

First release of the IPHAS Catalogue of New Extended Planetary Nebulae

* L. Sabin¹, Q.A. Parker^{2,3,4}, R.L.M Corradi^{5,6}, L. Guzman-Ramirez⁷, R.A.H. Morris⁸, A.A. Zijlstra⁹, I.S. Bojčić^{2,3,4}, D.J. Frew^{2,3}, M. Guerrero¹⁰, M. Stupar^{2,3}, M.J. Barlow¹¹, F. Cortés Mora¹, J.E. Drew¹², R. Greimel¹³, P. Groot¹⁴, J.M. Irwin¹⁵, M.J. Irwin¹⁶, A. Mampaso^{5,6}, B. Miszalski^{17,18}, L. Olguín¹⁹, S. Phillipps⁸, M. Santander García^{20,21}, K. Viironen²² and N.J. Wright¹²

¹Instituto de Astronomía y Meteorología, Departamento de Física, CUCEI, Universidad de Guadalajara, Av. Vallarta 2602, C.P. 44130, Guadalajara, Jal., México

²Macquarie University Research Centre in Astronomy, Astrophysics & Astrophotonics, Sydney, NSW 2109, Australia

³Department of Physics and Astronomy, Macquarie University, Sydney, NSW 2109, Australia

⁴Australian Astronomical Observatory, PO Box 296, Epping, NSW 1710, Australia

⁵Instituto de Astrofísica de Canarias, E-38200 La Laguna, Tenerife, Spain

⁶Departamento de Astrofísica, Universidad de La Laguna, E-38206 La Laguna, Tenerife, Spain

⁷European Southern Observatory, Alonso de Córdova 3107, Casilla 19001, Santiago, Chile

⁸School of Physics, Bristol University, Tyndall Avenue, Bristol, BS8 1TL, UK

⁹Jodrell Bank Centre for Astrophysics, Alan Turing Building, Manchester, M13 9PL, UK

¹⁰Instituto de Astrofísica de Andalucía, IAA-CSIC, Glorieta de la Astronomía s/n, 18008 Granada, Spain

¹¹Department of Physics and Astronomy, University College London, Gower Street, London WC1E 6BT, UK

¹²School of Physics, Astronomy & Mathematics, University of Hertfordshire, College Lane, Hatfield, AL10 9AB, UK

¹³IGAM, Institute of Physics, NAWI Graz, University of Graz, Universitätsplatz 5/II, 8010 Graz, Austria

¹⁴Department of Astrophysics/IMAPP, Radboud University Nijmegen, P.O. Box 9010, 6500 GL Nijmegen, The Netherlands

¹⁵Harvard-Smithsonian Center for Astrophysics, 60 Garden St., Cambridge, MA, 02138, US

¹⁶Institute of Astronomy, University of Cambridge, Madingley Road, Cambridge CB3 0HA, UK

¹⁷South African Astronomical Observatory, PO Box 9, Observatory, 7935, South Africa

¹⁸Southern African Large Telescope Foundation, PO Box 9, Observatory, 7935, South Africa

¹⁹Departamento de Investigación en Física, Universidad de Sonora, México

²⁰Observatorio Astronómico Nacional, Ap 112, 28803 Alcalá de Henares, Spain

²¹CAB, INTA-CSIC, Ctra de Torrejón a Ajalvir, km 4, 28850 Torrejón de Ardoz, Madrid, Spain

²²Centro de Estudios de Física del Cosmos de Aragón, Plaza San Juan 1, Planta 2, Teruel, 44001, Spain

Accepted . Received

ABSTRACT

We present the first results of our search for new, extended Planetary Nebulae (PNe) based on careful, systematic, visual scrutiny of the imaging data from the INT Photometric H α Survey of the Northern Galactic Plane (IPHAS). The newly uncovered PNe will help to improve the census of this important population of Galactic objects that serve as key windows into the late stage evolution of low to intermediate mass stars. They will also facilitate study of the faint end of the ensemble Galactic PN luminosity function. The sensitivity and coverage of IPHAS allows PNe to be found in regions of greater extinction in the Galactic Plane and/or those PNe in a more advanced evolutionary state and at larger distances compared to the general Galactic PN population. Using a set of newly revised optical diagnostic diagrams in combination with access to a powerful, new, multi-wavelength imaging database, we have identified 159 true, likely and possible PNe for this first catalogue release. The ability of IPHAS to unveil PNe at low Galactic latitudes and towards the Galactic Anticenter, compared to previous surveys, makes this survey an ideal tool to contribute to the improvement of our knowledge of the whole Galactic PN population.

Key words: Survey – ISM: planetary nebulae – .

1 INTRODUCTION

Planetary nebulae (PNe) are strong astrophysical tools allowing us to understand the late stage stellar evolution and the chemical evolution of our entire Galaxy. The ionised shell exhibits strong and numerous emission lines that are excellent laboratories for plasma physics. PNe are also visible to great distances where their strong lines permit determination of the sizes, expansion velocities and ages of the PNe, so probing the physics and timescales of stellar mass loss (e.g. Iben 1995). We can also use them to derive luminosity, temperature and mass of their central stars, and the chemical composition of the ejected gas. Finally PNe can be used to directly probe Galactic stellar and chemical evolution (Dopita et al. 1997; Maciel & Costa 2003). Adding to their number, particularly at their more evolved extremes, can help inform general models describing the physical and chemical processes occurring during this crucial late stage of stellar evolution.

The general knowledge of the Galactic PN population has traditionally been based on the ~ 1500 objects listed in the Strasbourg-ESO Catalogue and its supplement (Acker et al. 1992, 1996) and the largely overlapping compendium of Kohoutek (2001). More recently the Macquarie-AAO-Strasbourg $H\alpha$ Survey (MASH) catalogues (Parker et al. 2006, Miszalski et al. 2008) uncovered an additional ~ 1500 spectroscopically confirmed PNe. These discoveries were based on careful scrutiny of the SuperCOSMOS AAO/UKST $H\alpha$ Survey (SHS) of 4000 square degrees of the Southern Galactic plane which is described in full in Parker et al. (2005) and Frew et al. (2014, a). The detection rate of new Galactic PNe has been relatively low since the release of the MASH catalogue. Nevertheless, a further 200 or so confirmed PNe have been uncovered subsequently by a medley of other researchers including Boumis et al. (2006) and Górný (2006) who found 44 and 24 new PNe in the Galactic Bulge region respectively. Significant numbers (~ 70) have also come from the Deep Sky Hunters (DSH) 'amateur' consortium via the analysis of the on-line Digital Sky Survey plates e.g. Jacoby et al. (2010), Kronberger et al. (2006, 2012, 2014) and also from a group of French amateurs, Acker et al. (2012). Finally, several hundred unconfirmed compact candidates from the Isaac Newton Telescope Photometric $H\alpha$ Survey IPHAS survey (Drew et al. 2005) have also been found by Viironen et al. (2009). Their proper investigation and veracity has now been assessed during the construction of a new, comprehensive, multi-wavelength Galactic PN database by Bojicic et al. (in preparation and see later).

All the recent, confirmed discoveries takes the total current Galactic PN population to ~ 3300 , double what it was a decade ago. However, even this number falls a factor of ~ 1.5 short of even the most conservative Galactic PN number estimates. Population synthesis yields 6,600-46,000 PNe depending on whether the binary hypothesis for PN formation is invoked. For example, Frew & Parker (2006) predict a global PN population of $28\,000 \pm 5000$, Moe & De Marco (2006) derived $46\,000 \pm 13\,000$ Galactic PNe with a radius $r < 0.9$ pc, Zijlstra & Pottasch (1991) gave an estimation of the total number of PNe in the Galactic disk of $\sim 23\,000 \pm 6000$ while Moe & De Marco (2005) predicted only ~ 6600 if close binaries (e.g. a common envelope phase) is required to form PNe. In this last case at least there are prospects to rule out the PN binary hypothesis as known PN numbers are now within less than a factor or two of this prediction. This is especially true given that a significant population of Galactic PNe must still be lurking behind the extensive clouds of gas and dust that obscure large regions of our view across the optical regime (e.g. Parker et al. 2012). Indeed, it is the extension of previous PN discovery techniques away from the

optically dominant [OIII] emission line in un-reddened PN spectra towards the longer wavelength $H\alpha$ emission line (that can peer at least partially through the dust), that has led to the major discoveries of the previous decade.

The most studied PNe (particularly those used for abundance studies) currently belong to the bright end of the luminosity function (Ciardullo & et al. 2010). This means that they are nearby and/or relatively young and as such may not be representative of the true, underlying PNe population. Until the advent of MASH the faintest and more evolved PNe were not well represented and this remains the case for the Northern Galactic plane. PN studies have also mainly concentrated on the solar neighbourhood and on the inner Galaxy, with fewer objects investigated towards the Galactic Anticentre. This imbalance becomes very important when considering the existence of an abundance gradient in the Galaxy and the behaviour of that gradient in the outer regions of the Galactic plane. The IPHAS $H\alpha$ survey of the inner regions of the Northern Galactic Plane (Drew et al. 2005) allows us scope to tackle these issues.

We present here the first significant discoveries of spectroscopically confirmed, extended PNe from candidates selected via careful visual scrutiny of the IPHAS data. This paper represents the outcome of nearly eight years of candidate detections and spectroscopic follow-up including many evolved and (very) faint nebulae located in the Northern Galactic Plane. In this, the first of several papers on new IPHAS PNe, we present the basic information for 159 newly confirmed Galactic PNe including positions, sizes and morphologies concentrated primarily in a two hour Right Ascension (RA) zone between 18 and 19 hours. There still remain hundreds of IPHAS resolved PN candidates still waiting final confirmation that will be the subject of additional papers in the series. This paper is structured as follows. First the IPHAS survey itself is briefly described (§2), then the PNe candidate detection method (§3) and then the subsequent spectroscopic follow-up (§4). The catalogue is presented in §5 with some statistics based on the PN parameters given in §6. The online version of the catalogue which is included as a subset of the new Macquarie-AAO-Strasbourg multi-wavelength and spectroscopic PN database (MASPN; Bojicic et al, in preparation) is briefly presented in §7. Our concluding remarks are discussed in §8.

2 THE INT PHOTOMETRIC $H\alpha$ SURVEY: IPHAS

IPHAS is a fully photometric CCD survey of the Northern Galactic Plane that began in 2003 and is now essentially complete (see Drew et al. 2005, González-Solares et al. 2008). A careful photometric calibration of the survey has now been undertaken and is presented in Barentsen et al. 2014 (submitted). IPHAS targeted the inner regions of the Northern plane over the latitude range of $-5^\circ < b < 5^\circ$ and a longitude range of $29^\circ < l < 215^\circ$ covering a total of 1800 square degrees or about 45% of the coverage of the SHS in the south due to the more restricted range in b . The survey used the 2.5 m Isaac Newton Telescope (INT) at La Palma in the Canary Islands, Spain equipped with the Wide Field Camera (WFC). The WFC offered a field of view of 34×34 arcmin² thanks to its four EEV $2k \times 4$ CCDs¹. In addition to the 120 second $H\alpha$ filter exposures (95 Å FWHM, central wavelength at 6568 Å), IPHAS was also conducted with two broadband filters: Sloan r' (central wavelength at 6240Å, 30s exposure) and Sloan i' (central wavelength

¹ <http://www.ing.iac.es/Astronomy/telescopes/int/>

at 7743 Å, 10s exposure). The r' filter is a continuum 'off-band' filter which can be used with the narrow-band $H\alpha$ filter to detect emission line stars and nebulae. The IPHAS survey offered two main advantages over previous surveys of this kind in the north. First, the WFC has a small pixel scale (0.33 arcsec/pixel) and the observing site has generally good seeing (with a median value of 1.1 arcseconds) that resulted in better resolution than other existing wide-field, narrow band surveys. Secondly, IPHAS is generally deeper, covering point sources with r' magnitudes down to 19.5-20 (González-Solares et al. 2008), and also extended emission with a $H\alpha$ detection limit down to 2.5×10^{-16} erg cm $^{-2}$ s $^{-1}$ arcsec $^{-2}$ at full spatial resolution and $\sim 10^{-17}$ erg cm $^{-2}$ s $^{-1}$ arcsec $^{-2}$ with a 5" binning (Corradi et al. 2005). The resolution and the sensitivity offered by IPHAS make it an ideal tool for the detection of emission nebulae of all kinds. IPHAS is a survey sensitive to very low surface brightness nebulae and our group has been able to detect individual, morphologically exceptional PNe (Mampaso et al. 2006; Wesson et al. 2008; Corradi et al. 2011; Viironen et al. 2011, and we can also cite the external work by Hsia & Zhang 2014), PNe interacting with the ISM (Wareing et al. 2006; Sabin et al. 2010, 2012), symbiotic stars (Corradi et al. 2008, 2010), proplyd-like objects (Wright et al. 2012) and new Galactic supernova remnants (Sabin et al. 2013). Crucially though IPHAS has the sensitivity to reveal many new PNe belonging to the faint end of the PNe luminosity function and sample more of the evolved PN population previously unavailable for study in the Northern Galactic plane. Furthermore, the high resolution and sensitivity of IPHAS allows the discovery of new morphological structures including extremely faint Asymptotic Giant Branch (AGB) haloes around some known PNe. Finally, IPHAS is able to detect PNe through the more extinguished regions of Northern plane due to the longer narrow-band $H\alpha$ wavelength. Such PNe would not have been optically detected in [OIII] or broad-band optical filters.

3 DETECTION PROCESS

3.1 Mosaicking

As described by Sabin (2008), the search for new ionised nebulae is performed on IPHAS image mosaics based on two scales of binned data. This pragmatic approach was adopted as careful visual scrutiny of the 0.3 arcsecond/pixel full resolution data would have been too time consuming given the scale of the survey. Pixel binning has the significant advantage of making coherent, low surface brightness features easier to detect. Of course once any candidate nebulae has been found it can be subsequently examined at full resolution for further confirmation and examination.

Mosaicked $H\alpha - r$ difference maps are generated for a set of pre-defined $2^\circ \times 2^\circ$ regions on the sky, following a two-step process. First, a pair of $H\alpha$ and r band exposures is selected for each IPHAS survey field together with a corresponding separate pair for the "offset" fields used in IPHAS to fill the inter-chip CCD gaps on the Wide Field Camera. We use the data quality control parameters as stored in a PostgreSQL database generated automatically from the FITS headers of the existing IPHAS pipeline object catalogues (e.g. Irwin & Lewis 2001; Drew et al. 2005) to select survey field exposures taken in good observing conditions. These constraints are currently: sky brightness < 2400 ADU; median image ellipticity < 0.3 ; seeing < 2.0 arcseconds; 5σ magnitude limit > 18.0 ; astrometric fit rms < 0.75 arcseconds). Where multiple images are available, the one with the best calculated limiting magnitude is

used. All pairs of $H\alpha$ and r images comprising the $2^\circ \times 2^\circ$ tile are then subtracted, storing one subtracted image per CCD (four per telescope pointing, and eight per IPHAS field including the "offset" fields).

We use a simple pixel-by-pixel subtraction method based on using an accurately assigned image world coordinate system (WCS) to re-bin the two images onto the same pixel coordinate system using bilinear interpolation. The object catalogues are used to refine the frame-to-frame transformation by fitting for a standard 6-coefficient linear plate solution. An accurate astrometric registration is critical for difference imaging to avoid introducing additional, unwanted artefacts into the images. The confidence maps (e.g. Irwin & Lewis 2001) are used to flag bad pixels and other low-confidence regions of the image. We then derive the median sky background on the subtracted images, and subtract this (constant) offset from the pixel values to remove the effects of any varying difference in sky background between the $H\alpha$ and r images in the mosaic.

This subtraction method frequently introduces image artefacts when the PSF match between the image pair is poor (e.g. if the seeing was substantially different for the two images despite then being taken consecutively). Although we have implemented an adaptive kernel method based on that of Alard & Lupton (1998) and Alard (2000), the computational cost of this technique was prohibitively expensive given the size of the IPHAS data-set and the number of mosaics which must be processed (~ 1500), so it has not been used in practice for this project. However, it is made available via the Wide Field Survey interface² to allow individual fields to be processed in this fashion if required for other projects/purposes. The presence of image artefacts, although ubiquitous, does not prevent the recognition and discovery of resolved nebulae even if they are of exceptionally low surface brightness as they have the same general form and character.

Finally, the subtracted images of all the CCDs in each survey field are combined into a full mosaic for that field. The resulting images are initially binned by 5×5 pixels in each dimension that corresponds to ~ 1.7 arcseconds/pixel. This is only a little poorer than the median site seeing and is similar to the native seeing of the equivalent SHS survey in the south. The human visual system is quite immune to the effects of undersampling the PSF. This binning is done as before, by interpolating the input images onto the output map by using the WCS information stored in the FITS headers, and flagging bad pixels using the confidence maps. Since each pixel of the output image is typically covered by $\gg 1$ input pixel, this effectively removes a large fraction of the CCD artefacts present in the full resolution data quotient images. A second coarser binning factor of $15 \text{ pixels} \times 15 \text{ pixels}$ (equivalent resolution of ~ 5 arcseconds/pixel) was also employed to capture larger-scale diffuse nebulosity more easily (see below).

3.2 Visual search

Searches for extended but discrete ionised nebulae within the binned mosaics were done via careful and painstaking visual scrutiny of each processed IPHAS survey field. The most interesting tool, for our purposes, is the setting of two mosaic image scale factors or binning levels at $15 \text{ pixels} \times 15 \text{ pixels}$ (resolution of ~ 5 arcseconds/pixel) and at the original $5 \text{ pixels} \times 5 \text{ pixels}$ (resolution of ~ 1.7 arcseconds/pixel) as mentioned above. The

² <http://www.ast.cam.ac.uk/wfcsur/data/dqc/>

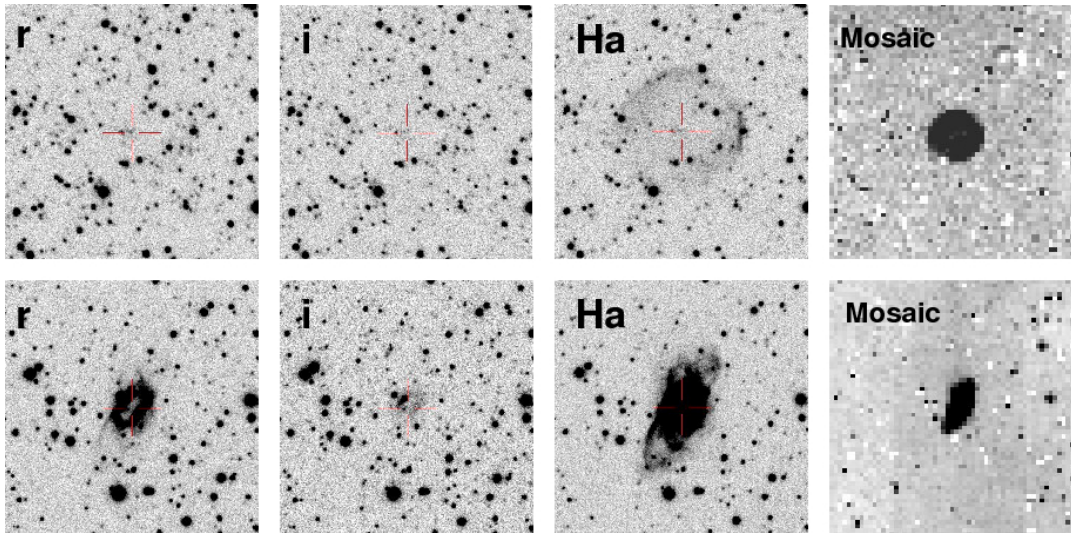


Figure 1. The top row shows the faint, new PN IPHASX J190512.4+161347 in the r , i and $H\alpha$ filter (FoV=2 arcmin and resolution 0.33 arcseconds/pixel) and the region of the mosaic where it was first clearly spotted (FoV= 5 arcmin and resolution 4.95 arcseconds/pixel). For comparison purposes we show in the second row the IPHAS images of the known and brighter PN M1-75 (FoV=2 arcmin and resolution 0.33 arcseconds/pixel) and also the region where it lies in the 15 pixels binned mosaic (FoV= 5 arcmin and resolution 4.95 arcseconds/pixel). The advantage in using the binned mosaicking technique to unveil low surface brightness nebulae such as those found with IPHAS is clear. In both cases North is up and East to the left.

cruder binning level helps to resolve low surface brightness objects (Fig.1-Top row) down to the IPHAS limit (Sabin et al. 2010) and to accentuate the contours/shape of such extended nebulae (this is particularly useful to see the full extent of an outflow for example). The second, finer binning is used to detect intermediate size nebulae, i.e those smaller than ~ 15 -20 arcseconds in diameter which constitutes a decent fraction of the total discoveries. These objects are too small to be seen with the crudest binning level (they are not resolved, and thus not distinguishable). They are also generally too faint to be detected via point source $H\alpha - r$ colour photometry as used by (Viironen et al. 2009) to uncover unresolved PN candidates as they drop out of the r -band completely. Some of the smallest new IPHAS PN candidates from ~ 3 -4 arcseconds up to ~ 10 -15 arcseconds were discovered using a semi-automated detection method. The technique, also used in the southern MASH survey (Miszalski et al. 2008), relies upon quotient imaging and combining $H\alpha$, r and i images into an RGB composite. Some smaller extended nebulae can be detected and we can also discriminate them from “late-type star” contaminants which can mimic emitters in $H\alpha - r$ due to their increasingly strong TiO bands whereas in the i band such stars are brighter.

Careful examination of the mosaics was done according to the following procedure. First, all the detected ionised nebulae were noted regardless of whether they are already known in the literature. This helped to ensure the completeness of the search. The large overlap between two adjacent mosaics is also a guarantee that no real object is easily missed. Candidate selection was then refined based on the objects’ morphology (which is particularly valid for PNe) and on whether the nebulae are detached or isolated, i.e. they are not merely part of a larger nebular conglomerate such as a large supernova remnant, HII region or other large-scale meandering, diffuse nebulae. Environmental considerations were also assessed such that objects in areas of high extinction, low stellar number density and general HII regions were considered to be likely of young provenance (but the candidates were not discarded).

Finally, objects unknown in Simbad and Vizier³ were separated from known sources. Despite the great care taken while performing the extensive search and in creating the mosaics we were still confronted with three main problems which complicated the selection process:

- The presence of image artefacts. These can be very easily mistaken for real objects under certain binning conditions. Such artefacts generally result from instrumental effects (e.g. CCD edge reflections) or are generated during the $H\alpha$ - r image subtraction due to psf mismatch. A simple way to check the veracity of a candidate is to look at the un-binned images (0.33 arcseconds/pixel) and also in the native $H\alpha$ band as each IPHAS field is observed at least twice. An artefact is highly unlikely to be repeated in all frames and so can be easily eliminated.
- Based on some independent comparisons from the DSH team it is clear that our selection process is not sensitive to a group of true candidate objects i.e. those extending over a couple of pixels in the 15×15 mosaics (which were also not picked up during the semi-automated search of 5×5 pixel mosaics). Some of these are likely to be genuine PNe. The only solution is to perform a scan of the full resolution mosaics. This massive work will be undertaken in the future.
- The bad quality of some mosaics early in the search process due to the need to initially use frames taken in non-optimal weather conditions. Many of these frames have now been replaced with higher quality equivalents as the survey nears completion and it would be worthwhile revisiting the affected fields in the future.

As this is the first in a series of papers of new IPHAS PNe we mainly present the visual detection and spectroscopic confirmation from the hundreds of PN candidates in the two hour right ascension range RA=18 to 19 hours that has been examined most thoroughly. However, we have also included a limited number of additional confirmed PNe in the RA range from 20 hours through to 06h30m

³ <http://cdsportal.u-strasbg.fr/>

acquired and confirmed due to the vagaries of telescope time allocations for the spectroscopic follow-up. All the newly discovered objects with IPHAS, including the new PNe presented here, are named according the International Astronomical Union convention: IPHASX JHHMMSS.s+DDMMSS (exclusively used for extended sources).

4 FOLLOW-UP SPECTROSCOPY

4.1 Observations

The large number of PN candidates discovered required the use of several telescopes worldwide for an efficient spectroscopic follow-up program as given in Table 1. On the whole 2-m class telescopes were sufficient to provide the necessary spectroscopic confirmation which is all that is required at this stage. Detailed abundance, kinematics and photo-ionisation studies for selected high-interest candidates will be performed later but has already been done for a few selected objects including the so-called 'Necklace' PN (e.g. Mampaso et al. 2006; Corradi et al. 2011; Viironen et al. 2011).

During the initial stages of our spectroscopic follow-up we used the Intermediate Dispersion Spectrograph (IDS) on the 2.5m INT and the spectrograph ISIS on the 4.2 m William Herschel Telescope (WHT) located at the Observatorio del Roque de los Muchachos on La Palma in the Canary Islands. Many subsequent observations were performed with the 2.1m San Pedro Martir Telescope (SPM) in Mexico with its Boller & Chivens spectrograph and with the 1.5m telescope associated to the ALBIREO spectrograph at the Observatory of Sierra Nevada (OSN) in Spain. One valuable run was performed with the 2.1m telescope at the Kitt Peak National Observatory (KPNO) and a few observations were made with the 10.4m Gran Telescopio Canarias (GTC) and OSIRIS spectrograph also on La Palma. Other observations for those IPHAS PNe candidates also accessible from the south were observed with the ANU 2.3 m Telescope at Siding Spring Observatory in Australia, initially with its Dual Beam Spectrograph (DBS) and later with the Wide Field Spectrograph (WiFeS; Dopita et al. 2007) IFU and also with the 1.9m Radcliffe Telescope at the South African Astronomical Observatory (SAAO) at Sutherland. Details of each telescope run together with the configurations of the associated spectrographs are listed in Table 1. In total more than 500 spectroscopic observations were carried out mostly between 2006 and 2014 (see some examples in Fig.2). The general faintness of the IPHAS targets also necessitated long exposure times typically ranging from 900 seconds to 2×1800 seconds, some of them repeated once or twice depending on the weather conditions or result obtained. Due to some modest overlapping with the coverage of the MASH survey in the southern Galactic plane as well as with the area searched by the DSH community some of our targets were common to both of these independent studies. In cases where the basic information on a common source has already been published by one of the two aforementioned groups, we only present the IPHAS detected PNe for which a clear classification and confirmation has not previously been clearly determined although such PNe are indicated in the main catalogue table.

The majority of the new IPHAS PNe uncovered have low surface brightness which is either intrinsic (evolved PNe), due to heavy intervening extinction in the plane and/or is because the candidates are located at large distance. Consequently, for many nebulae only the strongest few emission lines could be detected. Fortunately, these are also generally the minimum necessary to allow object identification following the usual diagnostic

diagrams (i.e. $H\alpha$, $[\text{NII}]\lambda\lambda 6548, 6583\text{\AA}$; $[\text{SII}]\lambda\lambda 6717, 6731\text{\AA}$ and $[\text{OIII}]\lambda 4959, 5007\text{\AA}$). Parker et al. (2012) showed that the most obscured PNe discovered from optical images have a V -band extinction in excess of 10 magnitudes. For such objects the $H\beta$ line can be very difficult to detect spectroscopically. For some of the more obscured IPHAS PNe, this line was undetected so we were not able to derive an extinction value for them based on the Balmer decrement technique, although with an estimation of the upper limit of the $H\beta$ flux we can derive a lower limit of $cH\beta$. Other basic physical properties such as the electron density (n_e) can come from the observed $[\text{SII}]$ line ratio available for many of our existing spectra. However, other parameters such as the electron temperature (T_e) and abundances for individual PNe require far higher S/N spectra to detect the faint diagnostic lines required. Such determinations will be reported in forthcoming papers and in the MASP database as available spectra allow.

The spectral data reduction including bias removal, flat-fielding, cosmic ray removal, wavelength and flux calibration and 1-D spectrum extraction was generally performed with standard long-slit IRAF routines (Valdes 1986) with some specific, minor differences according to the various data formats, calibration lamps used etc. In the case of the WiFeS IFU data specially developed reduction pipelines were used (e.g. Dopita et al. 2010). Given the large number of objects, for some suitable data sets the automatic analysis software ANNEB, developed by Olguín et al. (2011), which includes the *Nebular* packages of IRAF/STSDAS (Shaw & Dufour 1995), could be employed on the reduced 1-D spectra. It conveniently provides a set of useful information such as the emission line identifications, the extinction $c(H\beta)$ according to the chosen extinction law and for any Balmer line, the dereddened fluxes, physical parameters (T_e, n_e) where the spectra S/N and detections allow and crucially, the most important line ratios for use in the diagnostic diagrams. The extinction correction applied to our spectra was performed using the Fitzpatrick and Massa extinction curve (Fitzpatrick & Massa 2007) for $R_V = 3.1$.

4.2 Spectroscopic object identification and confirmation

An accurate determination of the PN nature of many of the IPHAS candidate nebulae is challenging for two reasons. First, there are a large number of other morphologically similar nebular mimics such as Wolf-Rayet (WR) shells, symmetric HII regions, symbiotic stars, Herbig Haro objects, CVs with highly collimated bipolar outflows, reflection nebulae and shell supernova remnants (e.g. Sabin et al. 2013) which can all be confused with true PNe. Secondly, the low surface brightness of the sources generally leads to low S/N emission-line spectra and small numbers of diagnostic identified lines. In several cases similar emission-line ratios are found for totally different types of equally faint astrophysical objects. In these cases the use of supplementary multi-wavelength imaging data, now increasingly available, has proven extremely valuable (see later). The removal of contaminants (i.e. non-PNe) is a critical and important step in delivering a catalogue of IPHAS PNe of high integrity. The issue of PN mimics has been thoroughly discussed by Parker et al. (2006) and Frew & Parker (2010) who also provide robust tests and other indicators of PN veracity that were adopted here.

The new IPHAS PNe were confirmed through using a combination of new, multi-wavelength imagery from the UV through the optical, NIR, MIR and radio and improved sets of optical diagnostic diagrams by Frew & Parker (2010) and more recently Sabin et al.

Table 1. Details of the spectroscopic follow-up performed on a variety of telescopes.

Telescope	Instrument	Grating(s)	Wavelength Coverage Å	Dispersion Å/pix	Resolution Å	Run dates yyyy-mm-dd	Observers
WHT-4.2m	ISIS	R300B	3500-6100	0.86	3	2004-09-23:27	-†
-	-	R158R	6000-10500	1.82	6		
SPM-2.1m	B&Ch	600 l/mm	3590-5650	2	3.2	2005-12-03:04	KV
-	-	-	5310-7450	2	3.2		
INT-2.5m	IDS	R300V	3030-8960	1.8	5	2006-06-14:15	RC,LS
INT-2.5m	IDS	R300V	3030-8960	1.8	5	2006-08-01	RC
WHT-4.2m	ISIS	R300B	3040-5460	0.86	3	2006-08-23:24	MB,LS
-	-	R158R	5140-9700	1.82	6		
INT-2.5m	IDS	R300V	3030-8960	1.8	5	2006-08-28:29	MB,LS
INT-2.5m	IDS	R300V	3030-8960	1.8	5	2006-09-08	RG,RC
SPM-2.1m	B&Ch	400 l/mm	4330-7530	5	4.8	2007-01-23:25	KV
WHT-4.2m	ISIS	R300B	3040-5460	0.86	3	2007-07-16:17	KV,LS
-	-	R158R	5140-9700	1.82	6		
MSSO-2.3m	DBS ⁽²⁾	300B	3630-7390	1.9	6	2007-09-05	BM
INT-2.5m	IDS	R300V	3030-8960	1.8	5	2007-08-02	-†
INT-2.5m	IDS	R300V	3030-8960	1.8	5	2008-06-27:29	RC
KPNO	GoldCam	240	3980-7020	1.52	4.1	2009-08-12:18	LG,KV
GTC-10.2m	Osiris	R1000B	3600-7760	2.12	2.15	2009-11-09	-†
SPM-2.1m	B&Ch	400 l/mm	4330-7530	5	4.8	2010-06-02:03	LS
SPM-2.1m	B&Ch	400 l/mm	4330-7530	5	4.8	2010-07-09:12	LS
SPM-2.1m	B&Ch	400 l/mm	4330-7530	5	4.8	2010-09-17	LS
OSN-1.5m ⁽³⁾	Albireo	R600	3650-7180	3.49	6.5	2010-09-18	MG
SPM-2.1m	B&Ch	400 l/mm	4330-7530	5	4.8	2010-09-20	LS
GTC-10.2m	Osiris	R1000B	3600-7760	2.12	2.15	2011-04-13	-†
SPM-2.1m	B&Ch	400 l/mm	4330-7530	5	4.8	2011-05-04:06	LS
GTC-10.2m	Osiris	R1000B	3600-7760	2.12	2.15	2011-06-07:28	-†
SAAO-1.9m	CCDSPEC	Grating 7	3000-7200	210 (Å/mm)	5	2011-07-01:04	QP,MS
SAAO-1.9m	CCDSPEC	Grating 7	3000-7200	210 (Å/mm)	5	2011-07-05:11	AZ
MSSSO-2.3m	WiFeS	B7000	4180-5580			2011-07-01:05	LS,LG
-	-	R7000	5290-7060				
SPM-2.1m	B&Ch	400 l/mm	4330-7530	5	4.8	2011-09-22:26	LS
OSN-1.5m	Albireo	R600	3650-7180	3.49	6.5	2011-10-04:10	MG
OSN-1.5m	Albireo	R600	3650-7180	3.49	6.5	2011-11-23:28	MG
SPM-2.1m	B&Ch	400 l/mm	4330-7530	5	4.8	2012-04-12:15	IB
OSN-1.5m	Albireo	R600	3650-7180	3.49	6.5	2012-05-17:25	MG
SPM-2.1m	B&Ch	400 l/mm	4330-7530	5	4.8	2013-02-10:11	LS
SPM-2.1m	B&Ch	400 l/mm	4330-7530	5	4.8	2013-05-07:09	LS

† Observations performed in service mode.

(2013) and Frew et al. (2014, b). These diagrams are based on improved determinations of the traditional Sabbadin et al. (1977) and Baldwin et al. (1981) emission line ratio plots. Contrary to older versions of such diagrams (from Riesgo & López 2006 for example) these new sets have the advantage of including more robustly determined line measurements from the very best data and several more types of well identified ionised nebulae which occupy distinct zones in these diagrams. These newly established plots offer more reliable constraints for an accurate determination of the nature of the investigated source. In order to keep some coherency between the diverse PNe catalogues we chose to adopt the flags used by the MASH survey of Parker et al. (2006) to estimate the quality of the identification. Those flags are:

True “T”: To indicate a spectroscopically and morphologically well defined PN across perhaps several multi-wavelength images.

Likely “L”: To indicate a not completely conclusive spectroscopic and/or morphological identification though a PN ID is likely.

Possible “P”: To indicate a non conclusive identification due to the insufficient quality or ambiguous nature of spectroscopic and/or

morphological data. Such objects cannot yet be ruled out as PNe but the current data could also support identification as several other possible astrophysical objects such as HII regions.

5 IPHAS CATALOGUE OF NEWLY DISCOVERED PNE

As a result of our spectroscopic, multi-wavelength and morphological investigation we were able to identify 159 candidate PNe. Following our adopted criteria we have classified 113 True, 26 Likely and 20 Possible PNe. The complete list of PNe can be found at the end of this paper (Table 3) as well as the catalogue of images (from Fig. A1 to Fig. A40). The different column entries for each object in the catalogue are described below.

Flag: True “T”, Likely “L” and Possible “P” as mentioned above.

IAU designation: Based on the Galactic coordinates and set to fit the general galactic PN nomenclature i.e. PN GIII.l+bb.b

IPHAS designation: IPHASX JHHMMSS.s+DDMMSS as described following the adopted IAU convention and based on the measured RA/DEC of the PNe.

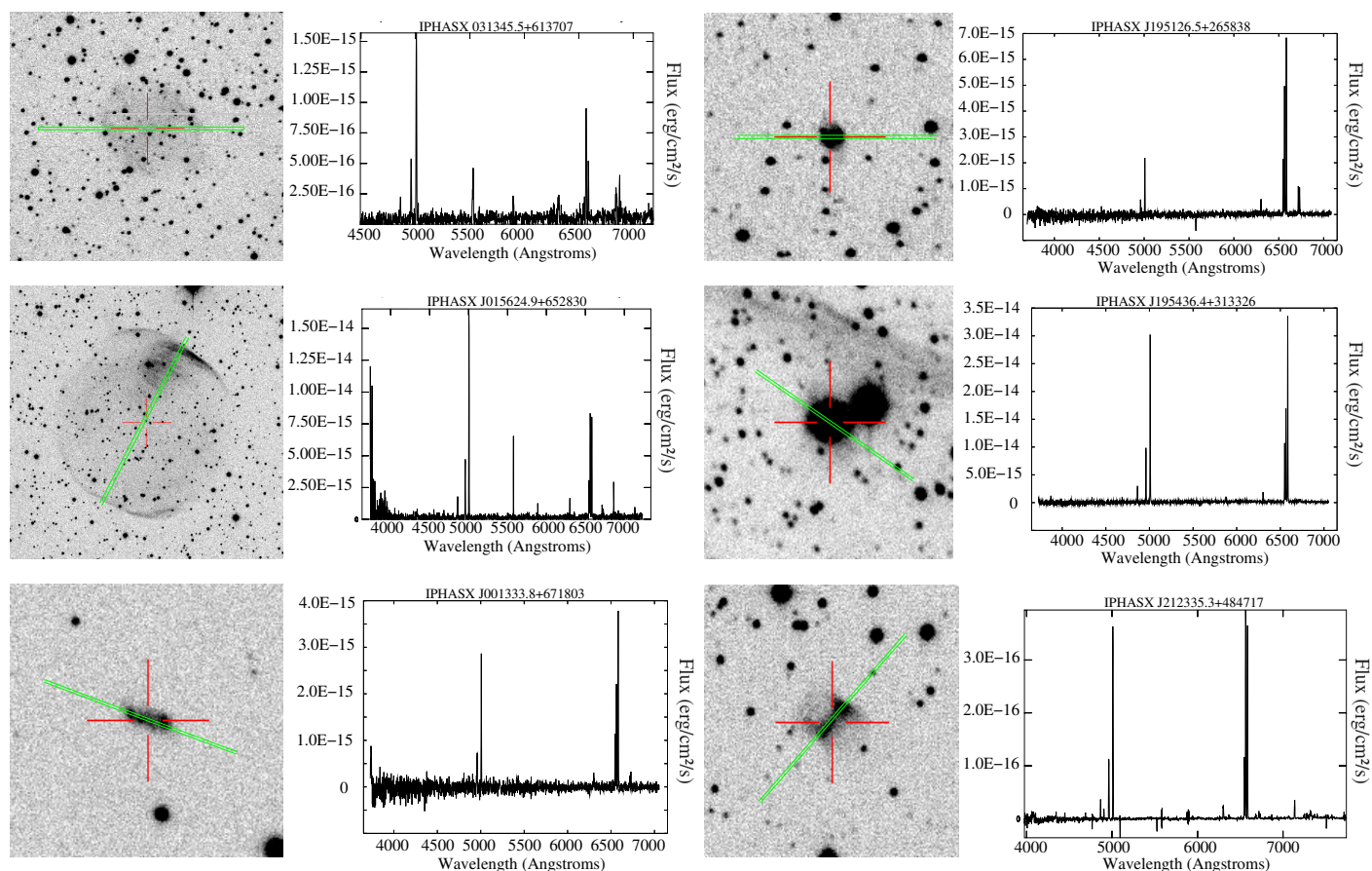


Figure 2. Example images and spectra of selected, newly discovered IPHAS PNe. For each object we indicate its official name followed by the field of view (in arcminutes), the binning of the image (in pixels) and the telescope where the confirmatory spectroscopy was performed such as (FoV,Bin,Telescope). North is up and East is left. We show a wide variety of morphologies and peak fluxes ranging from 10^{-14} to 10^{-16} erg/cm²/s. From top to bottom in the left column we present successively: IPHASX J031345.5+613707 (5,3,SPM) which is relatively faint and round, IPHASX J015624.9+652830 (5,2,SPM) a large (radius ~ 100 arcseconds) and well defined transparent bubble and IPHASX J001333.8+671803 (1,1,KPNO) which has an irregular and knotty structure. In the right column we present: IPHASX J195126.5+265838 (1,1,KPNO) is a small (3.8×3.4 arcseconds semi axis) new bipolar PN, IPHASX J195436.4+313326 (1,1,KPNO) is a ring PN and IPHASX J212335.3+484717 (1,1,GTC) is a faint bipolar (butterfly type) PN. All the PNe shown here are classified as True PNe (see text). The green lines indicate the position of the slit.

RA, DEC J2000 equatorial coordinates: The coordinates were defined based on the best estimate of the geometric centre of each object from the IPHAS H α or quotient image, or in the case of highly asymmetric or one sided nebulae, based on the middle of this arc or zone. When a candidate central star (CSPN) was identified its location was not adopted as the position of the PN. This is because in many cases of evolved and large angular size PNe the likely CSPN is clearly not centrally located. A separate list of unequivocally identified CSPN with positions, including those which exhibit [WR] or WELS or PG1159 spectral signatures, will be provided in a subsequent publication.

Galactic coordinates l,b : They are based on the RA,DEC defined previously.

Major and where relevant, minor axis dimensions in arcseconds: The measurement of PNe size was done from the 120 second exposure H α + [NII] images so we are limited in description of the exact extent of the nebulae.

Morphological classification Assigned following the identical scheme used for the sister MASH survey (see below).

Telescope and date for first spectroscopic confirmation: A two letter code is used to identify each telescope used for spectroscopic

confirmations as follows: WH - WHT 4.2m; IN - INT 2.5m ; SM - San Pedro Martir 2m; KP - KPNO 2m ; GC - Grantecan 10m, OS - OSN 1.5m, MS - ANU 2.3m with DBS, WI - ANU 2.3m with WiFeS; SA - SAAO 1.9m.

5.1 Comments on table column values

Although our search focused on extended objects, i.e. with a lower limit on the total size of 3 arcseconds in the 5×5 binned pixel data, we also found quasi-stellar (essentially unresolved) PNe which were still picked up through the binned images. Some objects are not well defined, e.g. when only a rim is seen. In such cases the exact size will be slightly inaccurate as we rely on the best determined geometric centre of the structure encompassing the detected nebulae to establish the major axis. A comment to this effect is made in the notes accompanying such cases in the MASP database (e.g. IPHASX J194240.5+275109). This of course can introduce a (large) bias in the assumption of the optical size of the nebulae, but with no other high quality narrow-band optical data available, we adopted this scheme for the time being. Hence, the positional accuracy of some large, irregular nebulae (such as IPHASX

J192534.9+200334), of certain examples of bipolar nebulae (such as IPHASX J193718.6+202102) and some PNe with a possible ISM/interaction (e.g. IPHASX J195358.2+312120) could be off by tens-of-arcseconds compared to their actual centroids. Recall each observed nebulae is merely the 2-D projection of a 3-D source so we do not pretend to present a position for the projected physical object's centre. Deeper, high resolution images may be needed to establish the best coordinates to use for some of the IPHAS PNe listed here. Nevertheless, we have endeavoured to provide the best coordinates that the current IPHAS images can provide and also a best estimate of the angular extent to assist any observer in locating these PNe for further studies. Of course these may still not be sufficiently deep to pick up any faint, external AGB haloes or the extremely faint lobes of highly evolved bipolar PNe.

In order to facilitate easy inter-comparison with both the earlier MASH survey in the south and the new, full-scale catalogue of all known PNe recently put together by Parker et al. (2014) and Bojicic et al. (in preparation) we adopted the “ERBIAS” morphological classifiers to indicate Elliptical, Round, Bipolar, Irregular, Asymmetric or quasi-Stellar (unresolved or barely resolved) PNe. The additional sub-classifiers of “amprs” were also used where evident where a one sided enhancement/asymmetries denoted with “a”, multiple shells or external structure as “m”, point symmetry “p”, well defined ring structure or annulus “r” and resolved, internal structure as “s”. We emphasize that this initial morphological classification is based on the short $H\alpha$ + $[NII]$ exposure IPHAS image. Further investigations based on IFU data coupled with morpho-kinematical modelling will be needed to assert the “true” shape and geometry of many of these newly discovered PNe. Such detailed kinematical study would help, for example to disentangle cases of apparently round annular PNe that are actually face-on bipolar PNe (e.g. Jones et al. 2012), while longer exposure times will likely reduce the number of apparently irregular PNe by revealing an overall more coherent structure.

6 PRELIMINARY STATISTICAL ANALYSIS

6.1 Galactic distribution of new IPHAS PNe

Fig.3-Top shows the general distribution profile of new IPHAS PNe found in the longitude range $l^\circ=29-204$ degrees. We compared our data with earlier surveys such as the Strasbourg/ESO survey (Acker et al. 1992, 1996) and to a lesser extent with the overlapping zone of the southern MASH-I&II surveys (Parker et al. 2006; Miszalski et al. 2008) both restricted to the same area. Our new IPHAS sample increases the number of known PNe in this region of the Northern Galactic plane by nearly doubling it. Indeed, 181 PNe were previously found with the Strasbourg/ESO survey and 21 with the MASH survey in the region overlapping with the IPHAS survey area. As expected the detection rate declines when we move to larger Galactic longitudes but it is important to note that we have uncovered additional new PNe towards the Galactic Anticenter region i.e. $l^\circ > 115^\circ$ (Fig.3-Middle). These new objects will be of high importance for the estimation of the metallicity gradient which is one of the major issues that PN studies can help address as they provide an easily detectable target population that can be traced to great distance and whose emission lines can provide decent abundance estimates given decent S/N (Viironen et al. 2011; Henry et al. 2010; Costa et al. 2004). We also increase the number of detections close to the Galactic Plane (Fig.3-Bottom) including in more heavily obscured zones as can

be seen by comparing our new IPHAS PNe distribution to the extinction map by González-Solares et al. (2008). This trend is particularly well seen at $-0.5^\circ \leq b \leq 0.5^\circ$ where the detection rate is multiplied by a factor ~ 2 .

6.2 Estimated angular sizes

Our investigation, which is strongly biased towards extended (nearby and/or evolved) PNe, shows a large scatter in observed angular size. We detected PNe with an average major-axis dimension of 42 arcseconds and a median of 22 arcseconds (Fig.4) which is comparable to the results found in the MASH survey by Parker et al. (2006) with had an average size of 51 arcseconds and also a median of 22 arcseconds as for IPHAS. Among our sample we identified a set of 13 large PNe with diameters ranging between 100 and 480 arcseconds. The largest PNe in our catalogue has a diameter of ≈ 8 arcmin (IPHASX J185225.8+005250). Our ability to detect such extended structures at low latitudes (Fig.4-bottom) underlines both the depth reached with IPHAS and its ability to at least partially peer through dust. Apart from their size, this group of larger PNe is spread over a wide range of different morphologies. As an example, while IPHASX J015624.9+652830 appears as a well defined circular structure (Fig.2-left-2nd row), IPHASX J195358.2+312120 shows a bright rim structure probably indicating its interaction with the surrounding interstellar medium (Fig.6). The geometry of the latter PN does not allow an accurate measurement of its size and in those cases the coordinates and dimensions are derived based on the best estimate of the geometric centre from the best fitting circle or ellipse.

6.3 Morphological classifications

As previously mentioned the morphological classifications were made using the “ERBIAS” and “aprms” classification scheme. The current IPHAS sample consists of 50 elliptical, 45 round, and 45 bipolar PNe, while 6 display an irregular morphology, 6 are asymmetric and 7 are classified as quasi-stellar (i.e. essentially unresolved) sources (Table 2). Even with the short exposure time of 120 seconds in $H\alpha$, we were able to observe additional or secondary morphological structures in many objects. Deeper imaging coupled in some cases with 3-D morpho-kinematic analysis will be required for a more robust classification. We have already started an observational campaign with this aim for some of the more interesting IPHAS PNe so far uncovered (Fig.5).

A large, relative fraction of PNe classified essentially as round have been found in the latitude range targeted by IPHAS. This is a potentially interesting result as difficulties in detection of such round objects is linked to their generally lower surface brightness compared to non-spherical and bipolar PNe and the likelihood of being detected in more restricted surveys in terms of depth (Soker & Subag 2005). Our new data will contribute to better investigate this interesting “group”. Nevertheless the majority of these new IPHAS PNe are non-circular.

6.4 Estimating IPHAS PNe distances

We are now in the process of determining distances to most of these new IPHAS PNe using the newly developed Surface-Brightness radius relation Frew et al. 2014 (submitted). These new distance estimates will help us to ascertain the evolutionary status of our

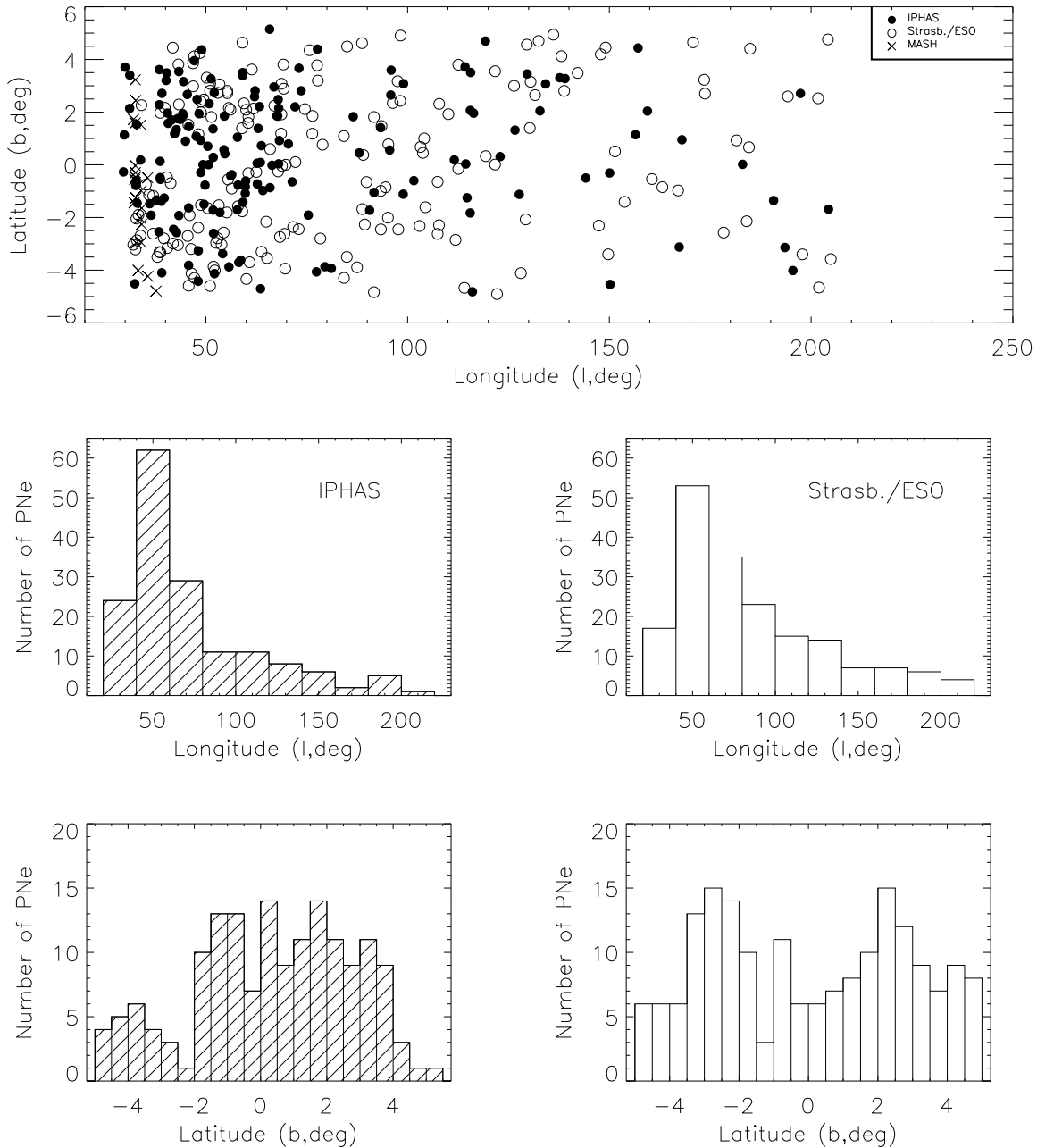


Figure 3. Top panel: Galactic distribution of the new IPHAS PNe (filled circles) shown against the sample from the Strasbourg/ESO catalogue (open circles) and the MASH catalogues (crosses) in the same area. Bottom panels: same as before with a histogram representation of the longitude and latitude distribution of the IPHAS PNe on the left and the Strasbourg/ESO data on the right. These plots underline the gain in terms of coverage and gap filling obtained with our new IPHAS PNe catalogue.

objects. Meanwhile we can still infer that the large sizes associated with the generally low surface brightness PNe suggest (highly) evolved more local PNe and hence provide a new sample with which to study the end stages of the PN evolution (i.e. several PNe with ISM interactions have also been found). The extinction method described by Giammanco et al. (2011) and Sale et al. (2009), which uses highly reliable photometric data from IPHAS, will be an additional, very useful tool to derive alternative distance

estimates with which to determine the age and evolutionary stage of these IPHAS PNe.

7 IPHAS PNE IN THE NEW ONLINE MACQUARIE-STRASBOURG PN DATABASE

All the newly discovered IPHAS PNe described and listed in this paper will also be accessible through the new Macquarie-Strasbourg PNe database MASP (Parker et al. 2014, Bojicic et

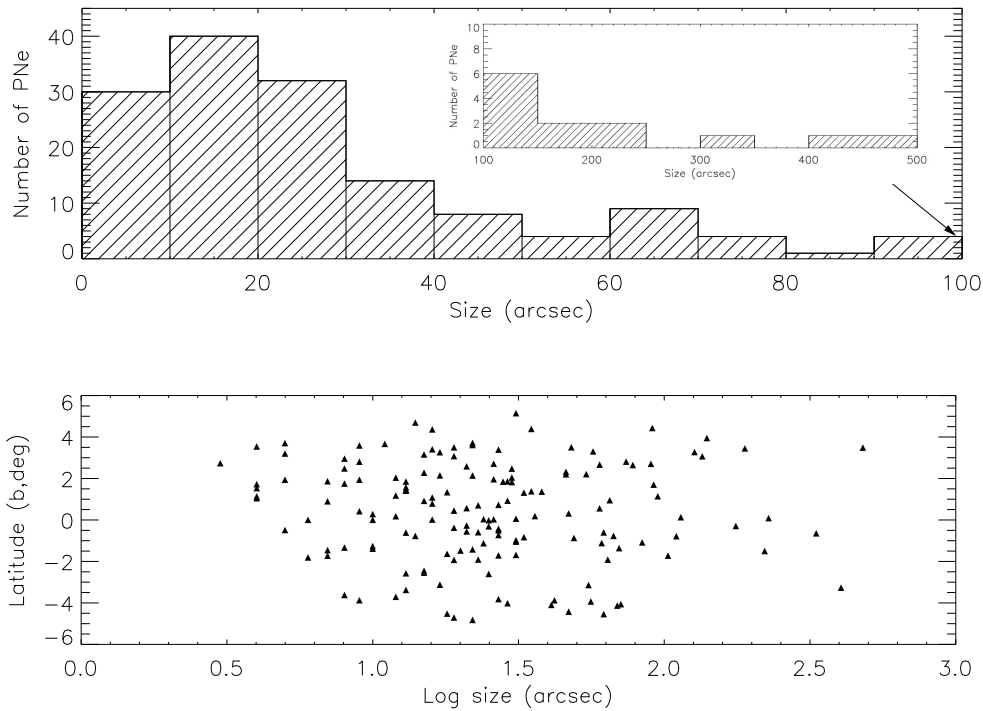


Figure 4. Estimated angular size distribution of the IPHAS PNe sample in the Northern Galactic plane. We observe a large scatter from compact barely resolved objects to those large objects 5 or more arcminutes in diameter even at low Galactic latitudes .

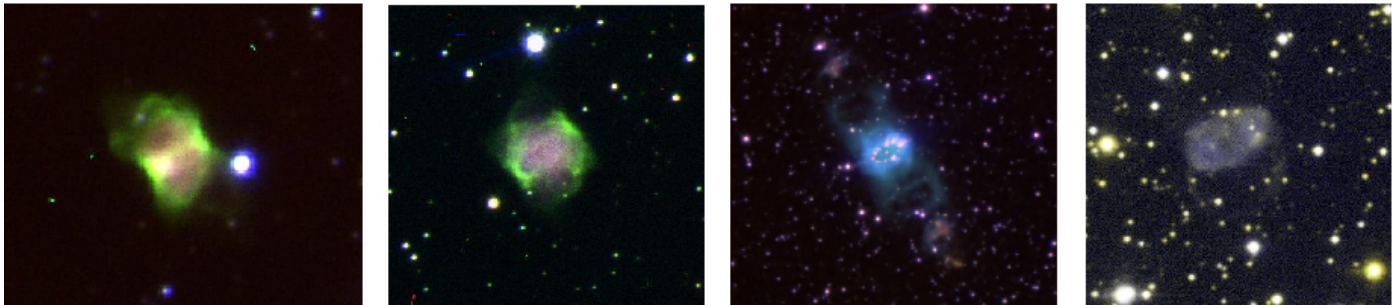


Figure 5. IPHAS image gallery of bipolar PNe with from left to right: IPHASX J194940.9+261521, IPHASX J205527.2+390359, IPHASX J194359.5+170901 (the Necklace) and IPHASX J221118.0+552841 (with its two faint lobes). All the images were taken at the Nordic Optical Telescope with ALFOSC and an average 20 min per filter (H α , [OIII] 5007 and [NII] 6583Å).

Table 2. Morphological distribution of the new IPHAS PNe.

Morphology	Elliptical	Round	Bipolar	Irregular	Asymmetric	Quasi-Stellar
Total Number	50	45	45	6	6	7
Fraction(%)	32	28	28	4	4	4
$\langle b \rangle^\circ$	1.89	2.36	1.96	0.84	2.46	1.66
$\langle \text{Major axis} \rangle''$	53	36	30	72	96	–

essential, up-to date information for all known Galactic PN and provides the community with the most complete data with which to undertake new science. It provides quick and easy access to information such as a multi-wavelength image service, spectroscopy, morphologies and other useful data. Fig. 7 shows the specific dedicated MASPNe entries available for each PNe in the catalogue for the PN IPHASX J194727.5+230816. MASPNe allows for the retrieval of detailed information such as the identification spectra and direct links to the SIMBAD and VIZIER entries for the selected object. As a preliminary demonstration of the MASPNe database, the catalogue entries for the complete list of a set of our newly discovered IPHAS PNe are presented in Fig. 8 in the form of selected multi-wavelength images.

al in preparation). This powerful, new database and research tool gathers all known Galactic PNe in a single place. It provides, for the first time, an accessible, reliable, on-line “one-stop” shop for

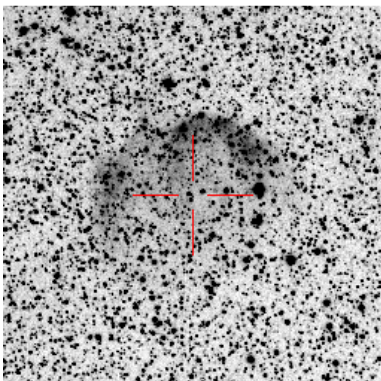


Figure 6. $H\alpha$ + $[NII]$ image of IPHASX J195358.2+312120 (North is up, East on the left). This new and large PN (~ 3.8 arcmin size) is an example of the many objects found during the survey which only show a bright rim inferred to be coincident with an interaction with the surrounding interstellar medium. The accurate estimation of the angular sizes of such objects is not currently straightforward due to the relatively short $H\alpha$ exposure time of 120 seconds.

8 CONCLUSIONS AND FUTURE WORK

We present the first major release of the preliminary catalogue of new, extended PNe discovered in the framework of the IPHAS Survey. We have detected 159 new PNe by visually scanning binned IPHAS image mosaics predominately over a two hour RA region from 18-19 hours. These newly discovered objects nearly double the number of known Northern PNe close to the Galactic mid-plane in the regions covered. Most of the newly found objects are relatively faint, attesting to their generally more advanced evolutionary stage and/or location in more obscured regions. The survey now provides access to a class of evolved and distant Galactic PNe previously under-represented in the Northern plane and vital for a proper evaluation of the global PN population across the whole Galaxy. Our sample also includes new PNe towards the Galactic Anticentre, a crucial region for abundance gradient studies. The IPHAS PNe are generally of low surface brightnesses and also of low excitation which makes their spectroscopic confirmation more difficult due to similar lines ratios sometimes existing for totally different classes of objects (which are equally faint and also show a few number of emission lines). However, the use of newly implemented diagnostic diagrams and associated environmental, morphological and multi-wavelength analysis allows us to largely overcome this problem. The first statistical studies indicate that our catalogue shows a large scatter in PNe sizes (though we are biased towards non point source PNe) and morphological structures. Also, within our sample we unveiled an important group of, what appeared to be genuine, round PNe at low Galactic latitudes. Their study would allow us to have a new look at this class of objects which are usually found at higher latitudes. By extension their progenitor characteristics could also be derived.

The work on extended, new IPHAS PNe presented here is the first in a series of associated papers in terms of discoveries as more IPHAS PNe have yet to be found and spectroscopically investigated. Additional work is planned on detailed kinematical analysis using IFUs for velocity and morphological determination of selected sub-samples combined with deep spectroscopy for accurate chemical analysis and abundance determinations. The study of identified CSPN and derivation of the distances (which could both benefit from the future GAIA mission) are also part of a non-exhaustive list of works still to be performed by our team. We in-

tend to measure the integrated $H\alpha$ fluxes of all these new nebulae directly from the IPHAS imaging data now that it has been properly calibrated (e.g. Barentsen et al. 2014, submitted), to complete the recent catalogue of Frew et al. (2014, a). The flux data is necessary to determine the distances of these new PNe independently using the $H\alpha$ surface brightness – radius relation of Frew et al. 2014 (submitted), and to be reported in a forthcoming paper. This investigation on the discovery and preliminary analysis of these new extended IPHAS PNe will be supplemented with data from the UVEX survey (“blue” counterpart of IPHAS in the North; Groot et al. 2009) and the VPHAS+ survey Drew et al. (2014) in the South.

ACKNOWLEDGEMENTS

We would like to thank Margaret Meixner for her careful review and highly appreciate the comments which contributed to improving the quality of the publication. LS is supported by the CONACYT grant CB-2011-01-0168078, MS was partially supported by Spanish MICINN within the program CONSOLIDER INGENIO 2010, under grant “Molecular Astrophysics: The Herschel and ALMA Era, ASTROMOL” (ref: CSD2009-00038), LO acknowledges support by project PROMEP/103.5/12/3590. We also thank the Bristol University students Greg Mould, William Howie, Luke Davies, Heidi Naumann, Will Summers, Alex Townshend, Paul May, Matina Mitchell, Finn Hoolahan, Tom Burgess, Ashley Akerman, James Jordan, Simon Palmer, Anna Kovacevic, Jai Taylor, Olivia Smedley and Daniel Huggins for their participation in the search in the framework of their undergraduate thesis.

This paper makes use of data obtained as part of the INT Photometric $H\alpha$ Survey of the Northern Galactic Plane (IPHAS) carried out at the Isaac Newton Telescope (INT). All IPHAS data are processed by the Cambridge Astronomical Survey Unit, at the Institute of Astronomy in Cambridge. The INT and WHT telescopes are operated on the island of La Palma by the Isaac Newton Group in the Spanish Observatorio del Roque de los Muchachos of the Instituto de Astrofísica de Canarias. This research has been partially carried out with telescope time awarded by the CCI International Time Programme. The Observatorio Astronómico Nacional at San Pedro Mártir, is a facility operated by Instituto de Astronomía of the Universidad Nacional Autónoma de México. We acknowledge the staff of the San Pedro Mártir Observatory for their support. This research also made use of data from Kitt Peak National Observatory, National Optical Astronomy Observatory, which is operated by the Association of Universities for Research in Astronomy (AURA) under cooperative agreement with the National Science Foundation. This paper uses observations made at the South African Astronomical Observatory (SAAO) as well as at the Siding Spring Observatory (SSO-Australia), which is part of the Research School of Astronomy & Astrophysics (RSAA) at the Australian National University (ANU). The 1.5m and ALBIREO spectrograph are operated by the Instituto de Astrofísica de Andalucía at the Sierra Nevada Observatory. Some observations were also made with the Gran Telescopio Canarias (GTC), installed in the Spanish Observatorio del Roque de los Muchachos of the Instituto de Astrofísica de Canarias, in the island of La Palma. This research has made use of the SIMBAD and VizieR databases, operated at CDS, Strasbourg, France. This research made use of APLpy, an open-source plotting package for Python hosted at <http://aplpy.github.com>. This research made use of Montage, funded by the National Aeronautics and Space Administration’s Earth Science Technology Office,

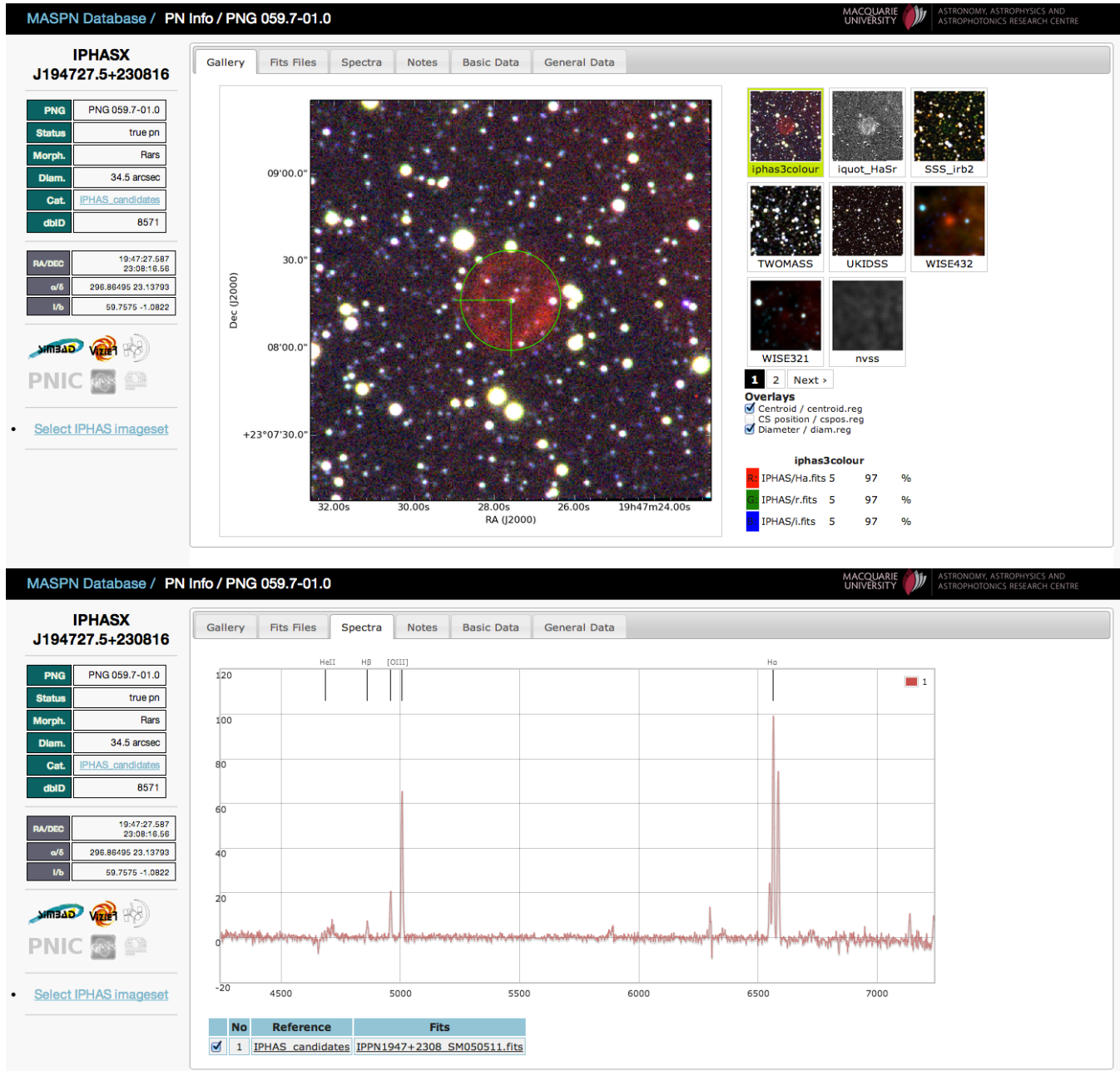


Figure 7. Multi-wavelength images of IPHASX J194727.5+230816 (Top) with its associated optical spectrum (Bottom).

Computation Technologies Project, under Cooperative Agreement Number NCC5-626 between NASA and the California Institute of Technology. Montage is maintained by the NASA/IPAC Infrared Science Archive. This publication makes use of data products from the Wide-field Infrared Survey Explorer, which is a joint project of the University of California, Los Angeles, and the Jet Propulsion Laboratory/California Institute of Technology, funded by the National Aeronautics and Space Administration.

Macquarie University GPN Database / Views / Image View 2

MACQUARIE UNIVERSITY ASTRONOMY, ASTROPHYSICS AND ASTROPHOTONICS RESEARCH CENTRE

Table View Image View Image View 2 Restart View Current Selection Check Objects Add New Object ivan

DATA	shs/iphaz_RGB	shs/iphaz_quot	2mass_RGB	vista/ukidss_RGB	wise432_RGB	spitzer432_RGB	nvss/mgps
<p>PNG056.1-00.4 IPHASX J193718.8-202102 true pn / Bas  19:37:18.680 20:21:02.99 56.16810 -0.42006</p>							
<p>PNG056.4-00.3 IPHAS XJ193740.8-203548 true pn / las  19:37:40.473 20:35:47.82 56.42408 -0.37400</p>							
<p>PNG057.8-01.0 IPHASX J193517.8-223120 likely pn / Ras  19:35:17.844 22:31:20.52 57.83543 1.04805</p>							
<p>PNG057.9-00.7 Kn 7 true pn / B  19:42:26.033 21:45:21.11 57.97967 -0.76769</p>							

Records:43 Page: 1 Items per page: 100

Text search... Select sample... Select images...

Figure 8. Selection of IPHAS PNe from the new MASPn database that gives an idea of how this new utility can be used.

REFERENCES

- Acker A., Boffin H. M. J., Outters N., Miszalski B., Sabin L., Le Dû P., Alves F., 2012, *Revista Mexicana de Astronomía y Astrofísica*, 48, 223
- Acker A., Marcout J., Ochsenbein F., 1996, First Supplement to the SECPGN. Observatoire de Strasbourg, 1996
- Acker A., Marcout J., Ochsenbein F., Stenholm B., Tylenda R., 1992, Strasbourg - ESO catalogue of galactic planetary nebulae. Part 1; Part 2. Garching: European Southern Observatory, 1992
- Acker A., Marcout J., Ochsenbein F., Stenholm B., Tylenda R., Schohn C., 1992, The Strasbourg-ESO Catalogue of Galactic Planetary Nebulae. Parts I, II.
- Alard C., 2000, *A&A*, 144, 363
- Alard C., Lupton R. H., 1998, *ApJ*, 503, 325
- Baldwin J. A., Phillips M. M., Terlevich R., 1981, *PASP*, 93, 5
- Boumis P., Akras S., van Hoof P. A. M., van de Steene G. C., Papamastorakis J., López J. A., 2006, in Barlow M. J., Méndez R. H., eds, *Planetary Nebulae in our Galaxy and Beyond Vol. 234 of IAU Symposium*, . pp 373–374
- Ciardullo R., et al. 2010, *PASA*, 27, 149
- Corradi R. L. M., Mampaso A., Viironen K., Kovacevic A., Zijlstra A., Greimel R., Irwin J., Drew J. E., Wright N., Morris R., Phillipps S., et al. 2005, in R. Szczerba, G. Stasińska, & S. K. Gorny ed., *Planetary Nebulae as Astronomical Tools Vol. 804 of American Institute of Physics Conference Series*, . pp 7–10
- Corradi R. L. M., Rodríguez-Flores E. R., Mampaso A., Greimel R., Viironen K., Drew J. E., Lennon D. J., Mikolajewska J., Sabin L., Sokolowski J. L., 2008, *A&A*, 480, 409
- Corradi R. L. M., Sabin L., Miszalski B., Rodríguez-Gil P., Santander-García M., Jones D., Drew J. E., Mampaso A., et al. 2011, *MNRAS*, 410, 1349
- Corradi R. L. M., Valentini M., Munari U., Drew J. E., Rodríguez-Flores E. R., Viironen K., 2010, *A&A*, 509, A41
- Costa R. D. D., Uchida M. M. M., Maciel W. J., 2004, *A&A*, 423, 199
- Dopita M., Hart J., McGregor P., Oates P., Bloxham G., Jones D., 2007, *Astrophysics and Space Science*, 310, 255
- Dopita M., Rhee J., Farage C., McGregor P., Bloxham G., Green A., Roberts B., Neilson J., Wilson G., Young P., Firth P., Busarello G., Merluzzi P., 2010, *Astrophysics and Space Science*, 327, 245
- Dopita M. A., Vassiliadis E., Wood P. R., Meatheringham S. J., Harrington J. P., Bohlin R. C., Ford H. C., Stecher T. P., Maran S. P., 1997, *ApJ*, 474, 188
- Drew J. E., Gonzalez-Solares E., Greimel R., Irwin M. J., Küpcü Yoldas A., Lewis J., Barentsen G., Eisloffel J., Farnhill H. J., et al. 2014, *MNRAS*, 440, 2036
- Drew J. E., Greimel R., Irwin M. J., Aungwerojwit A., Barlow M. J., Corradi R. L. M., Drake J. J., Gänsicke B. T., Groot P., and IPHAS collaboration 2005, *MNRAS*, 362, 753
- Fitzpatrick E. L., Massa D., 2007, *ApJ*, 663, 320
- Frew D. J., Bojčić I. S., Parker Q. A., Pierce M. J., Gunawardhana M. L. P., Reid W. A., 2014, *MNRAS*, 440, 1080
- Frew D. J., Bojčić I. S., Parker Q. A., Stupar M., Wachter S., DePew K., Danekhar A., Fitzgerald M. T., Douchin D., 2014, *MNRAS*, 440, 1345
- Frew D. J., Parker Q. A., 2006, in Barlow M. J., Méndez R. H., eds, *Planetary Nebulae in our Galaxy and Beyond Vol. 234 of IAU Symposium*, . pp 49–54
- Frew D. J., Parker Q. A., 2010, *PASA*, 27, 129
- Giammanco C., Sale S. E., Corradi R. L. M., Barlow M. J., Viironen K., Sabin L., Santander-García M., Frew D. J., Greimel R., Miszalski B., Phillipps S., Zijlstra A. A., Mampaso A., Drew J. E., Parker Q. A., Napiwotzki R., 2011, *A&A*, 525, A58
- González-Solares E. A., Walton N. A., Greimel R., Drew J. E., Irwin M. J., Sale S. E., Andrews K., Aungwerojwit A., Barlow M. J. e. a., 2008, *MNRAS*, 388, 89
- Górny S. K., 2006, in Barlow M. J., Méndez R. H., eds, *Planetary Nebulae in our Galaxy and Beyond Vol. 234 of IAU Symposium*, . pp 409–410
- Groot P. J., Verbeek K., Greimel R., Irwin M., González-Solares E., Gänsicke B. T., de Groot E., Drew J., et al. 2009, *MNRAS*, 399, 323
- Henry R. B. C., Kwitter K. B., Jaskot A. E., Balick B., Morrison M. A., Milingo J. B., 2010, *ApJ*, 724, 748
- Hsia C.-H., Zhang Y., 2014, *A&A*, 563, A63
- Iben Jr. I., 1995, *Physics Reports*, 250, 2
- Irwin M., Lewis J., 2001, *NAR*, 45, 105
- Jacoby G. H., Kronberger M., Patchick D., Teutsch P., Saloranta J., Howell M., Crisp R., Riddle D., Acker A., Frew D. J., Parker Q. A., 2010, *PASA*, 27, 156
- Jones D., Mitchell D. L., Lloyd M., Pollacco D., O'Brien T. J., Meaburn J., Vaytet N. M. H., 2012, *MNRAS*, 420, 2271
- Kohoutek L., 2001, *A&A*, 378, 843
- Kronberger M., Jacoby G. H., Acker A., Alves F., Frew D. J., Goldman D., Guillem P., Harmer D., Lilge S., Mulato L., Parker Q. A., Patchick D., Sabin L., Zoll S., 2014, in *Asymmetrical Planetary Nebulae VI conference, Proceedings of the conference held 4-8 November, 2013*. Edited by C. Morisset, G. Delgado-Inglada and S. Torres-Peimbert
- Kronberger M., Jacoby G. H., Ciardullo R., Crisp R. D., De Marco O., Douchin D., Frew D. J., Harmer D., Howell M., Howell S. B., Parker Q. A., Patchick D., Rector T., Riddle D., Teutsch P., 2012, in *IAU Symposium Vol. 283 of IAU Symposium*, . pp 414–415
- Kronberger M., Teutsch P., Alessi B., Steine M., Ferrero L., Graczewski K., Juchert M., Patchick D., Riddle D., Saloranta J., Schoenball M., Watson C., 2006, *A&A*, 447, 921
- Maciel W. J., Costa R. D. D., 2003, in Kwok S., Dopita M., Sutherland R., eds, *Planetary Nebulae: Their Evolution and Role in the Universe Vol. 209 of IAU Symposium*, . p 551
- Mampaso A., Corradi R. L. M., Viironen K., Leisy P., Greimel R., Drew J. E., Barlow M. J., Frew D. J., Irwin J., Morris R. A. H., Parker Q. A., Phillipps S., Rodríguez-Flores E. R., Zijlstra A. A., 2006, *A&A*, 458, 203
- Miszalski B., Parker Q. A., Acker A., Birkby J. L., Frew D. J., Kovacevic A., 2008, *MNRAS*, 384, 525
- Moe M., De Marco O., 2006, *ApJ*, 650, 916
- Olguín L., Vázquez R., Contreras M. E., Jiménez M. Y., 2011, in *Revista Mexicana de Astronomía y Astrofísica Conference Series Vol. 40 of Revista Mexicana de Astronomía y Astrofísica*, vol. 27, . pp 193–193
- Parker Q., Bojčić I., Frew D., Day T., Acker A., Ochsenbein F., 2014, in *Asymmetrical Planetary Nebulae VI conference, Proceedings of the conference held 4-8 November, 2013*. Edited by C. Morisset, G. Delgado-Inglada and S. Torres-Peimbert.
- Parker Q. A., Acker A., Frew D. J., Hartley M., Peyaud A. E. J., Ochsenbein F., Phillipps S., Russeil D., Beaulieu S. F., Cohen M., Köppen J., Miszalski B., Morgan D. H., Morris R. A. H., Pierce M. J., Vaughan A. E., 2006, *MNRAS*, 373, 79
- Parker Q. A., Acker A., Frew D. J., Hartley M., Peyaud A. E. J., Phillipps S., Russeil D., Beaulieu S. F., Cohen M., Köppen J., Marcout J., Miszalski B., Morgan D. H., Morris R. A. H.,

- Ochsenbein F., Pierce M. J., 2006, VizieR Online Data Catalog, 5127, 0
- Parker Q. A., Cohen M., Stupar M., Frew D. J., Green A. J., Bojicic I., Guzman-Ramirez L., Sabin L., Vogt F., 2012, MNRAS, 427, 3016
- Parker Q. A., Phillipps S., Pierce M. J., Hartley M., Hambly N. C., Read M. A., MacGillivray H. T., Tritton S. B., Cass C. P., Cannon R. D., Cohen M., Drew J. E., 2005, MNRAS, 362, 689
- Preite-Martinez A., 1988, A&A, 76, 317
- Riesgo H., López J. A., 2006, Revista Mexicana de Astronomia y Astrofisica, 42, 47
- Sabbadin F., Minello S., Bianchini A., 1977, A&A, 60, 147
- Sabin L., 2008, PhD thesis, Jodrell Bank Centre for Astrophysics, University of Manchester, UK
- Sabin L., Corradi R. L. M., Parker Q., Mampaso A., Zijlstra A., 2012, in IAU Symposium Vol. 283 of IAU Symposium, . pp 492–493
- Sabin L., Parker Q. A., Contreras M. E., Olguín L., Frew D. J., Stupar M., Vázquez R., Wright N. J., Corradi R. L. M., Morris R. A. H., 2013, MNRAS, 431, 279
- Sabin L., Zijlstra A. A., Wareing C., Corradi R. L. M., Mampaso A., Viironen K., Wright N. J., Parker Q. A., 2010, PASA, 27, 166
- Sale S. E., Drew J. E., Unruh Y. C., Irwin M. J., Knigge C., Phillipps S., Zijlstra A. A., Gänsicke B. T., Greimel R., Groot P. J., Mampaso A., Morris R. A. H., Napiwotzki R., Steeghs D., Walton N. A., 2009, MNRAS, 392, 497
- Shaw R. A., Dufour R. J., 1995, PASP, 107, 896
- Soker N., Subag E., 2005, ApJ, 130, 2717
- Urquhart J. S., Hoare M. G., Purcell C. R., Lumsden S. L., Oudmaijer R. D., Moore T. J. T., Busfield A. L., Mottram J. C., Davies B., 2009, A&A, 501, 539
- Valdes F., 1986, in Crawford D. L., ed., Society of Photo-Optical Instrumentation Engineers (SPIE) Conference Series Vol. 627 of Society of Photo-Optical Instrumentation Engineers (SPIE) Conference Series, . pp 749–756
- Viironen K., Greimel R., Corradi R. L. M., Mampaso A., Rodríguez M., Sabin L., Delgado-Inglada G., Drew J. E., 2009, A&A, 504, 291
- Viironen K., Mampaso A., Corradi R. L. M., Drew J. E., Frew D. J., Giammanco C., Greimel R., Liimets T., Lindberg J. E., Rodríguez M., Sabin L., Sale S. E., Wilson P. A., Zijlstra A., 2011, A&A, 530, A107
- Wareing C. J., O'Brien T. J., Zijlstra A. A., Kwitter K. B., Irwin J., Wright N., Greimel R., Drew J. E., 2006, MNRAS, 366, 387
- Wesson R., Barlow M. J., Corradi R. L. M., Drew J. E., Groot P. J., Knigge C., Steeghs D., Gänsicke B. T., Napiwotzki R., Rodríguez-Gil P., Zijlstra A. A., Bode M. F., Drake J. J., Frew D. J. e. a., 2008, ApJ, 688, L21
- Wright N. J., Drake J. J., Drew J. E., Guarcello M. G., Gutermuth R. A., Hora J. L., Kraemer K. E., 2012, ApJ, 746, L21
- Zijlstra A. A., Pottasch S. R., 1991, A&A, 243, 478

Table 3. IPHAS PNe catalogue. See the text for the description of the database. There are 20 objects that were suggested as possible PN prior to IPHAS spectroscopic confirmation. These are identified by one of the following symbols appended to the PN status flag with the associated reference indicated: * Acker et al. (1992), † Jacoby et al. (2010), ‡ Kohoutek (2001), ⊕ Urquhart et al. (2009), * Preite-Martinez (1988), × Kronberger et al. (2006)

Number	PN status (T,L,P)	IAU PNG designation	IPHAS ID: IPHASX	RA (J2000)	DEC (J2000)	Galactic Longitude	Galactic Latitude	Major Diam axis (arcsec)	Morphology	No Spectra	Telescope	Obs.date yyyy-mm-dd
1	P	G116.0−04.8	J000021.4+572207	00:00:21.4	57:22:07	116.062	-4.8202	22	B	1	KP	2009-08-15
2	T†	G119.2+04.6	J001333.8+671803	00:13:33.8	67:18:03	119.28	4.6983	14	B	2	KP,OS	2009-08-17
3	P	G122.9+00.3	J005123.2+631059	00:51:23.2	63:10:59	122.926	0.3113	47	A	1	KP	2009-08-16
4	T	G126.6+01.3	J012507.9+635652	01:25:07.9	63:56:52	126.622	1.3177	33	Bapm	1	WH	2004-09-27
5	T	G127.6−01.1	J013108.9+612258	01:31:08.9	61:22:58	127.67	-1.1229	24	Ra	1	KP	2009-08-16
6	T	G129.6+03.4	J015624.9+652830	01:56:24.9	65:28:30	129.612	3.4496	189	Rar	1	SM	2011-09-23
7	T	G132.8+02.0	J022045.0+631134	02:20:45.0	63:11:34	132.804	2.046	30	Eas	1	OS	2011-10-04
8	P	G134.1+03.0	J023539.3+633823	02:35:39.3	63:38:23	134.194	3.0706	135	E	1	SM	2013-02-11
9	T	G137.7+03.3	J030421.3+621802	03:04:21.3	62:18:02	137.714	3.3066	57	Rr	2	OS,SM	2010-09-19
10	T	G139.0+03.2	J031345.5+613707	03:13:45.5	61:37:07	139.015	3.2741	127	Bs	1	SM	2011-09-24
11	T	G144.1−00.5	J033105.3+553851	03:31:05.3	55:38:51	144.159	-0.5012	27	Rar	1	SM	2010-09-18
12	L	G150.1−04.5	J034659.8+484900	03:46:59.8	48:49:00	150.186	-4.5403	62	Ra	1	OS	2012-09-20
13	T†	G150.0−00.3	J040329.5+520825	04:03:29.5	52:08:25	150.074	-0.3084	25	Bp	1	SM	2010-09-18
14	L	G156.4+01.1	J043826.1+483907	04:38:26.1	48:39:07	156.476	1.1425	95	Eas	2	OS,SM	2010-09-20
15	P	G159.4+02.0	J045358.6+465842	04:53:58.6	46:58:42	159.444	2.0407	12	Am	1	OS	2011-10-08
16	T	G157.1+04.4	J045627.6+501720	04:56:27.6	50:17:20	157.117	4.4347	91	Ra	1	SM	2011-09-24
17	T	G167.3−03.1	J045847.7+373640	04:58:47.7	37:36:40	167.314	-3.1209	17	Rs	1	SM	2010-09-18
18	P	G167.9+00.9	J051733.3+393027	05:17:33.3	39:30:27	167.988	0.9515	65	A	1	OS	2012-09-22
19	L	G183.0+00.0	J055242.8+262116	05:52:42.8	26:21:16	183.022	0.0176	16	Rar	1	GC	2009-11-09
20	T	G193.5−03.1	J060328.1+154108	06:03:28.1	15:41:08	193.522	-3.1388	55	Ba	1	SM	2011-09-24
21	T	G190.7−01.3	J060412.2+190031	06:04:12.2	19:00:31	190.709	-1.3567	70	Ba	1	SM	2010-09-18
22	T	G195.4−04.0	J060416.2+133250	06:04:16.2	13:32:50	195.486	-4.014	29	Ba	1	SM	2007-01-23
23	T	G204.3−01.6	J062937.8+065220	06:29:37.8	06:52:20	204.33	-1.6839	31	Ba	1	SM	2011-09-25
24	T	G197.3+02.7	J063223.9+150410	06:32:23.9	15:04:10	197.373	2.7078	90	B	1	SM	2011-09-26
25	T	G029.9+03.7	J183249.6−005638	18:32:49.6	-00:56:38	29.9655	3.7077	5	S	1	SA	2011-07-10
26	L*	G031.1+03.4	J183602.3−000227	18:36:02.3	-00:02:27	31.1381	3.4069	16	E	2	WI	2011-07-04
27	L	G031.1+02.1	J184030.1−003822	18:40:30.1	-00:38:22	31.1151	2.1411	22	B	1	WI	2011-07-04
28	L	G029.7+01.1	J184139.1−021649	18:41:39.1	-02:16:49	29.7865	1.1354	−	S	1	SA	2011-07-06
29	T	G032.8+01.5	J184546.7+003631	18:45:46.7	00:36:31	32.8287	1.5367	4	R	1	SA	2011-07-12
30	T	G029.5−00.2	J184616.3−030625	18:46:16.3	-03:06:25	29.578	-0.2684	4	Sm	1	SA	2011-07-10
31	P	G038.4+03.6	J184834.6+063302	18:48:34.6	06:33:02	38.4449	3.6152	21	Ba	2	SA	2011-07-09
32	T	G040.3+03.4	J185225.0+080843	18:52:25.0	08:08:43	40.3013	3.4883	22	R	3	WI,SM	2010-06-02
33	P	G033.8+00.1	J185225.8+005250	18:52:25.8	00:52:50	33.8287	0.1807	480	Ears	2	SM	2010-06-01
34	L*	G039.1+02.7	J185301.9+064415	18:53:01.9	06:44:15	39.114	2.7138	−	S	1	SA	2011-07-08
35	T	G040.1+03.2	J185309.4+075241	18:53:09.4	07:52:41	40.1456	3.2038	12	Eam	3	SA,IN	2008-06-30
36	L	G032.7−00.5	J185312.9−002529	18:53:12.9	-00:25:29	32.7563	-0.5893	26	E	1	WI	2011-07-03
37	T	G038.4+02.2	J185321.7+055641	18:53:21.7	05:56:41	38.4445	2.2806	5	R	2	SA,KP	2009-08-18
38	P	G032.6−00.7	J185342.6−003628	18:53:42.6	-00:36:28	32.6498	-0.7828	23	E	2	WI	2011-07-03
39	T	G032.9−01.4	J185640.0−003804	18:56:40.0	-00:38:04	32.9632	-1.4528	15	Bp	1	SM	2010-07-09
40	P	G043.3+03.5	J185744.4+105053	18:57:44.4	10:50:53	43.3109	3.5424	110	Eams	2	SM	2010-07-10
41	T	G040.5+01.9	J185815.8+073753	18:58:15.8	07:37:53	40.5014	1.9648	7	Rrs	1	KP	2009-08-15
42	T	G040.6+01.5	J185957.0+073544	18:59:57.0	07:35:44	40.6602	1.5766	4	B	2	SA	2011-07-10
43	T†	G041.5+01.7	J190105.7+082536	19:01:05.7	08:25:36	41.5293	1.7038	−	S	1	SA	2011-07-08
44	T	G044.4+03.1	J190115.5+114150	19:01:15.5	11:41:50	44.4613	3.1594	26	Ear	1	KP	2009-08-12
45	P	G038.6+00.1	J190125.4+050858	19:01:25.4	05:08:58	38.6517	0.1329	13	B	1	SM	2011-09-25
46	T	G036.0−01.4	J190227.3+020804	19:02:27.3	02:08:04	36.0885	-1.4757	92	Ias	1	SM	2011-05-05
47	T	G047.1+03.9	J190319.0+142524	19:03:19.0	14:25:24	47.1224	3.9521	15	E	2	WI	2011-07-05
48	P	G038.6−00.4	J190340.4+045311	19:03:40.4	04:53:11	38.6745	-0.4857	114	I	1	WI	2011-07-01
49	T	G043.0+01.7	J190340.7+094639	19:03:40.7	09:46:39	43.023	1.7542	20	Em	2	SA	2011-07-01
50	P	G038.7−00.5	J190401.5+045433	19:04:01.5	04:54:33	38.7351	-0.5533	140	Ims	1	WI	2011-07-01
51	T	G042.2+01.1	J190417.9+084916	19:04:17.9	08:49:16	42.2425	1.1804	−	S	1	SM	2010-07-10
52	T	G042.6+01.3	J190432.9+091656	19:04:32.9	09:16:56	42.6809	1.3368	8	E	1	IN	2008-06-29
53	P†	G036.4−01.9	J190438.6+021424	19:04:38.6	02:14:24	36.4326	-1.9136	21	Bmp	3	SA,IN	2008-06-28
54	T	G045.4+02.6	J190447.9+121844	19:04:47.9	12:18:44	45.4047	2.6692	12	Er	2	SM	2011-09-25
55	T	G043.6+01.7	J190454.0+101801	19:04:54.0	10:18:01	43.6257	1.7262	18	Ears	1	SM	2011-05-04
56	T	G037.7−01.3	J190503.1+034225	19:05:03.1	03:42:25	37.7839	-1.3321	64	Ear	3	OS,WI	2011-07-02
57	T	G048.9+04.3	J190512.4+161347	19:05:12.4	16:13:47	48.9435	4.3662	60	Rar	2	KP,SM	2009-08-12
58	T	G044.2+01.9	J190518.3+105750	19:05:18.3	10:57:50	44.2615	1.942	4	R	1	SA	2011-07-06
59	T	G044.3+01.8	J190543.8+110018	19:05:43.8	11:00:18	44.346	1.8681	8	Rr	1	KP	2009-08-12

Table 3. (continued)

Number	PN status (T,L,P)	IAU PNG designation	IPHAS ID: IPHASX	RA (J2000)	DEC (J2000)	Galactic Longitude	Galactic Latitude	Major Diam axis (arcsec)	Morphology	No Spectra	Telescope	Obs.date yyyy-mm-dd
60	L	G032.3-04.5	J190631.5-023236	19:06:31.5	-02:32:36	32.3845	-4.5154	16	E	2	WI	2011-07-05
61	L	G038.9-01.3	J190718.1+044056	19:07:18.1	04:40:56	38.908	-1.3827	9	I	1	SA	2011-07-02
62	P	G039.6-01.2	J190816.8+052506	19:08:16.8	05:25:06	39.674	-1.2603	7	Es	2	SA	2011-07-08
63	T [×]	G045.7+01.4	J190954.7+120455	19:09:54.7	12:04:55	45.7737	1.4535	18	B	1	SA	2011-07-08
64	T	G047.8+02.4	J191001.1+142202	19:10:01.1	14:22:02	47.8155	2.4831	10	E	1	KP	2009-08-15
65	T	G044.9+00.8	J191022.1+110538	19:10:22.1	11:05:38	44.9485	0.8986	10	Ear	1	KP	2009-08-15
66	T	G038.3-02.5	J191027.4+034046	19:10:27.4	03:40:46	38.3792	-2.5422	13	Ra	1	KP	2009-08-16
67	T	G048.2+01.9	J191255.4+143248	19:12:55.4	14:32:48	48.2994	1.9417	8	Rar	1	KP	2009-08-17
68	T	G051.2+03.2	J191345.5+174752	19:13:45.5	17:47:52	51.2785	3.2661	7	Ras	1	WH	2007-07-17
69	T	G047.6+01.0	J191445.1+133219	19:14:45.1	13:32:19	47.6116	1.0818	15	Ears	2	SA,WH	2006-08-24
70	T	G050.8+02.3	J191621.4+165638	19:16:21.4	16:56:38	50.8082	2.3214	5	R	1	IN	2008-06-28
71	L	G042.0-02.4	J191651.6+065608	19:16:51.6	06:56:08	42.0067	-2.4494	17	A	2	WI	2011-07-05
72	L	G039.0-04.0	J191716.4+033447	19:17:16.4	03:34:47	39.0765	-4.0972	16	Emr	1	KP	2009-08-16
73	T	G052.0+02.7	J191716.5+181518	19:17:16.5	18:15:18	52.0719	2.7369	46	Rrs	1	SM	2010-07-12
74	T	G043.3-01.9	J191727.0+082036	19:17:27.0	08:20:36	43.3218	-1.9235	15	Ras	2	SA	2011-07-02
75	L	G048.7+00.9	J191727.2+142735	19:17:27.2	14:27:35	48.732	0.9305	-	S	1	SA	2011-07-10
76	T	G042.7-02.5	J191840.4+073131	19:18:40.4	07:31:31	42.7386	-2.5729	41	Ea	2	WI	2011-07-01
77	L	G045.7-01.6	J192101.1+103734	19:21:01.1	10:37:34	45.7521	-1.6335	3	E	1	SA	2011-07-10
78	L [⊕]	G050.4+00.7	J192140.4+155354	19:21:40.4	15:53:54	50.4801	0.7055	19	B	1	SM	2010-07-10
79	T	G051.7+01.3	J192146.7+172055	19:21:46.7	17:20:55	51.772	1.3658	29	Ears	1	SM	2010-07-12
80	P	G048.7-00.2	J192152.0+135223	19:21:52.0	13:52:23	48.7153	-0.2894	13	B	1	KP	2009-08-17
81	T	G049.2+00.0	J192153.9+143056	19:21:53.9	14:30:56	49.2858	0.0065	18	Ear	1	KP	2009-08-16
82	T	G050.6+00.0	J192436.3+154402	19:24:36.3	15:44:02	50.6681	0.0061	23	Ea	1	SM	2011-09-26
83	L	G054.5+01.8	J192534.9+200334	19:25:34.9	20:03:34	54.5879	1.8515	38	E	1	OS	2012-09-19
84	L	G049.7-00.7	J192543.2+143546	19:25:43.2	14:35:46	49.794	-0.7702	176	Rars	1	SP	2012-04-13
85	T	G051.8+00.2	J192553.5+165331	19:25:53.5	16:53:31	51.8341	0.2838	6	E	1	WH	2007-07-18
86	T [*]	G049.5-01.4	J192751.3+140127	19:27:51.3	14:01:27	49.5371	-1.4973	10	Rars	1	SA	2011-07-09
87	T	G059.1+03.5	J192837.7+245024	19:28:37.7	24:50:24	59.135	3.5009	13	Eas	1	KP	2009-08-17
88	T	G045.7-03.8	J192847.2+093436	19:28:47.2	09:34:36	45.7296	-3.8144	67	Br	1	WH	2006-08-25
89	T	G059.1+03.3	J192902.5+244646	19:29:02.5	24:46:46	59.1263	3.3897	10	Rms	1	WH	2007-07-17
90	T	G054.4+00.5	J193009.3+192129	19:30:09.3	19:21:29	54.4845	0.5712	221	Ears	2	SA,SM	2011-07-09
91	T	G054.7+00.4	J193110.7+192905	19:31:10.7	19:29:05	54.7118	0.4203	19	Ba	1	SM	2011-09-26
92	T	G048.1-03.2	J193127.0+115622	19:31:27.0	11:56:22	48.123	-3.2626	27	R	1	SM	2011-09-26
93	T	G051.7-01.7	J193308.9+155354	19:33:08.9	15:53:54	51.7956	-1.7197	27	Ears	2	WI	2011-07-03
94	L	G057.8+01.0	J193517.8+223120	19:35:17.8	22:31:20	57.8354	1.0481	21	Ras	1	OS	2012-09-22
95	T	G048.0-04.4	J193532.1+112115	19:35:32.1	11:21:15	48.0901	-4.421	9	R	2	KP,SM	2009-08-14
96	P	G065.8+05.1	J193630.2+312810	19:36:30.2	31:28:10	65.8057	5.1485	404	Aa	1	SP	2012-04-12
97	T	G051.9-02.5	J193633.5+153345	19:36:33.5	15:33:45	51.8995	-2.6003	103	R	2	WI	2011-07-02
98	T	G053.4-01.8	J193652.9+171940	19:36:52.9	17:19:40	53.4803	-1.8082	4	R	1	WH	2007-07-18
99	T	G056.1-00.4	J193718.6+202102	19:37:18.6	20:21:02	56.1681	-0.4201	47	Bas	1	IN	2006-06-15
100	T	G056.4-00.3	J193740.4+203547	19:37:40.4	20:35:47	56.4241	-0.374	31	Ias	1	SA	2011-07-10
101	T	G062.1+02.8	J193752.2+271119	19:37:52.2	27:11:19	62.1977	2.8117	25	E	1	SM	2010-07-10
102	T	G062.0+02.5	J193827.8+265752	19:38:27.8	26:57:52	62.0663	2.5868	6	R	1	WH	2007-07-18
103	T [×]	G057.9-00.7	J194226.0+214521	19:42:26.0	21:45:21	57.9797	-0.7679	27	B	1	KP	2009-08-16
104	T	G052.1-04.1	J194232.8+150034	19:42:32.8	15:00:34	52.1249	-4.1306	19	Rr	1	SM	2010-09-20
105	T	G063.3+02.2	J194240.5+275109	19:42:40.5	27:51:09	63.3005	2.2106	74	Rar	1	OS	2012-09-22
106	T	G054.2-03.4	J194359.5+170901	19:43:59.5	17:09:01	54.1615	-3.3735	21	Bamps	1	WH	2007-07-17
107	T	G062.9+01.3	J194510.6+270930	19:45:10.6	27:09:30	62.9747	1.3839	14	B	1	KP	2009-08-18
108	L	G057.8-01.7	J194533.6+210808	19:45:33.6	21:08:08	57.8047	-1.7077	69	Ear	1	SA	2011-07-10
109	T	G059.8-00.6	J194556.2+232833	19:45:56.2	23:28:33	59.8739	-0.6101	54	Bas	1	SM	2010-07-10
110	L	G059.7-00.8	J194633.0+231659	19:46:33.0	23:16:59	59.7778	-0.8285	13	Ea	1	IN	2007-08-03
111	T	G059.7-01.0	J194727.5+230816	19:47:27.5	23:08:16	59.7575	-1.0822	35	Rars	1	SM	2011-05-05
112	L	G059.1-01.4	J194728.8+222823	19:47:28.8	22:28:23	59.1857	-1.4214	27	Ras	1	SP	2012-04-12
113	T	G066.8+02.9	J194751.9+311818	19:47:51.9	31:18:18	66.8587	2.9572	13	B	1	WH	2007-07-17
114	P	G055.7-03.8	J194905.2+181503	19:49:05.2	18:15:03	55.7245	-3.8742	33	A	2	WI	2011-07-01
115	T	G063.7+00.7	J194930.9+273028	19:49:30.9	27:30:28	63.7622	0.7277	84	R	1	OS	2012-09-24
116	T	G062.7+00.0	J194940.9+261521	19:49:40.9	26:15:21	62.7024	0.0602	22	Bps	1	WH	2007-07-17
117	T	G063.5+00.0	J195126.5+265838	19:51:26.5	26:58:38	63.5236	0.0893	8	B	2	KP,SM	2009-08-14
118	T	G067.9+02.4	J195221.6+315859	19:52:21.6	31:58:59	67.9297	2.4762	42	Ear	1	SM	2011-09-25

Table 3. (continued)

Number	PN status (T,L,P)	IAU PNG designation	IPHAS ID: IPHASX	RA (J2000)	DEC (J2000)	Galactic Longitude	Galactic Latitude	Major Diam axis (arcsec)	Morphology	No Spectra	Telescope	Obs.date yyyy-mm-dd
119	T	G062.7−00.7	J195248.8+255359	19:52:48.8	25:53:59	62.7552	-0.7263	27	B	1	WH	2007-07-17
120	T	G058.1−03.7	J195343.7+202635	19:53:43.7	20:26:35	58.1744	-3.7047	31	B	1	SA	2011-07-10
121	T	G067.5+01.8	J195358.2+312120	19:53:58.2	31:21:20	67.5661	1.8605	228	Ems	1	SM	2011-05-06
122	T	G068.0+02.1	J195400.8+315554	19:54:00.8	31:55:54	68.0655	2.1488	30	Rar	1	SM	2010-07-10
123	T	G058.6−03.6	J195424.6+205252	19:54:24.6	20:52:52	58.6331	-3.6172	27	Bps	0	–	–
124	T	G067.8+01.8	J195436.4+313326	19:54:36.4	31:33:26	67.8091	1.8479	12	Emr	2	KP,IN	2008-06-28
125	T	G064.1−00.9	J195657.6+265713	19:56:57.6	26:57:13	64.1372	-0.9765	29	Bars	1	WH	2006-08-24
126	L	G066.4−00.0	J195836.4+292314	19:58:36.4	29:23:14	66.4028	-0.016	17	Ea	1	SM	2011-09-26
127	L	G068.2+00.9	J195919.0+312534	19:59:19.0	31:25:34	68.2195	0.9221	8	E	2	KP,SM	2009-08-14
128	T*	G073.0+03.6	J200018.6+365934	20:00:18.6	36:59:34	73.0711	3.6669	28	Ems	2	KP,IN	2006-09-08
129	T	G065.8−00.8	J200041.5+283023	20:00:41.5	28:30:23	65.8928	-0.867	31	Ra	1	SM	2011-09-26
130	T	G068.0+00.0	J200224.3+304845	20:02:24.3	30:48:45	68.0469	0.037	25	Bar	1	SM	2010-09-20
131	T	G072.0+02.2	J200353.5+352250	20:03:53.5	35:22:50	72.0824	2.2017	15	B	1	SM	2011-09-26
132	T	G073.6+02.8	J200522.0+36594	20:05:22.0	+36:59:4	73.6083	2.8113	11	Eas	1	KP	2009-08-17
133	P	G070.4+00.7	J200525.3+331424	20:05:25.3	33:14:24	70.4413	0.791	49	I	1	OS	2011-10-08
134	T	G063.5−04.7	J200937.3+242903	20:09:37.3	24:29:03	63.556	-4.7037	24	Ba	1	SM	2013-05-09
135	T†	G077.6+04.3	J200940.9+411442	20:09:40.9	41:14:42	77.6494	4.3915	46	Rars	1	SM	2011-09-25
136	T	G071.3−00.6	J201339.0+331507	20:13:39.0	33:15:07	71.3879	-0.6456	9	B	2	KP,GC	2009-08-15
137	T	G075.3−01.9	J202946.0+354926	20:29:46.0	35:49:26	75.3928	-1.9088	16	Rr	1	IN	2006-08-29
138	T	G077.4−04.0	J204414.1+360737	20:44:14.1	36:07:37	77.4005	-4.063	19	Es	1	SM	2013-05-07
139	T×	G079.5−03.8	J205002.8+375315	20:50:02.8	37:53:15	79.5049	-3.8688	35	Ears	1	SM	2013-05-09
140	L	G086.5+01.8	J205013.6+465515	20:50:13.6	46:55:15	86.5191	1.8283	332	Ea	2	WH	2007-07-17
141	T†	G081.0−03.9	J205527.2+390359	20:55:27.2	39:03:59	81.0914	-3.9315	23	B	2	SM,IN	2006-08-30
142	L×	G088.0+00.4	J210204.7+471015	21:02:04.7	47:10:15	88.0182	0.4528	71	Eamrs	3	OS,SM,IN	2006-08-29
143	T†	G093.3+01.4	J212000.0+514105	21:20:00.0	51:41:05	93.3035	1.4107	9	Bps	1	GC	2010-06-07
144	T	G090.5−01.7	J212151.8+473301	21:21:51.8	47:33:01	90.5918	-1.7251	30	Bs	1	IN	2006-08-29
145	T†	G095.9+03.5	J212200.9+550430	21:22:00.9	55:04:30	95.9178	3.5929	56	Bams	1	WH	2006-08-25
146	T	G091.6−01.0	J212335.3+484717	21:23:35.3	48:47:17	91.667	-1.0472	19	B	1	GC	2011-07-06
147	T	G095.8+02.6	J212608.3+542015	21:26:08.3	54:20:15	95.8257	2.6495	13	Bas	1	GC	2011-06-28
148	T*	G095.5+00.5	J213423.2+523727	21:34:23.2	52:37:27	95.5461	0.561	7	E	1	GC	2011-04-13
149	T	G098.9+03.0	J214032.5+564751	21:40:32.5	56:47:51	98.9933	3.0779	9	E	1	IN	2006-08-01
150	T	G098.9−01.1	J215842.3+533003	21:58:42.3	53:30:03	98.9076	-1.1146	31	Rar	1	SM	2011-09-25
151	T	G101.5−00.6	J221118.0+552841	22:11:18.0	55:28:41	101.551	-0.6008	78	Bas	1	IN	2006-08-29
152	L	G111.5+00.1	J231546.1+605551	23:15:46.1	60:55:51	111.572	0.187	60	Er	1	OS	2011-10-10
153	T†	G114.2+03.7	J232713.2+650923	23:27:13.2	65:09:23	114.232	3.717	19	Rs	1	KP	2009-08-16
154	T	G114.4+00.0	J233841.2+614146	23:38:41.2	61:41:46	114.421	0.0324	61	Ears	2	OS,IN	2006-08-30
155	P	G115.6+03.5	J234025.5+652147	23:40:25.5	65:21:47	115.616	3.5051	62	Ra	1	OS	2011-10-08
156	T	G115.5+02.0	J234318.0+635717	23:43:18.0	63:57:17	115.537	2.0656	36	R	1	OS	2011-10-07
157	T	G114.7−01.2	J234403.8+603242	23:44:03.8	60:32:42	114.738	-1.2504	22	Ras	3	KP,IN	2006-08-29
158	T	G116.3+01.9	J235044.2+640311	23:50:44.2	64:03:11	116.351	1.9598	26	Ba	1	SM	2011-09-23
159	P	G115.5−01.8	J235114.7+601026	23:51:14.7	60:10:26	115.509	-1.8274	48	Ra	1	OS	2011-10-08

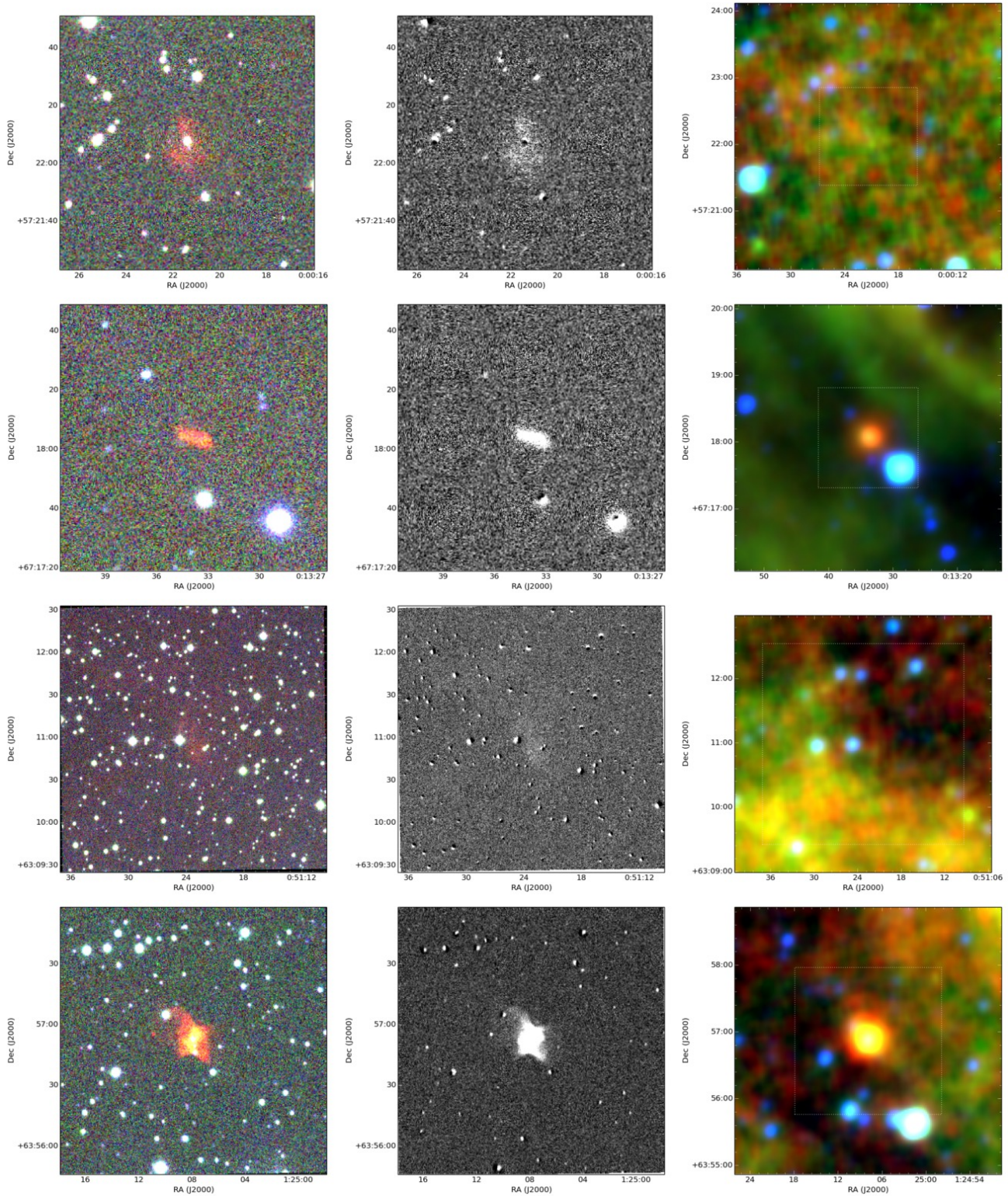


Figure A.1. Multiwavelength images of new IPHAS PNe. Columns from left to right: (1) IPHAS colour-composite image made from $H\alpha$ (R), r (G) and i (B), (2) IPHAS quotient ($H\alpha/r$) and (3) WISE colour-composite made from W4(R), W3(G) and W2(B). Dashed-line boxes in WISE image represent size of a field in the IPHAS image. All images have same orientation: NE at the top left. Objects shown (from top to bottom): PN G116.0-04.8, PN G119.2+04.6, PN G122.9+00.3, PN G126.6+01.3

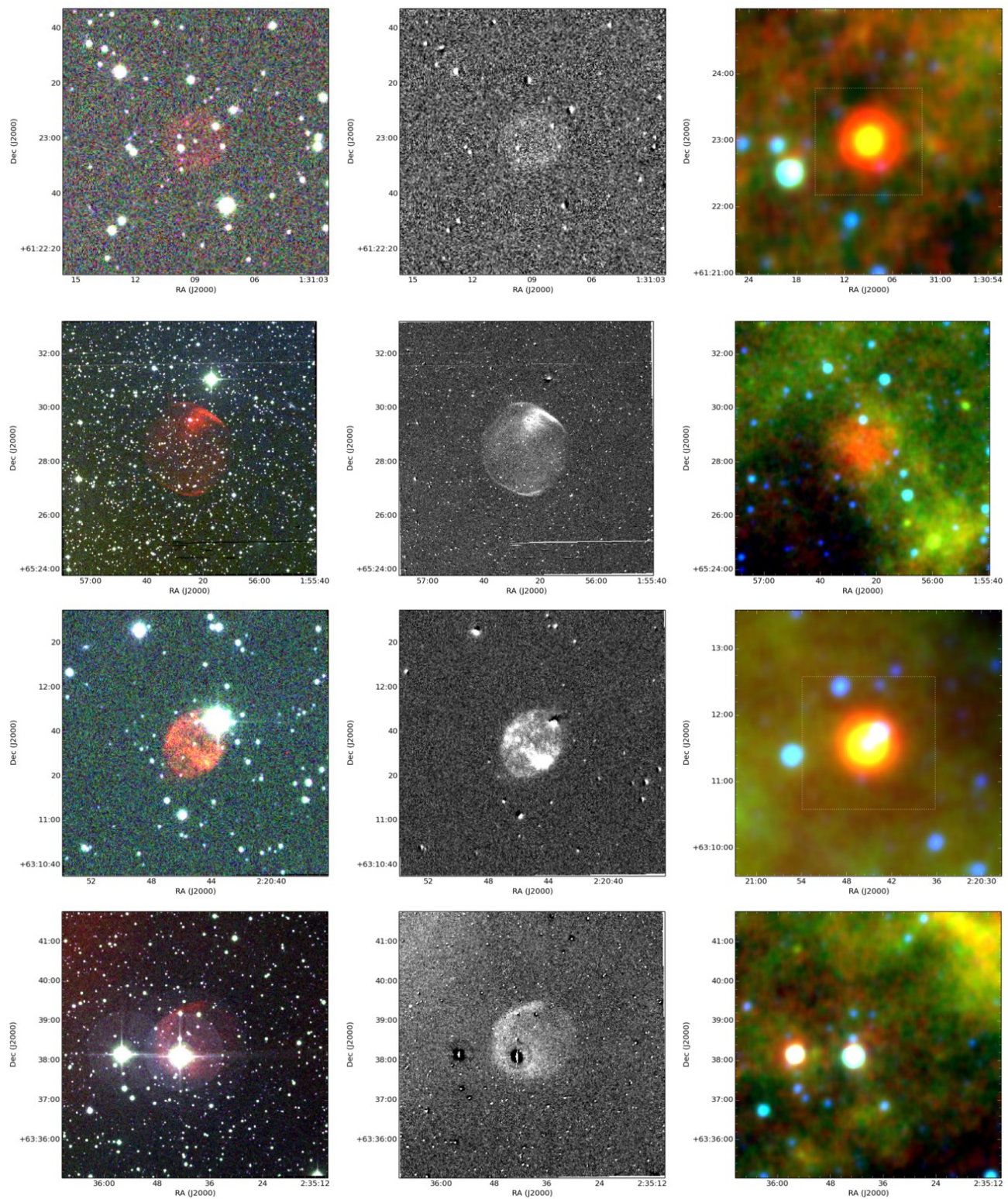


Figure A.2. Same as in Fig. A.1. Objects shown (from top to bottom): PN G127.6-01.1, PN G129.6+03.4, PN G132.8+02.0, PN G134.1+03.0

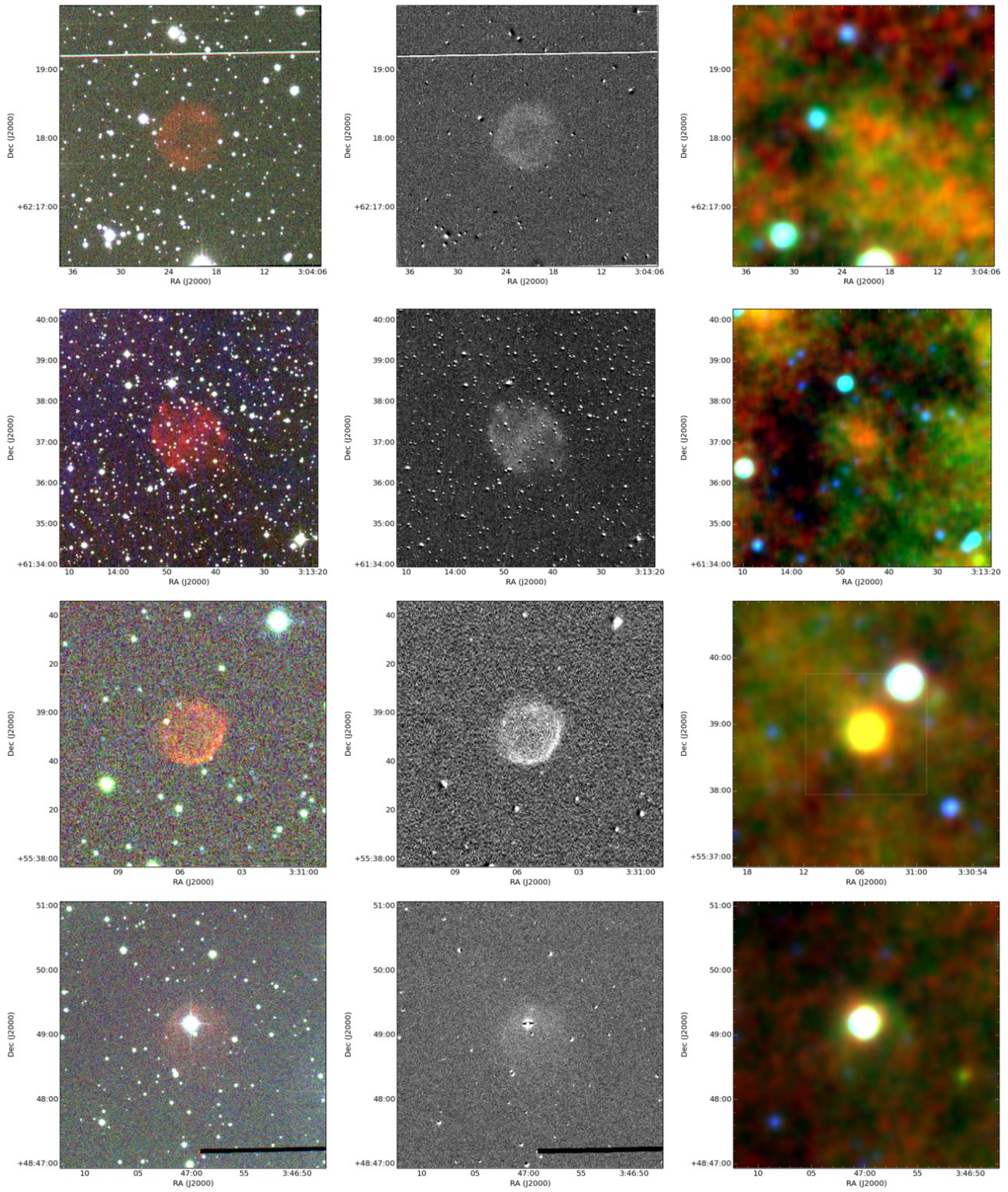


Figure A.3. Same as in Fig. A.1. Objects shown (from top to bottom): PN G137.7+03.3, PN G139.0+03.2, PN G144.1-00.5, PN G150.1-04.5

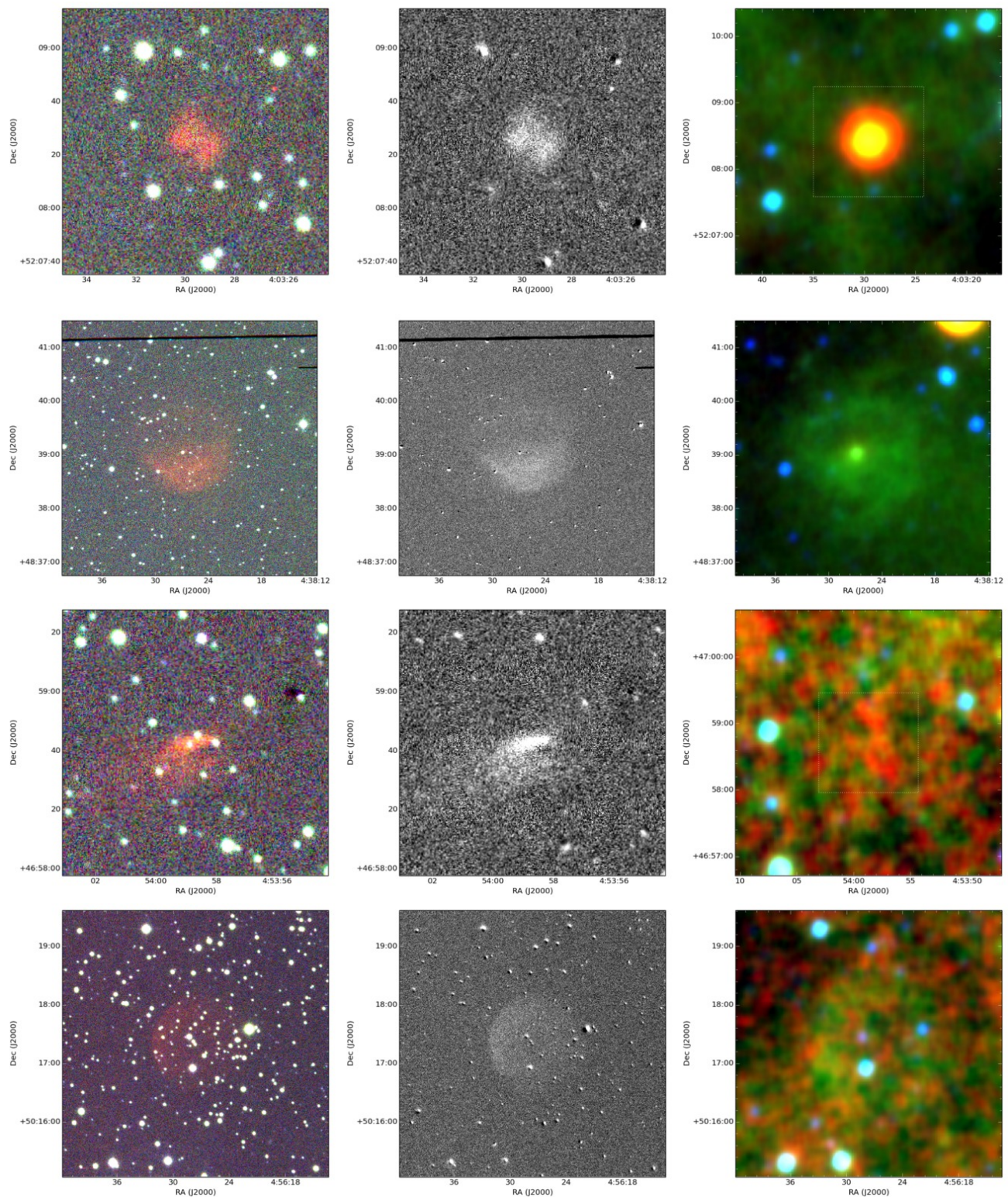


Figure A.4. Same as in Fig. A.1. Objects shown (from top to bottom): PN G150.0-00.3, PN G156.4+01.1, PN G159.4+02.0, PN G157.1+04.4

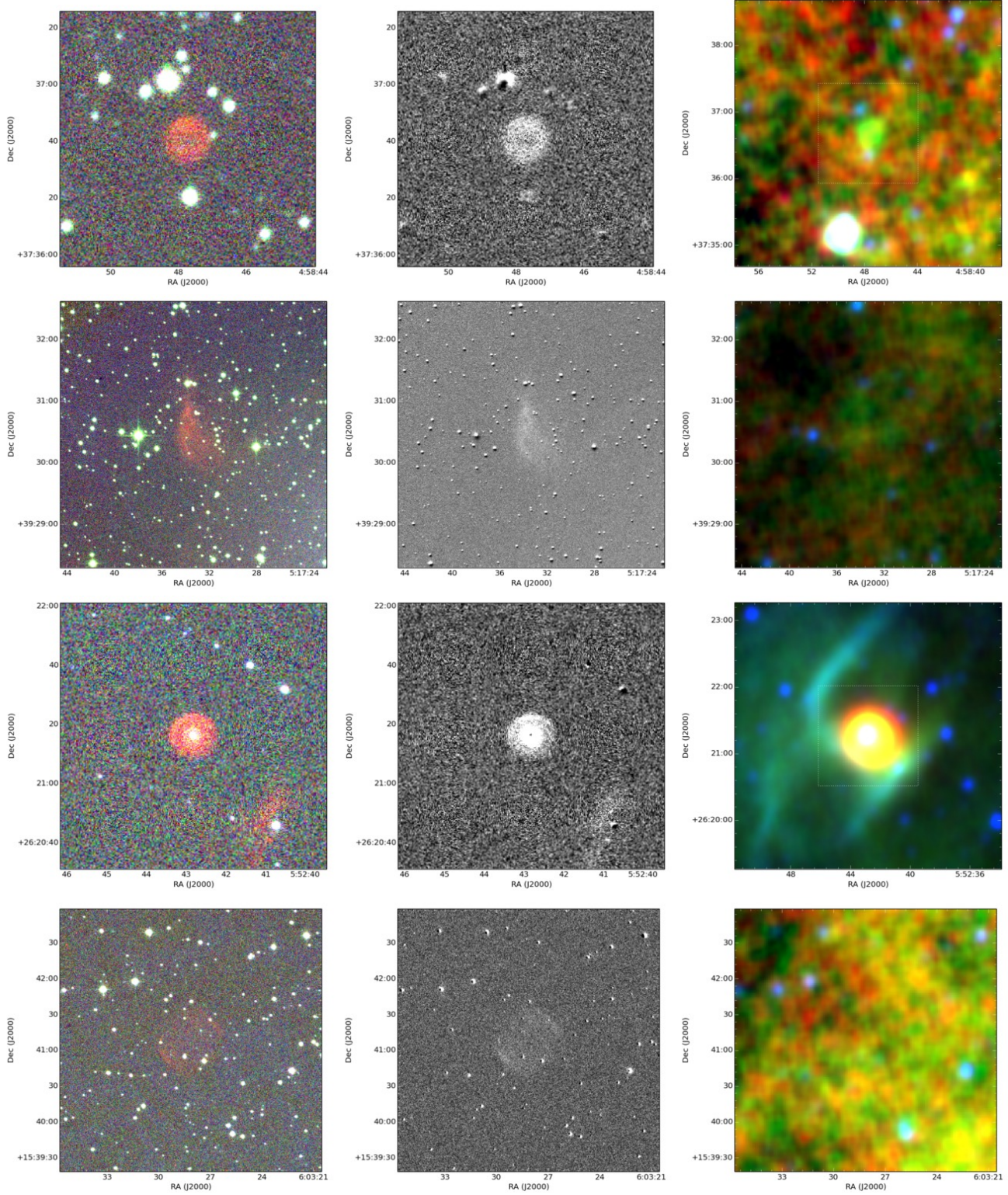


Figure A.5. Same as in Fig. A.1. Objects shown (from top to bottom): PN G167.3-03.1, PN G167.9+00.9, PN G183.0+00.0, PN G193.5-03.1

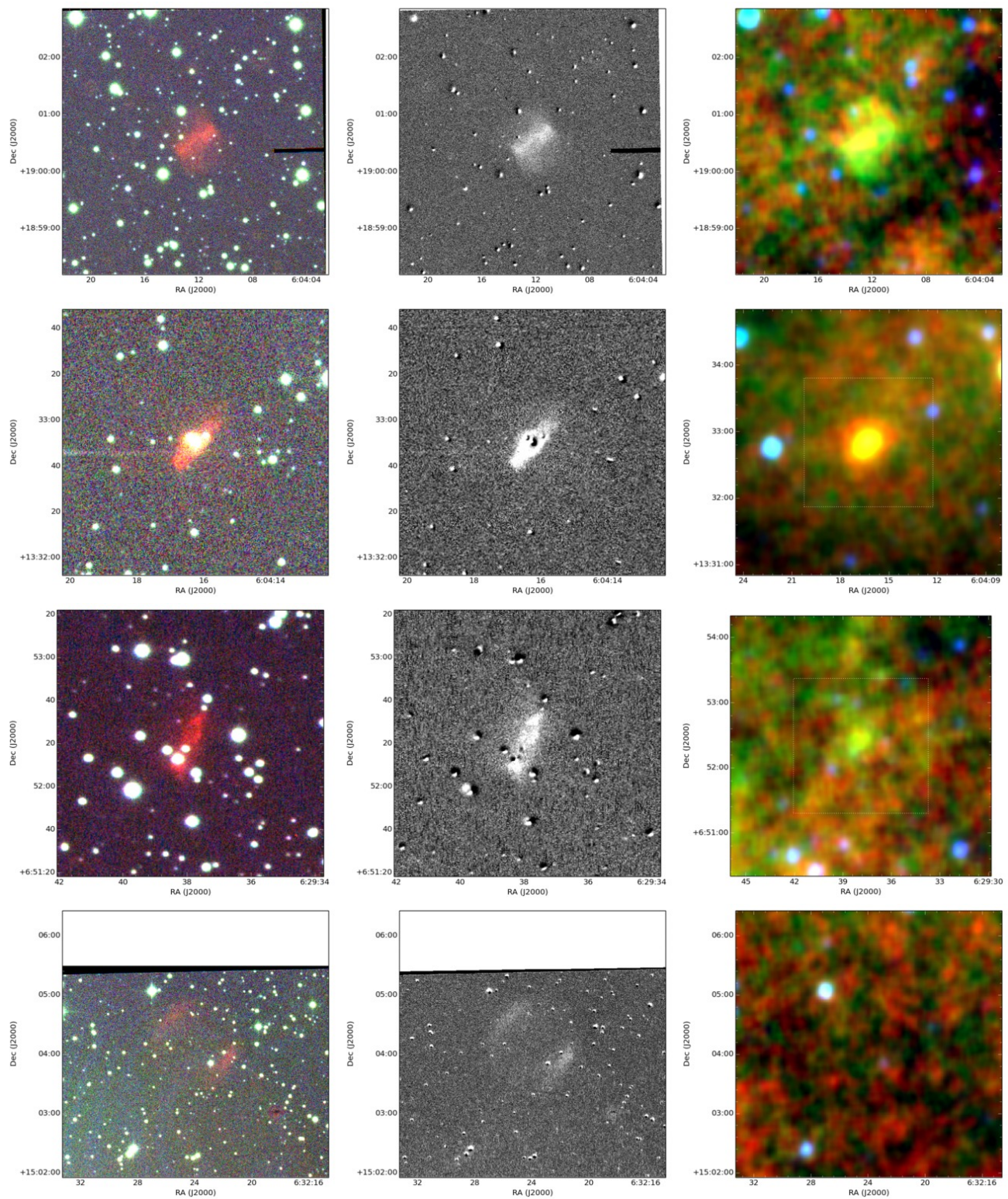


Figure A.6. Same as in Fig. A.1. Objects shown (from top to bottom): PN G190.7-01.3, PN G195.4-04.0, PN G204.3-01.6, PN G197.3+02.7

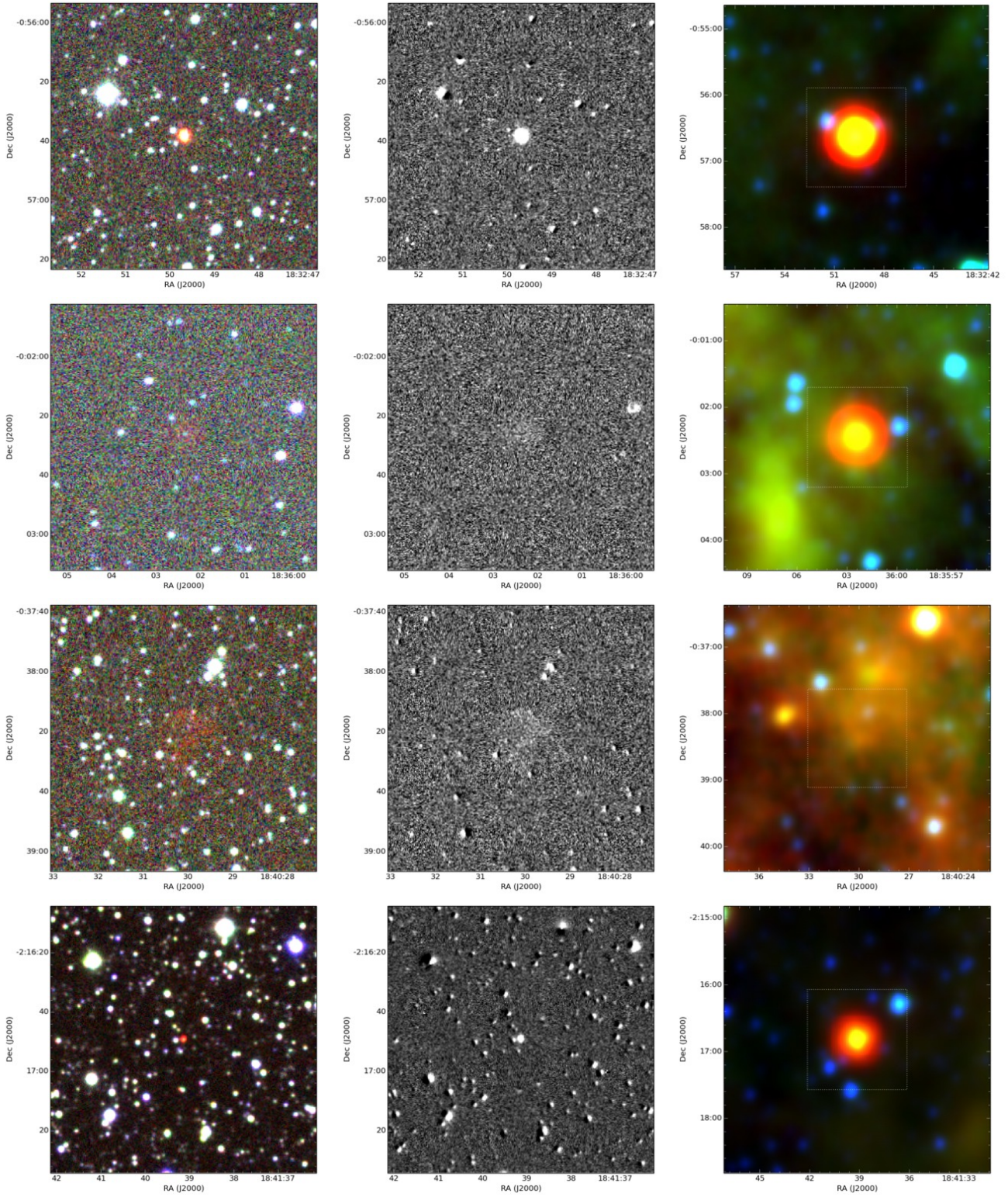


Figure A.7. Same as in Fig. A.1. Objects shown (from top to bottom): PN G029.9+03.7, PN G031.1+03.4, PN G031.1+02.1, PN G029.7+01.1

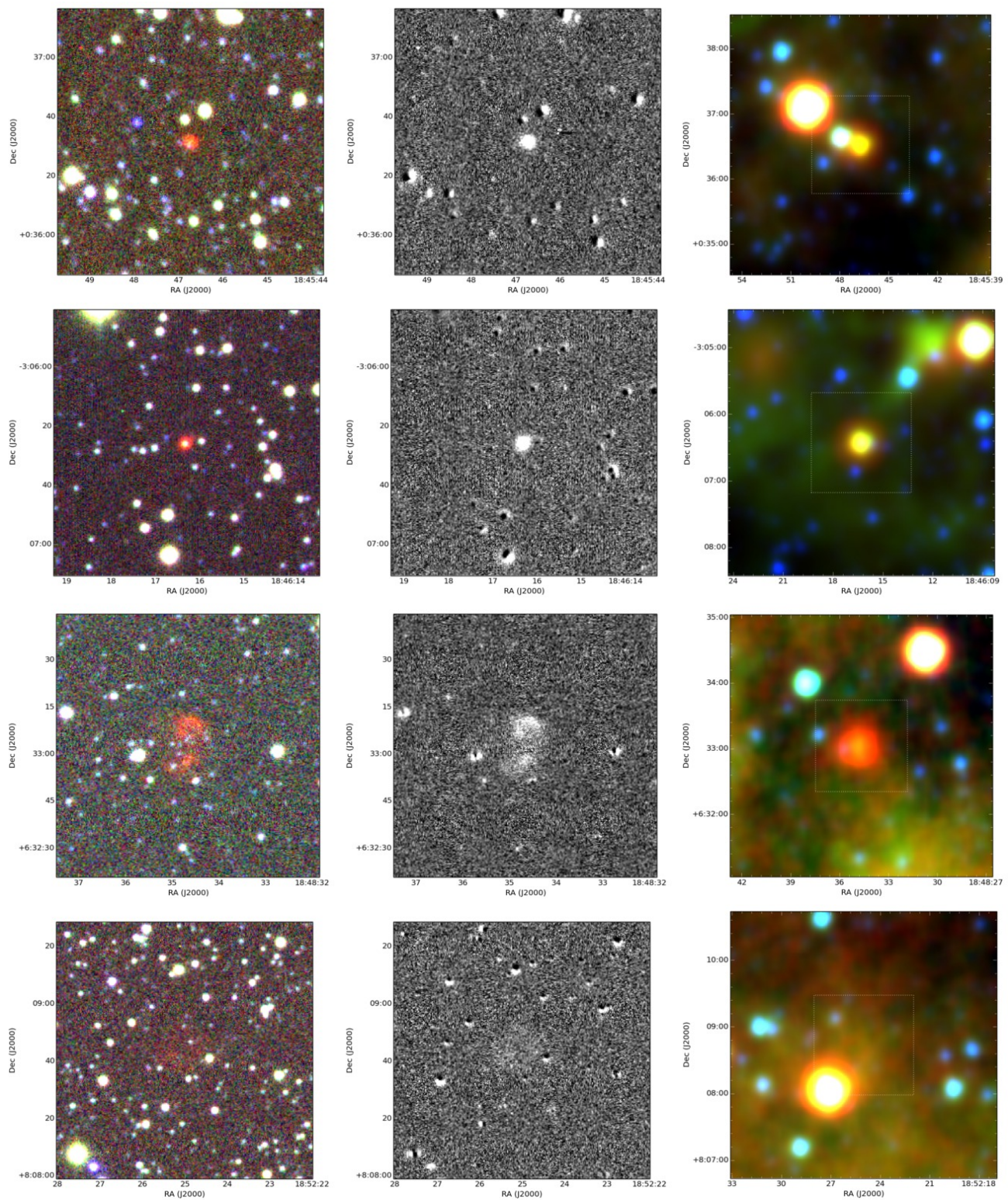


Figure A.8. Same as in Fig. A.1. Objects shown (from top to bottom): PN G032.8+01.5, PN G029.5-00.2, PN G038.4+03.6, PN G040.3+03.4

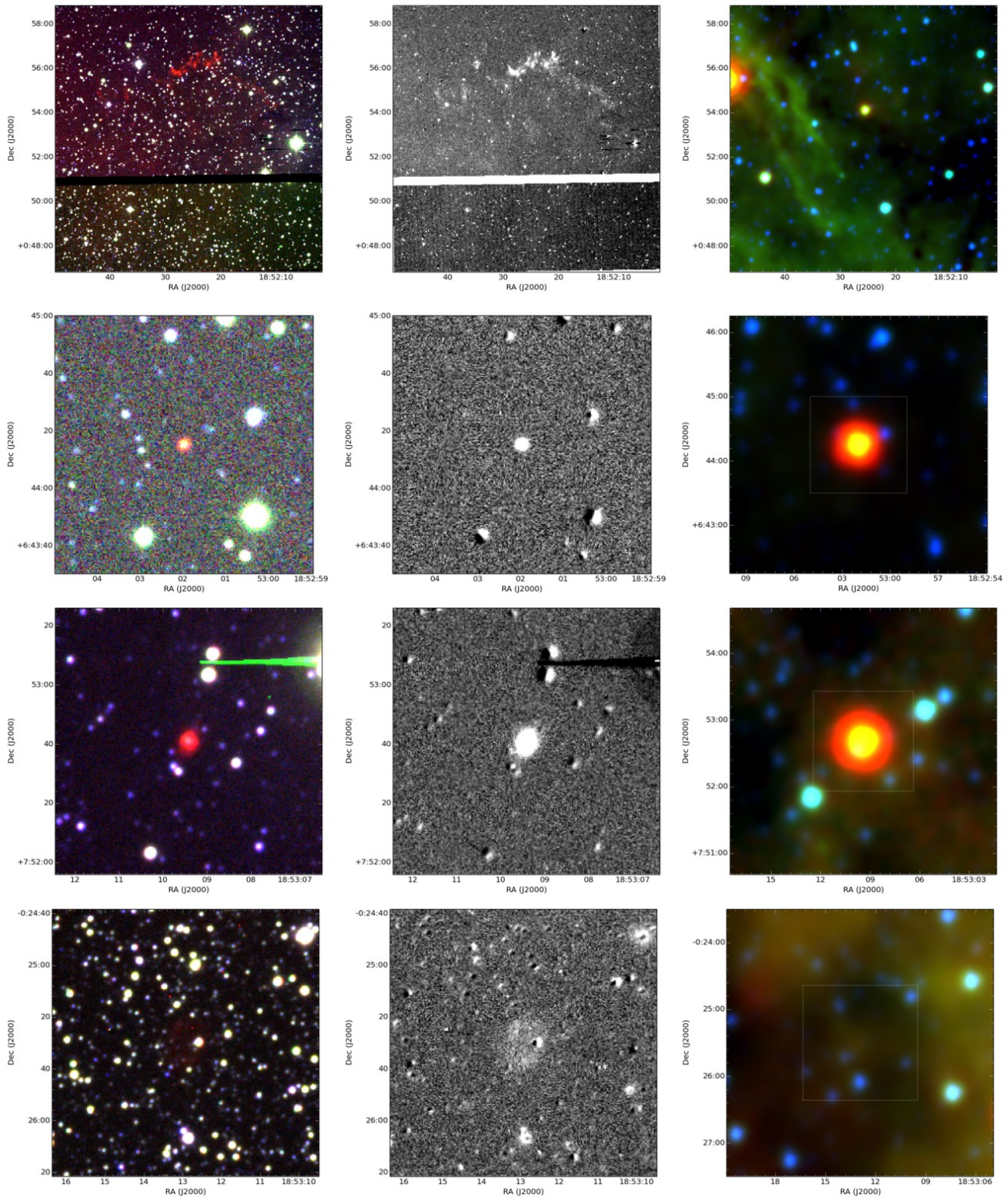


Figure A.9. Same as in Fig. A.1. Objects shown (from top to bottom): PN G033.8+00.1, PN G039.1+02.7, PN G040.1+03.2, PN G032.7-00.5

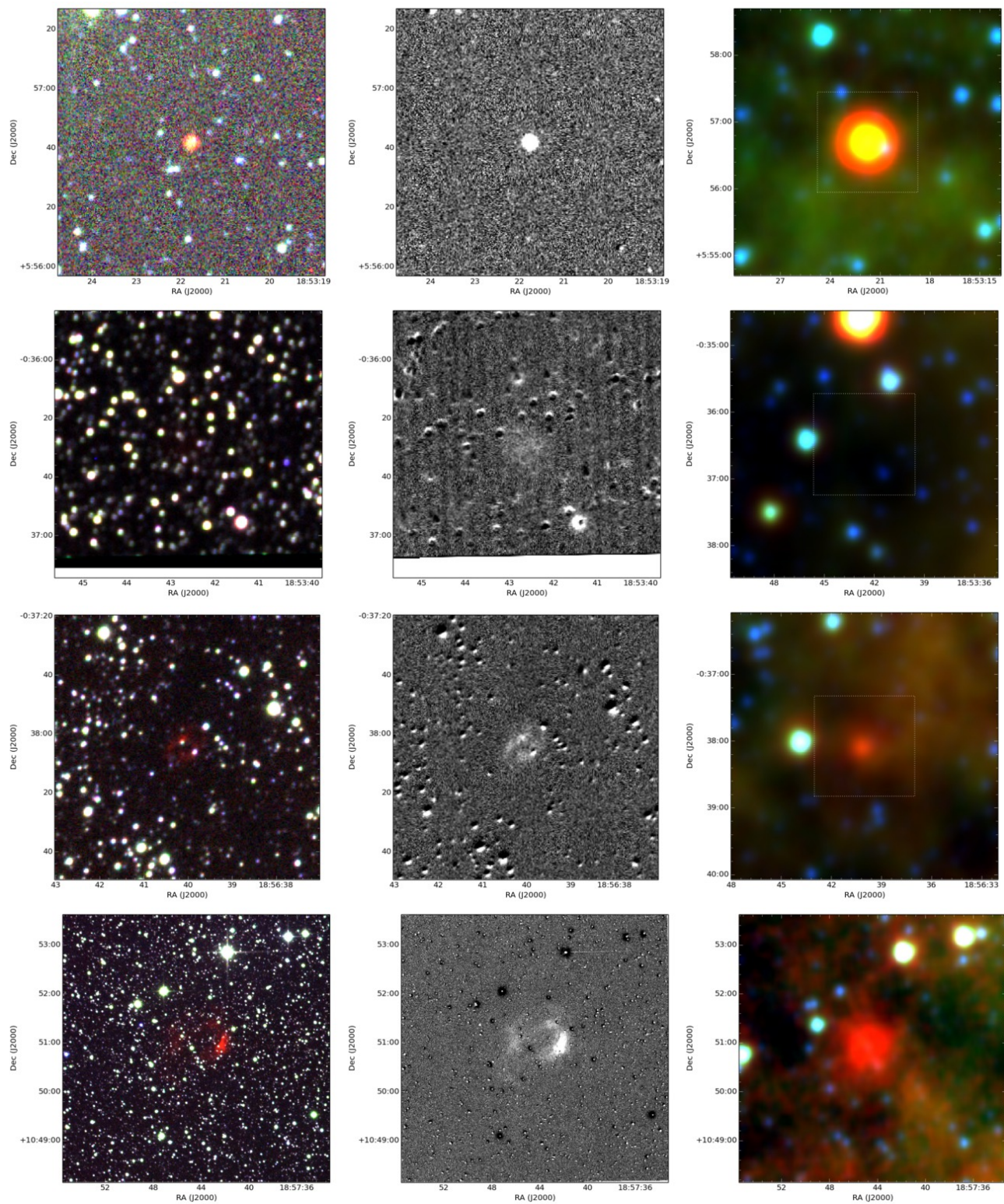


Figure A.10. Same as in Fig. A.1. Objects shown (from top to bottom): PN G038.4+02.2, PN G032.6-00.7, PN G032.9-01.4, PN G043.3+03.5

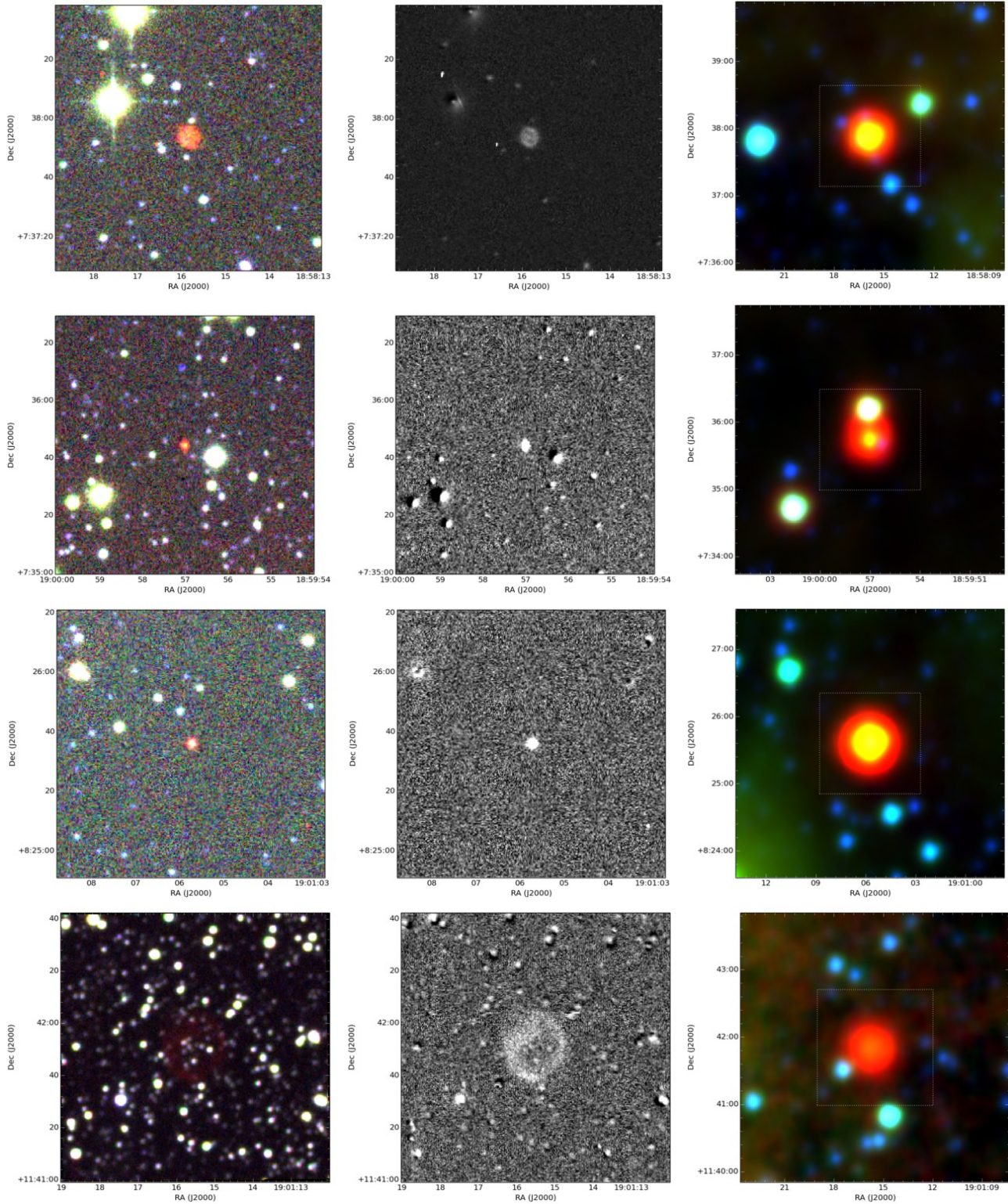


Figure A.11. Same as in Fig. A.1. Objects shown (from top to bottom): PN G040.5+01.9, PN G040.6+01.5, PN G041.5+01.7, PN G044.4+03.1

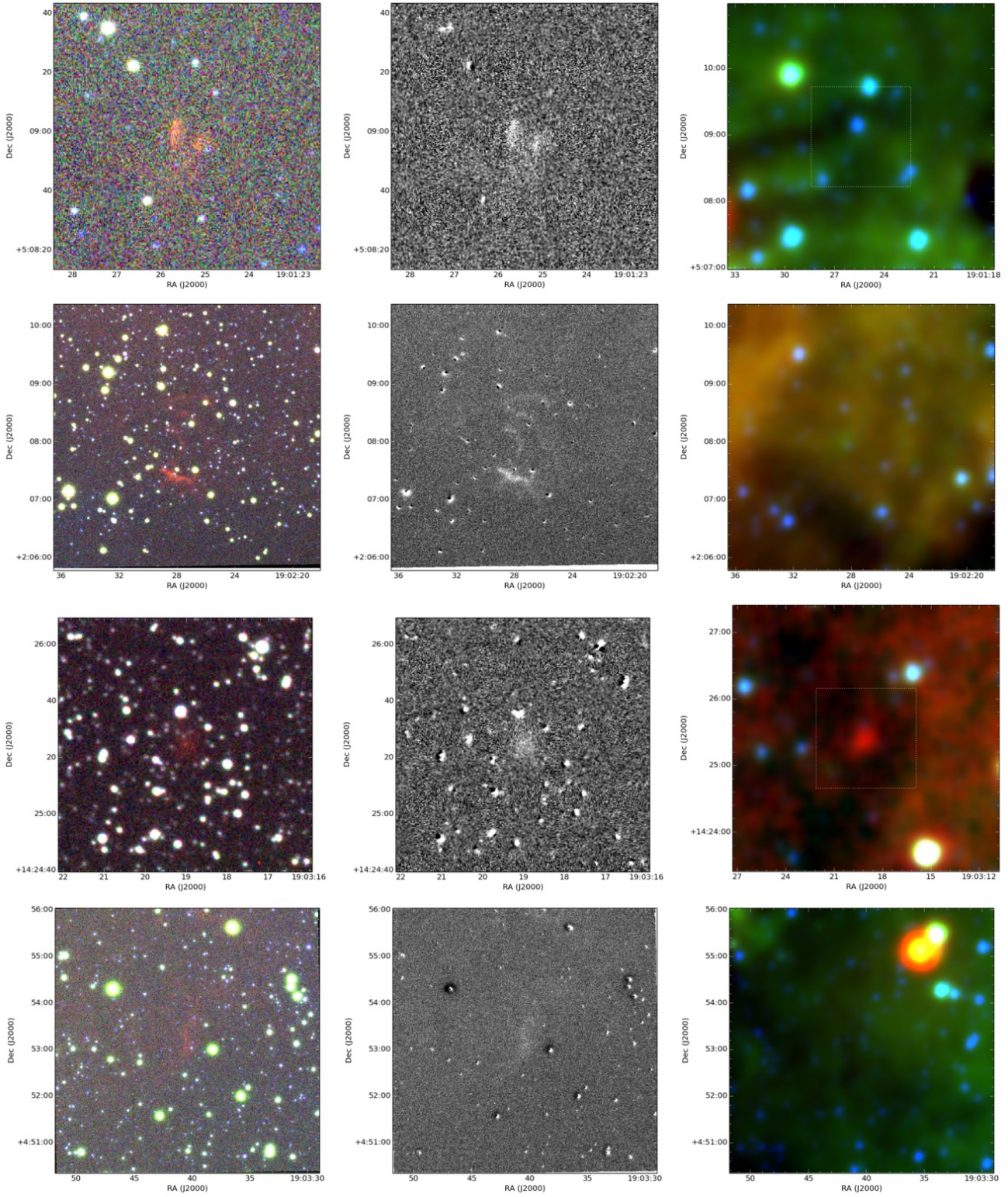


Figure A.12. Same as in Fig. A.1. Objects shown (from top to bottom): PN G038.6+00.1, PN G036.0-01.4, PN G047.1+03.9, PN G038.6-00.4

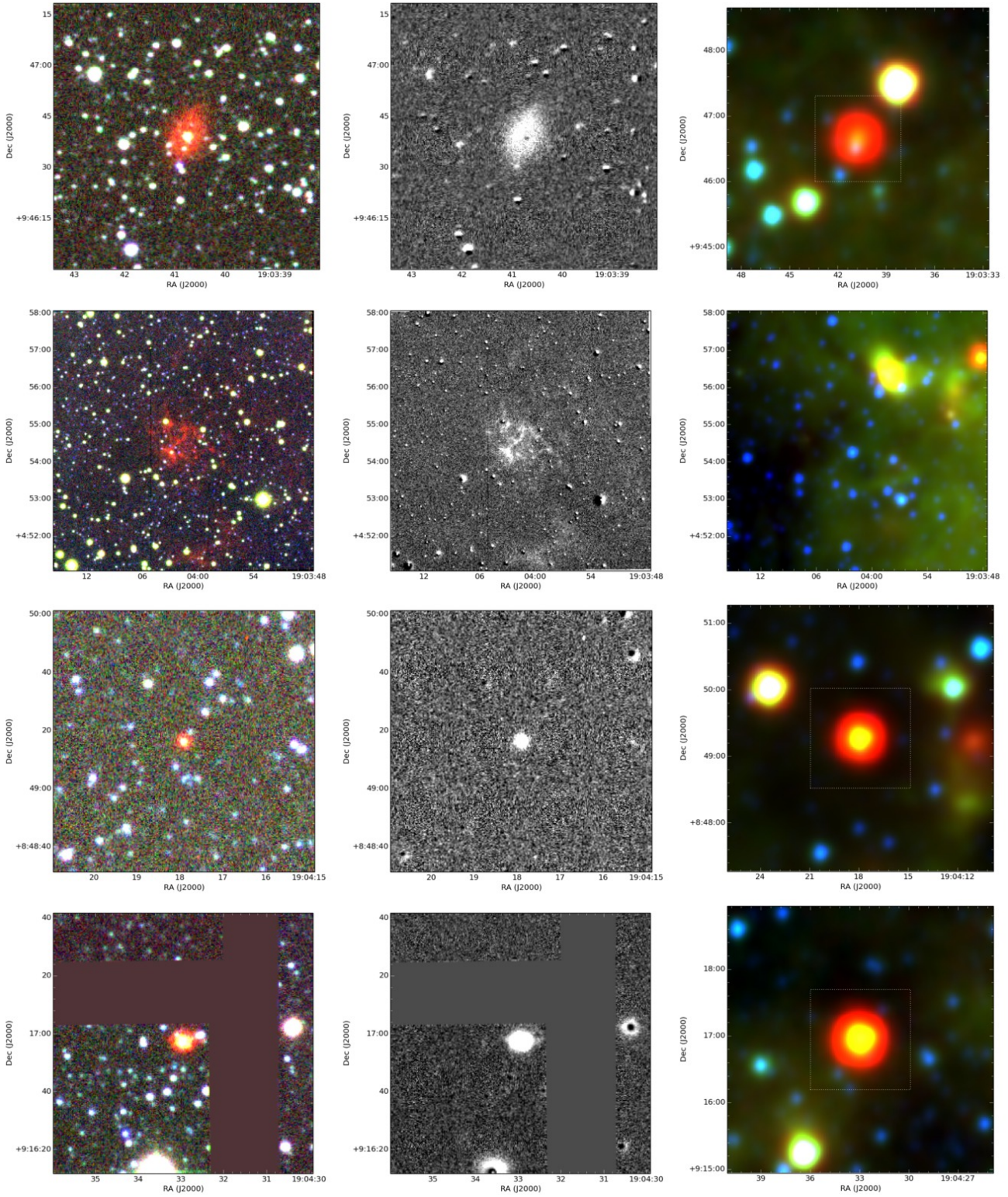


Figure A.13. Same as in Fig. A.1. Objects shown (from top to bottom): PN G043.0+01.7, PN G038.7-00.5, PN G042.2+01.1, PN G042.6+01.3

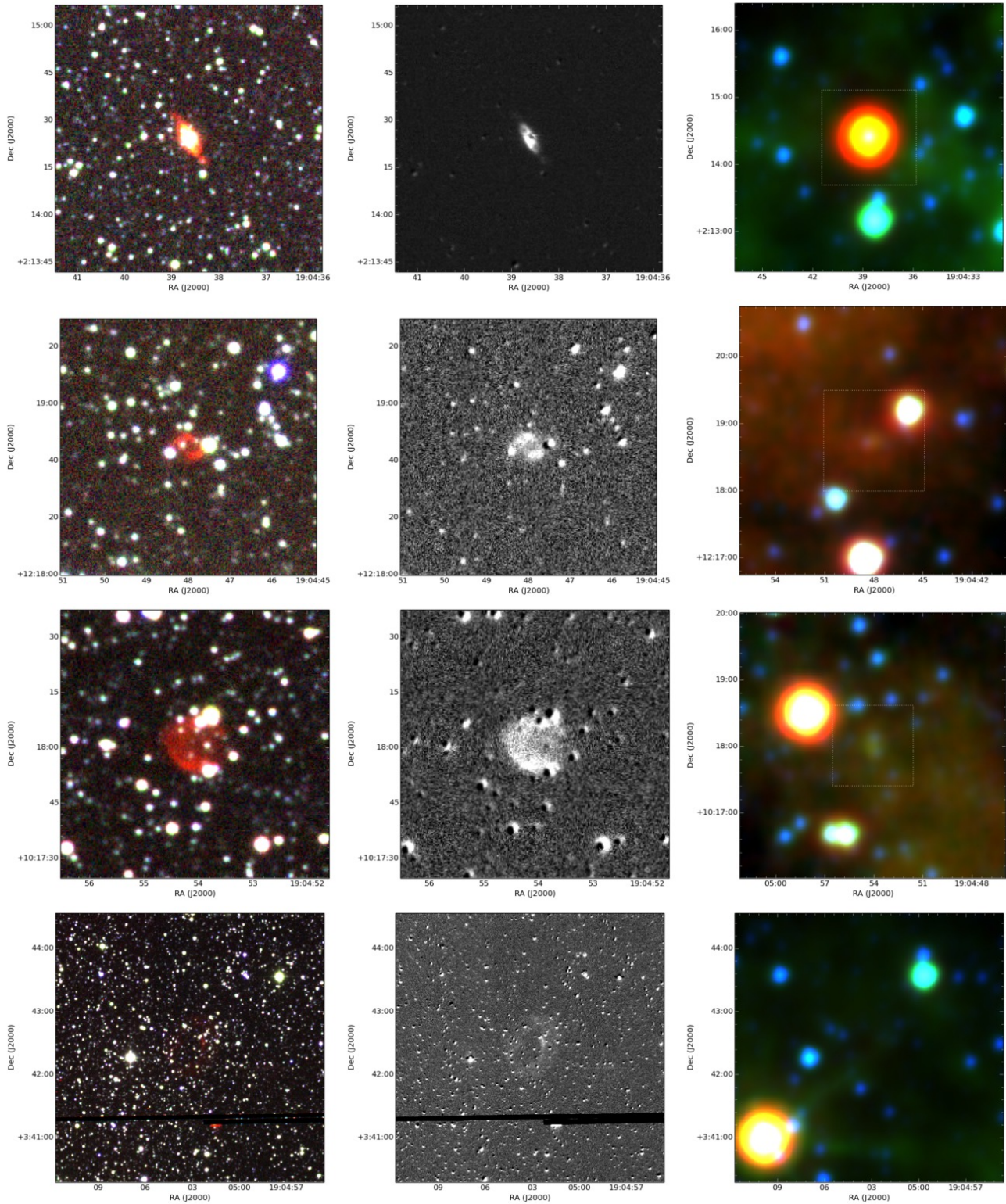


Figure A.14. Same as in Fig. A.1. Objects shown (from top to bottom): PN G036.4-01.9, PN G045.4+02.6, PN G043.6+01.7, PN G037.7-01.3

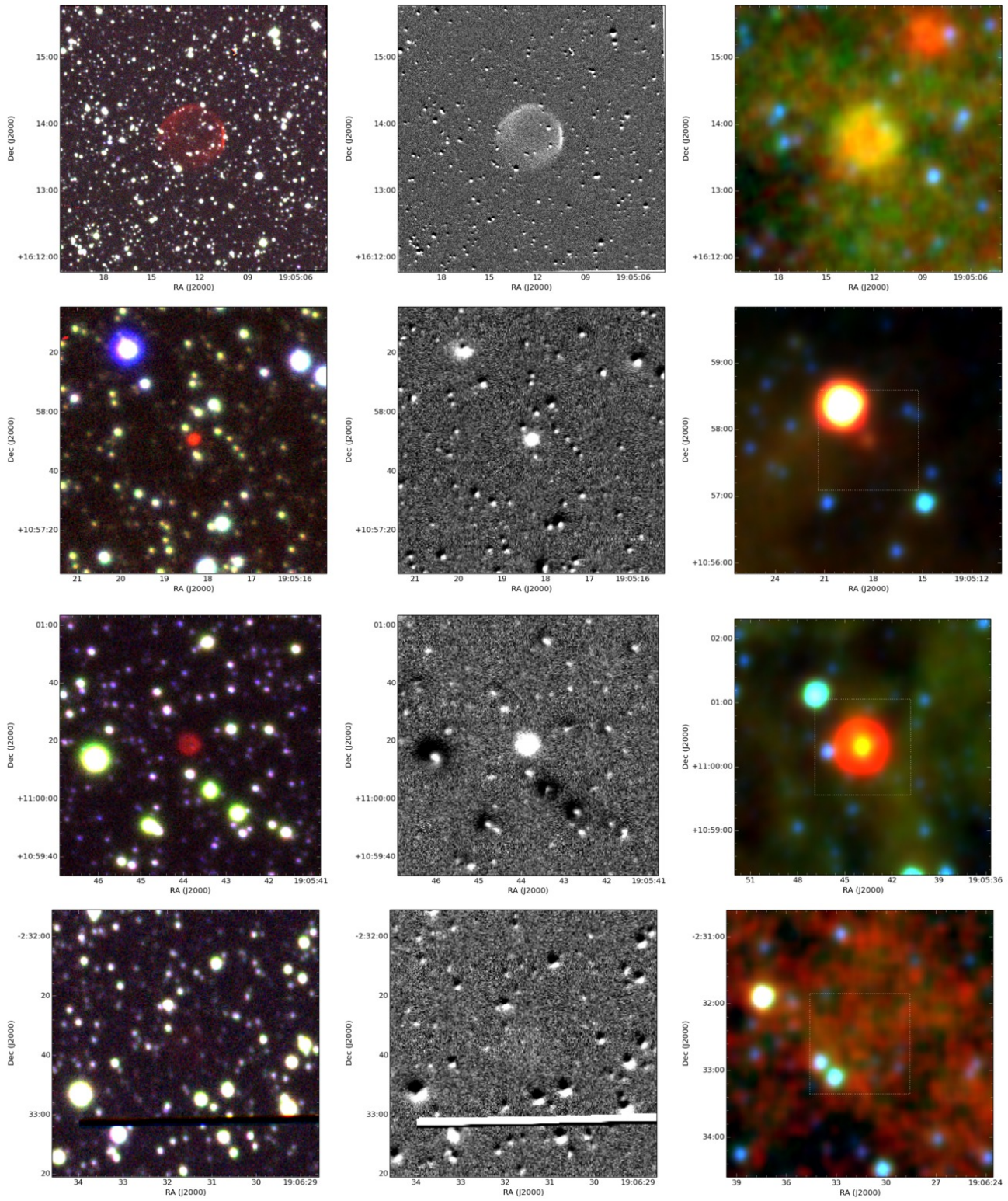


Figure A.15. Same as in Fig. A.1. Objects shown (from top to bottom): PN G048.9+04.3, PN G044.2+01.9, PN G044.3+01.8, PN G032.3-04.5

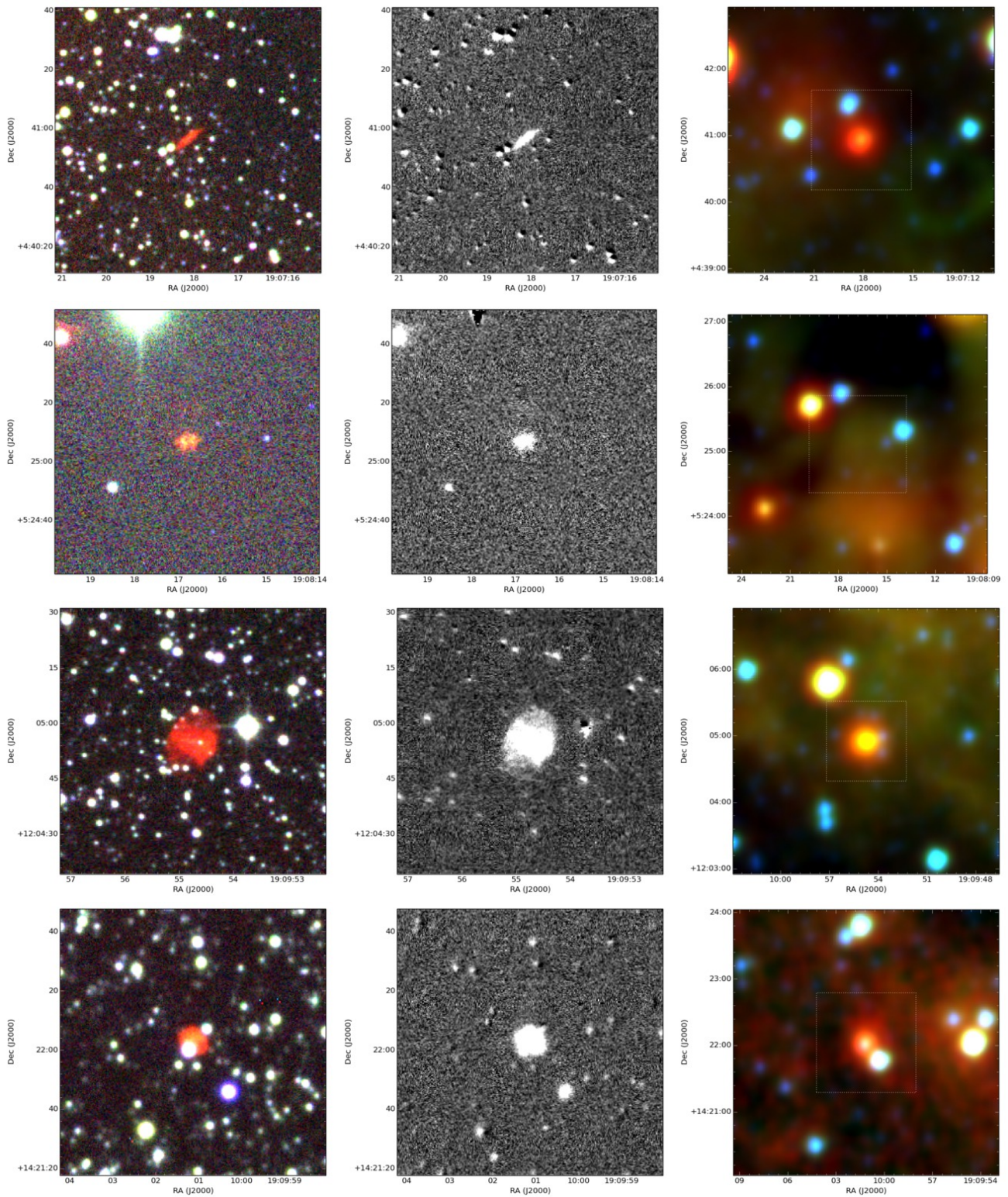


Figure A.16. Same as in Fig. A.1. Objects shown (from top to bottom): PN G038.9-01.3, PN G039.6-01.2, PN G045.7+01.4, PN G047.8+02.4

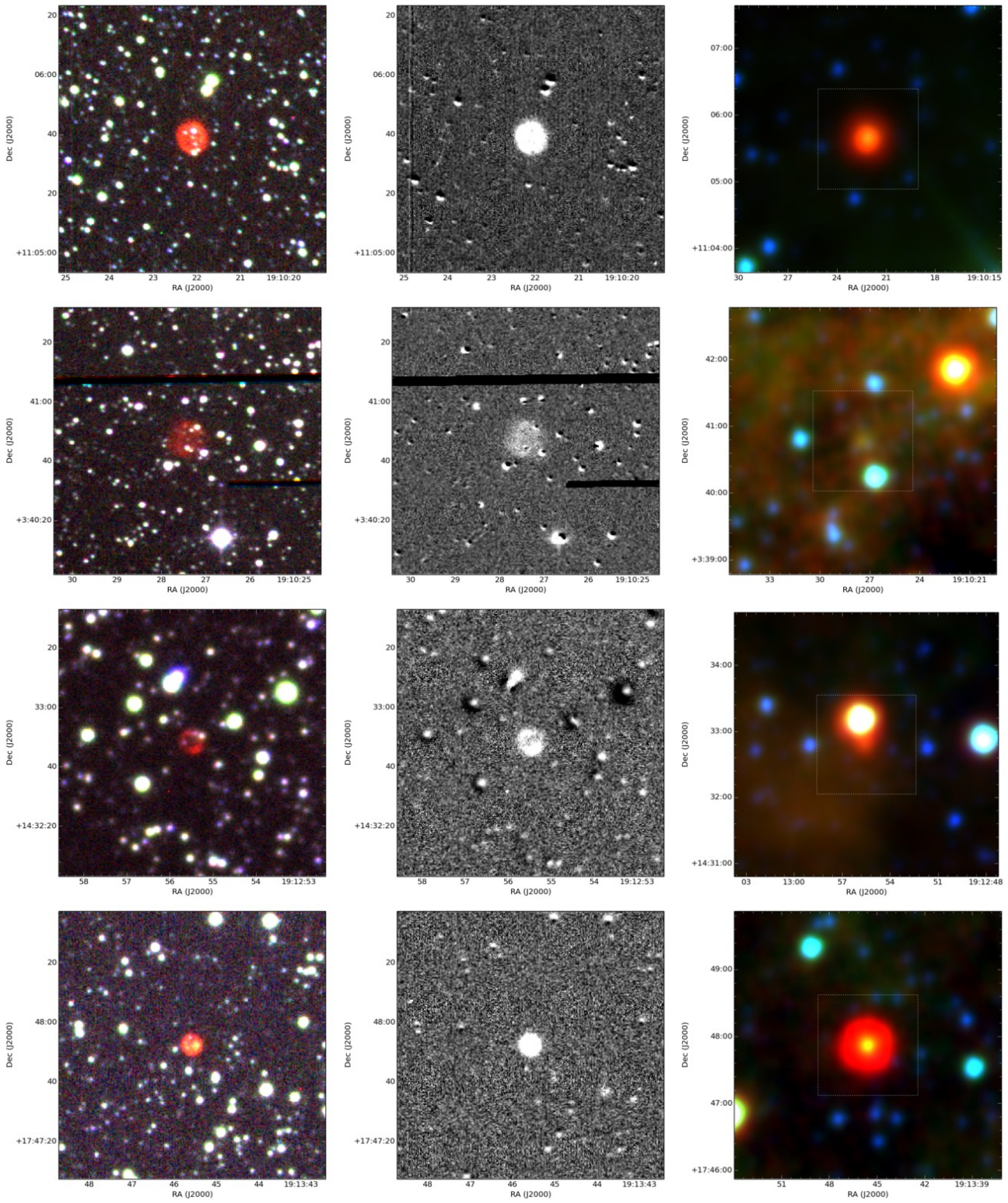


Figure A.17. Same as in Fig. A.1. Objects shown (from top to bottom): PN G044.9+00.8, PN G038.3-02.5, PN G048.2+01.9, PN G051.2+03.2

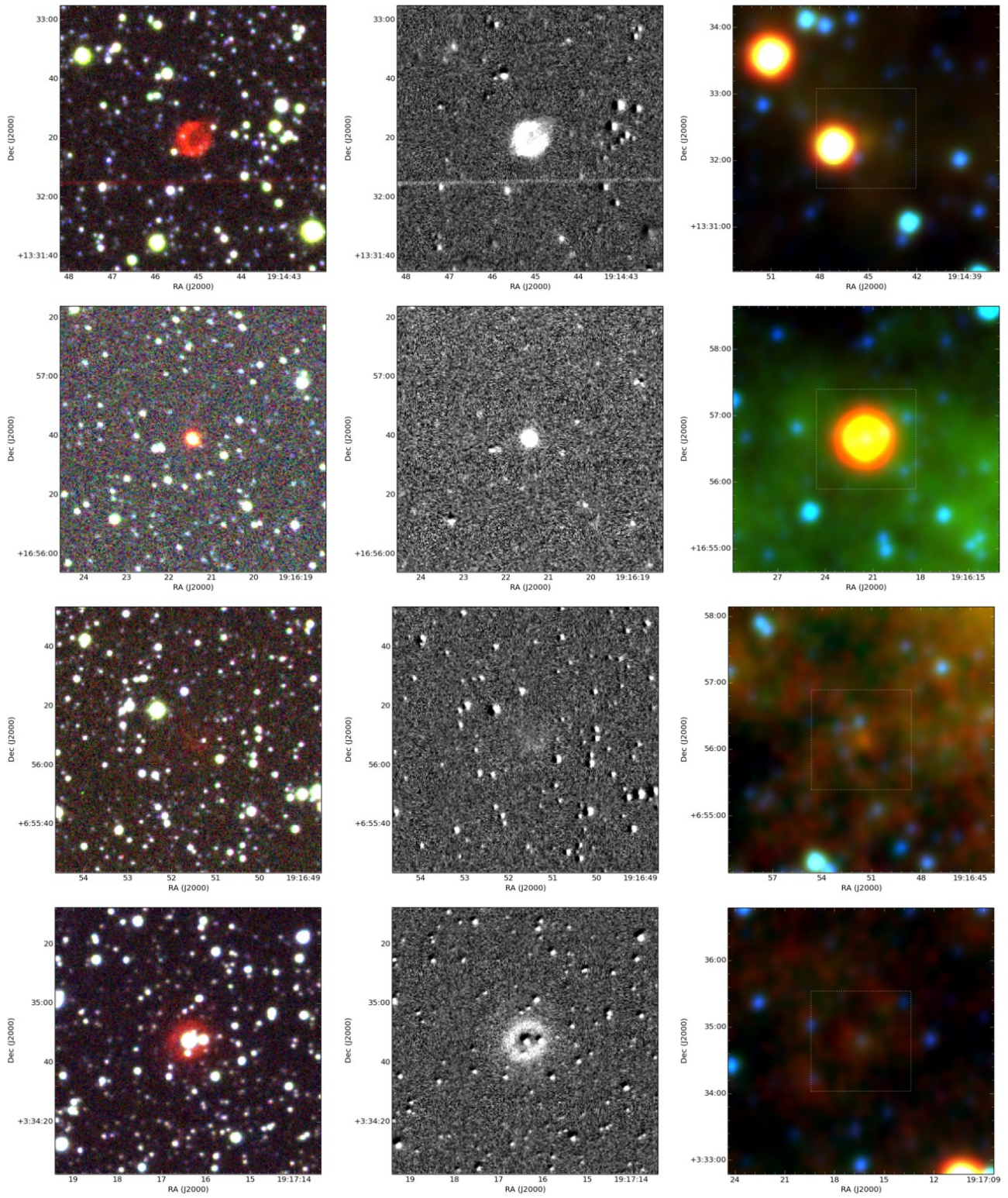


Figure A.18. Same as in Fig. A.1. Objects shown (from top to bottom): PN G047.6+01.0, PN G050.8+02.3, PN G042.0-02.4, PN G039.0-04.0

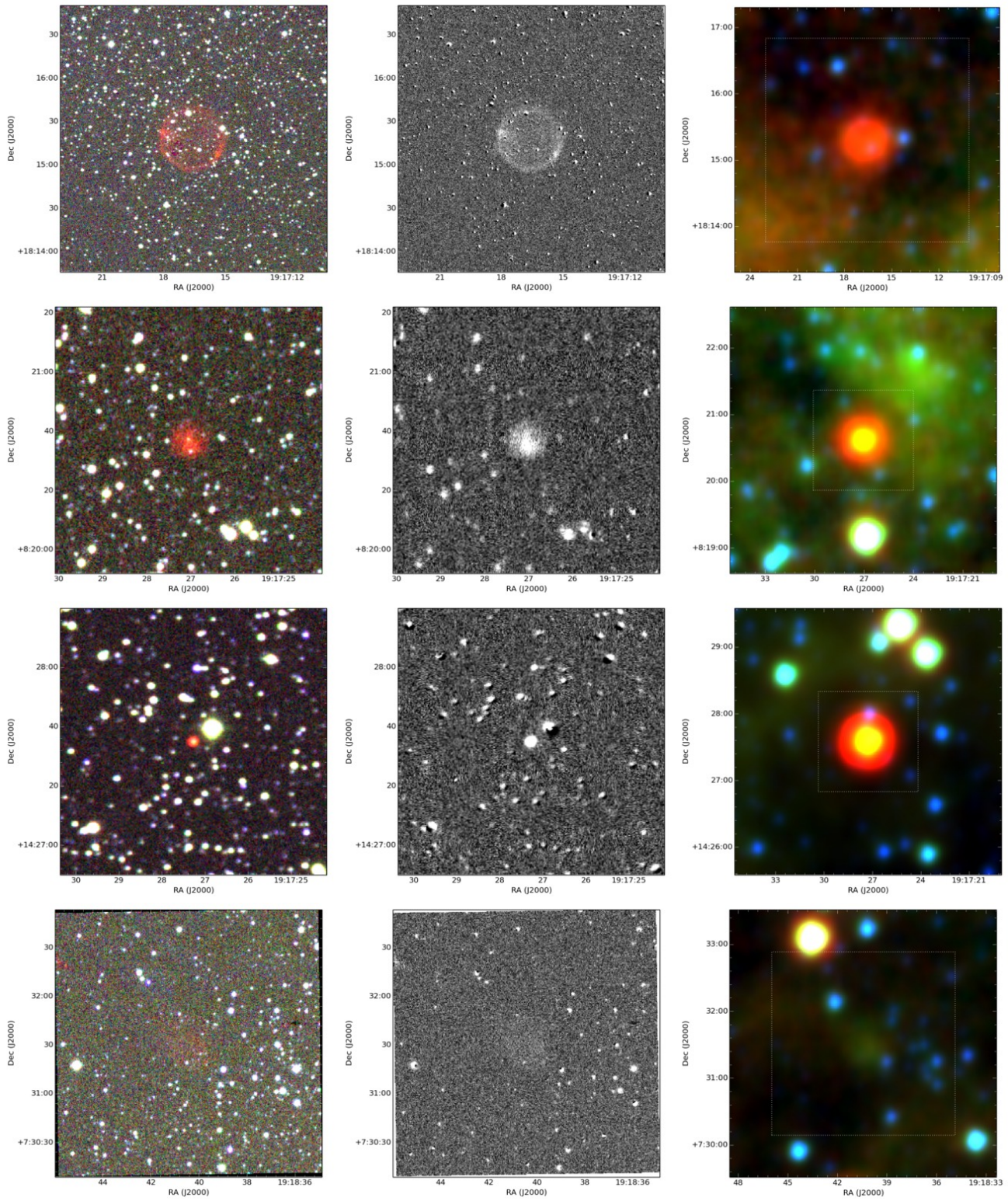


Figure A.19. Same as in Fig. A.1. Objects shown (from top to bottom): PN G052.0+02.7, PN G043.3-01.9, PN G048.7+00.9, PN G042.7-02.5

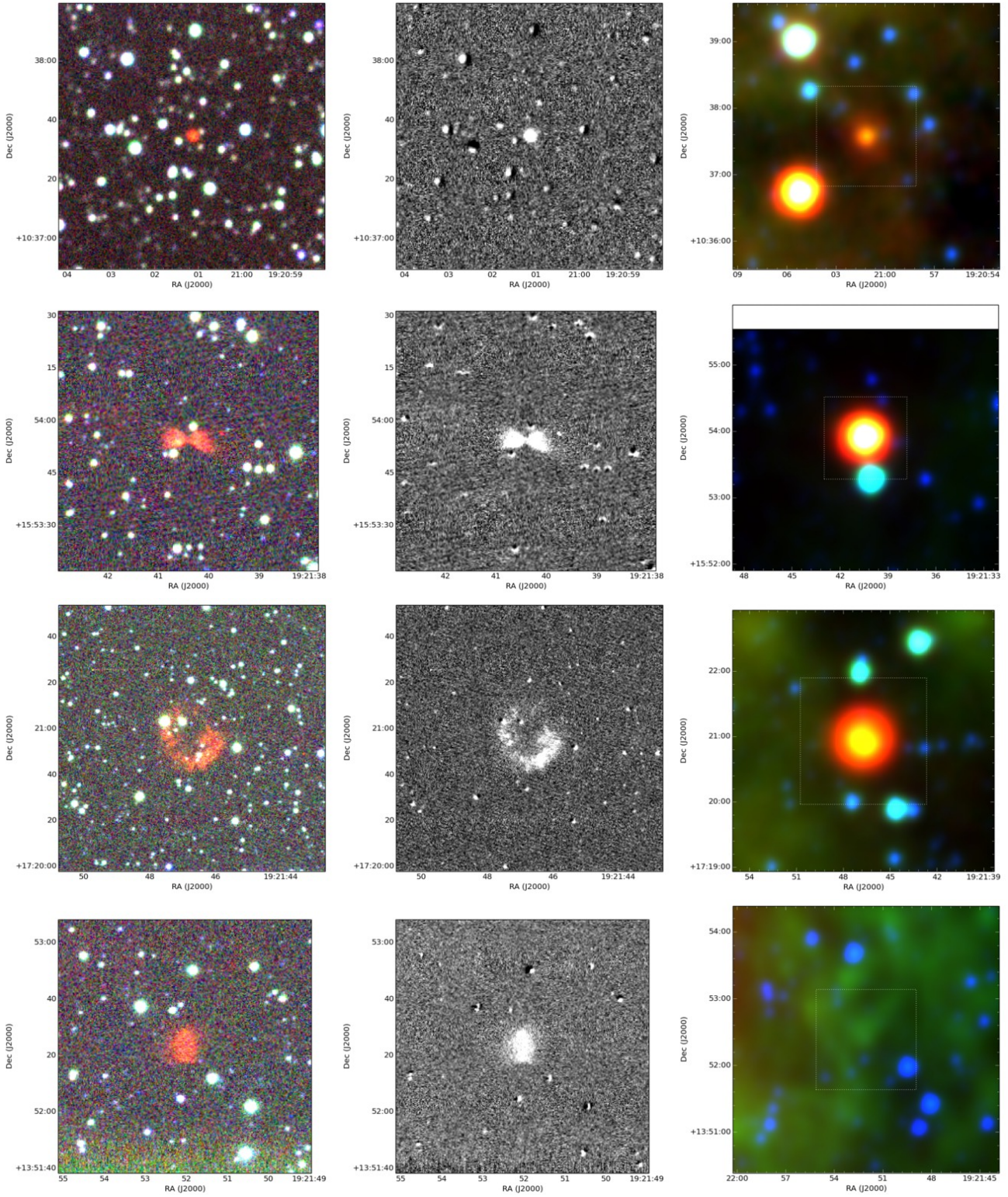


Figure A.20. Same as in Fig. A.1. Objects shown (from top to bottom): PN G045.7-01.6, PN G050.4+00.7, PN G051.7+01.3, PN G048.7-00.2

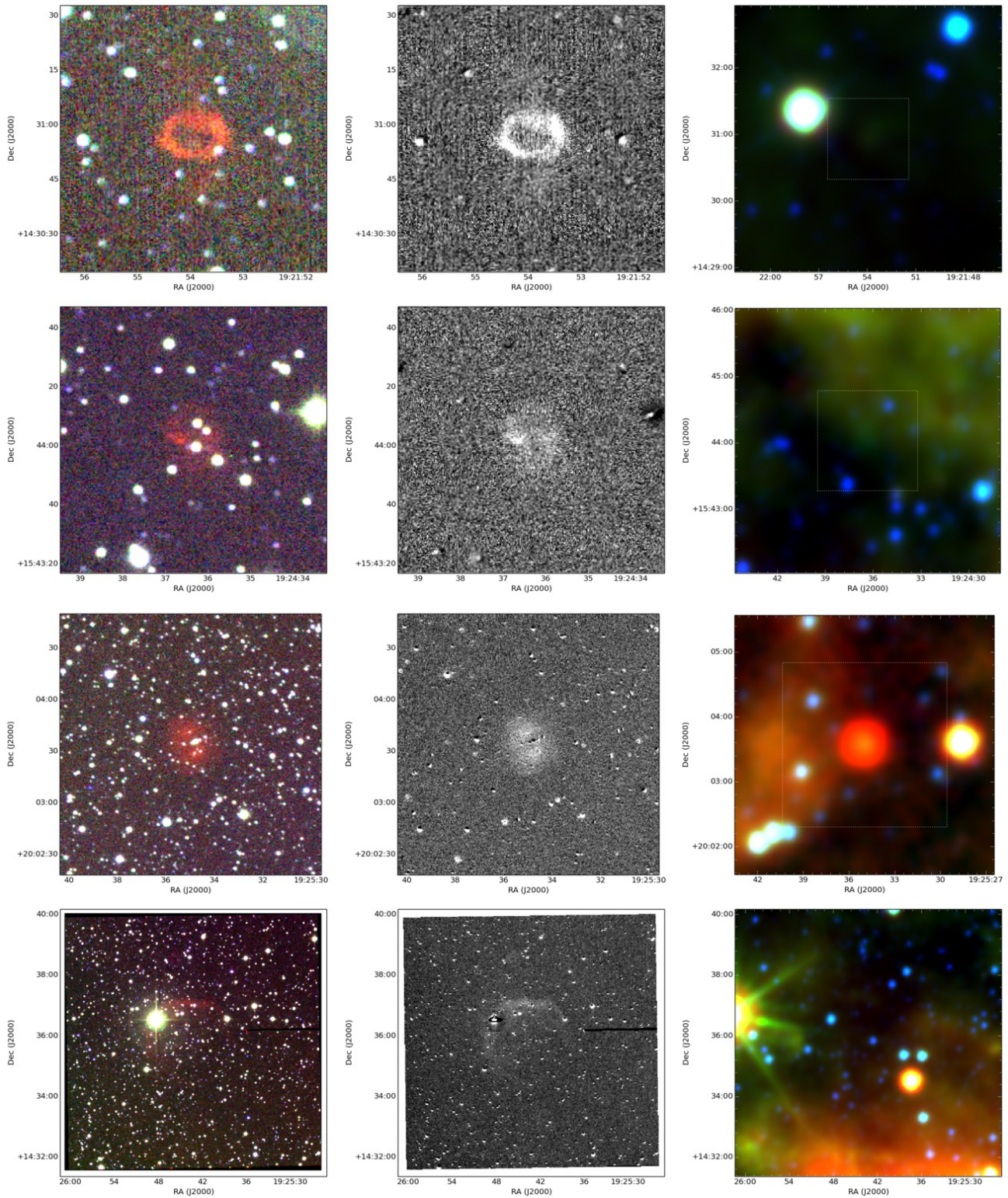


Figure A.21. Same as in Fig. A.1. Objects shown (from top to bottom): PN G049.2+00.0, PN G050.6+00.0, PN G054.5+01.8, PN G049.7-00.7

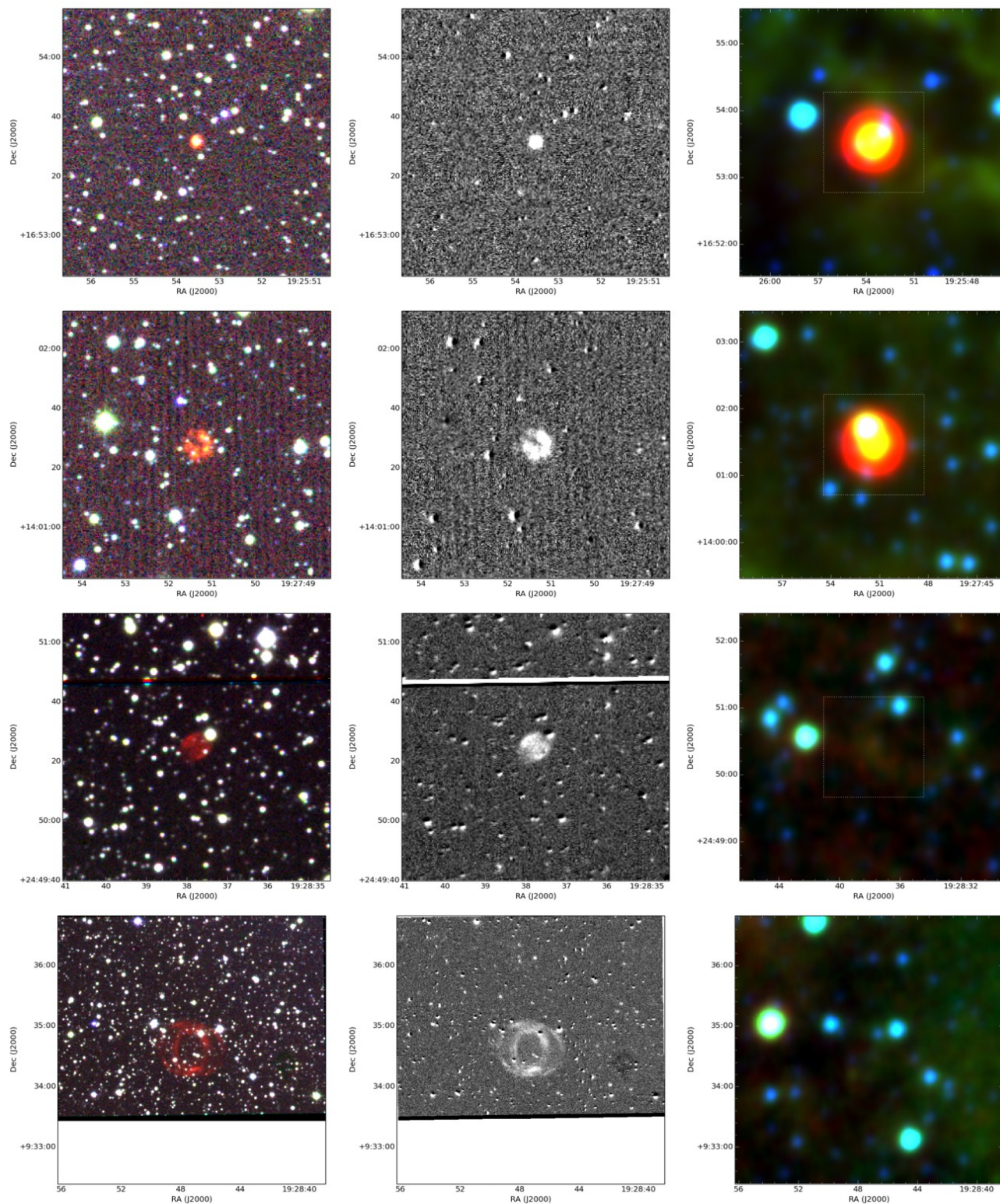


Figure A.22. Same as in Fig. A.1. Objects shown (from top to bottom): PN G051.8+00.2, PN G049.5-01.4, PN G059.1+03.5, PN G045.7-03.8

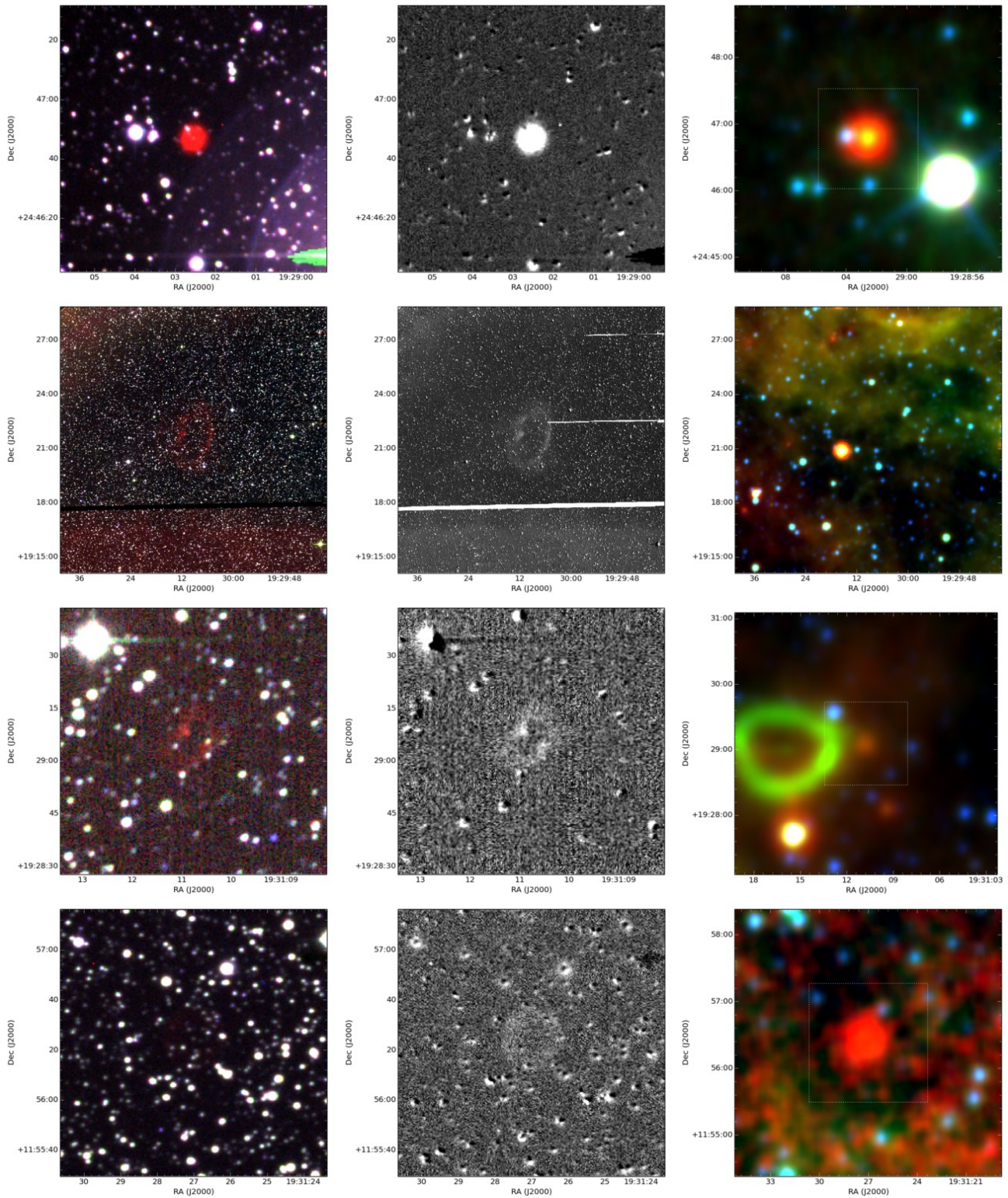


Figure A.23. Same as in Fig. A.1. Objects shown (from top to bottom): PN G059.1+03.3, PN G054.4+00.5, PN G054.7+00.4, PN G048.1-03.2

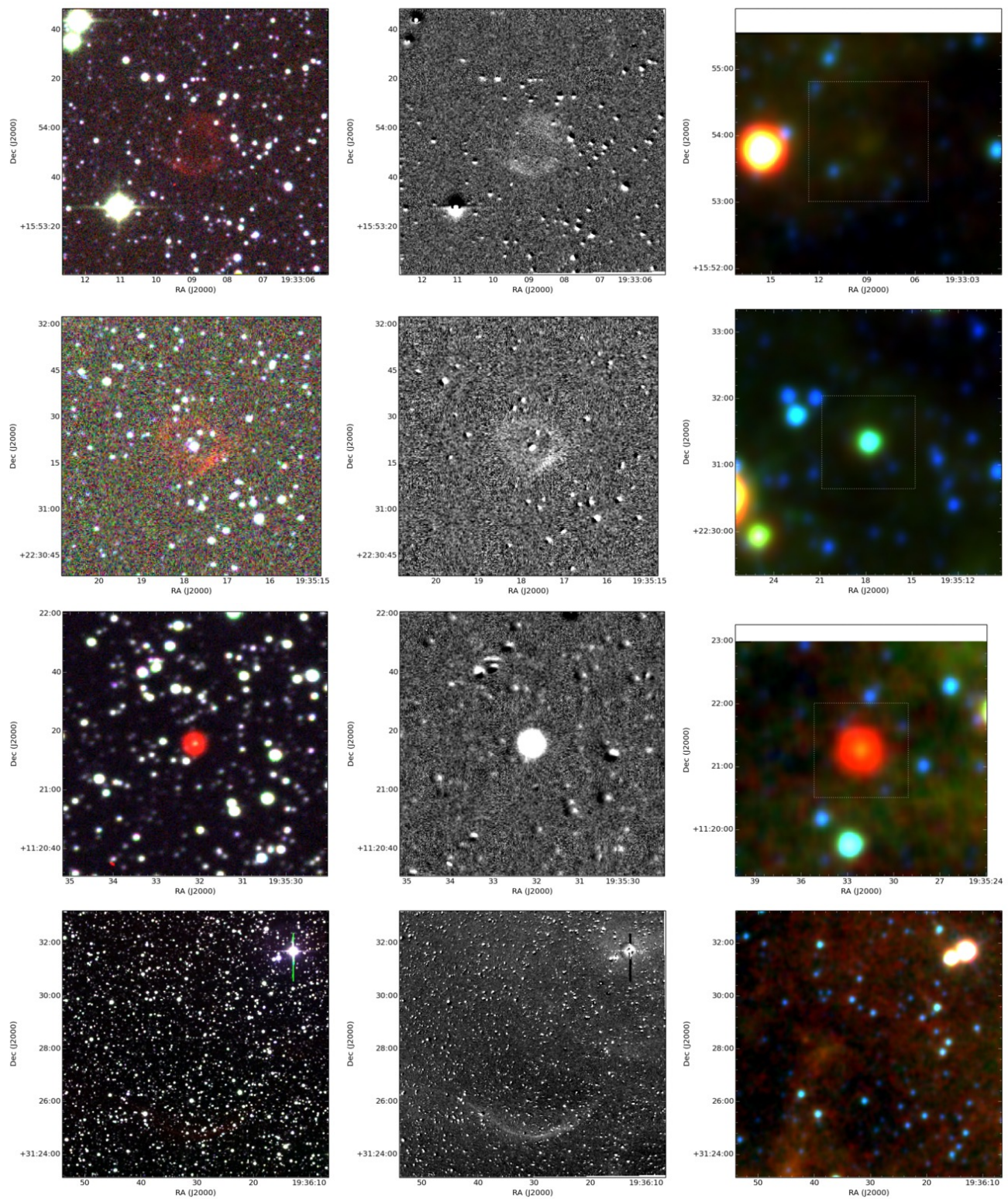


Figure A.24. Same as in Fig. A.1. Objects shown (from top to bottom): PN G051.7-01.7, PN G057.8+01.0, PN G048.0-04.4, PN G065.8+05.1

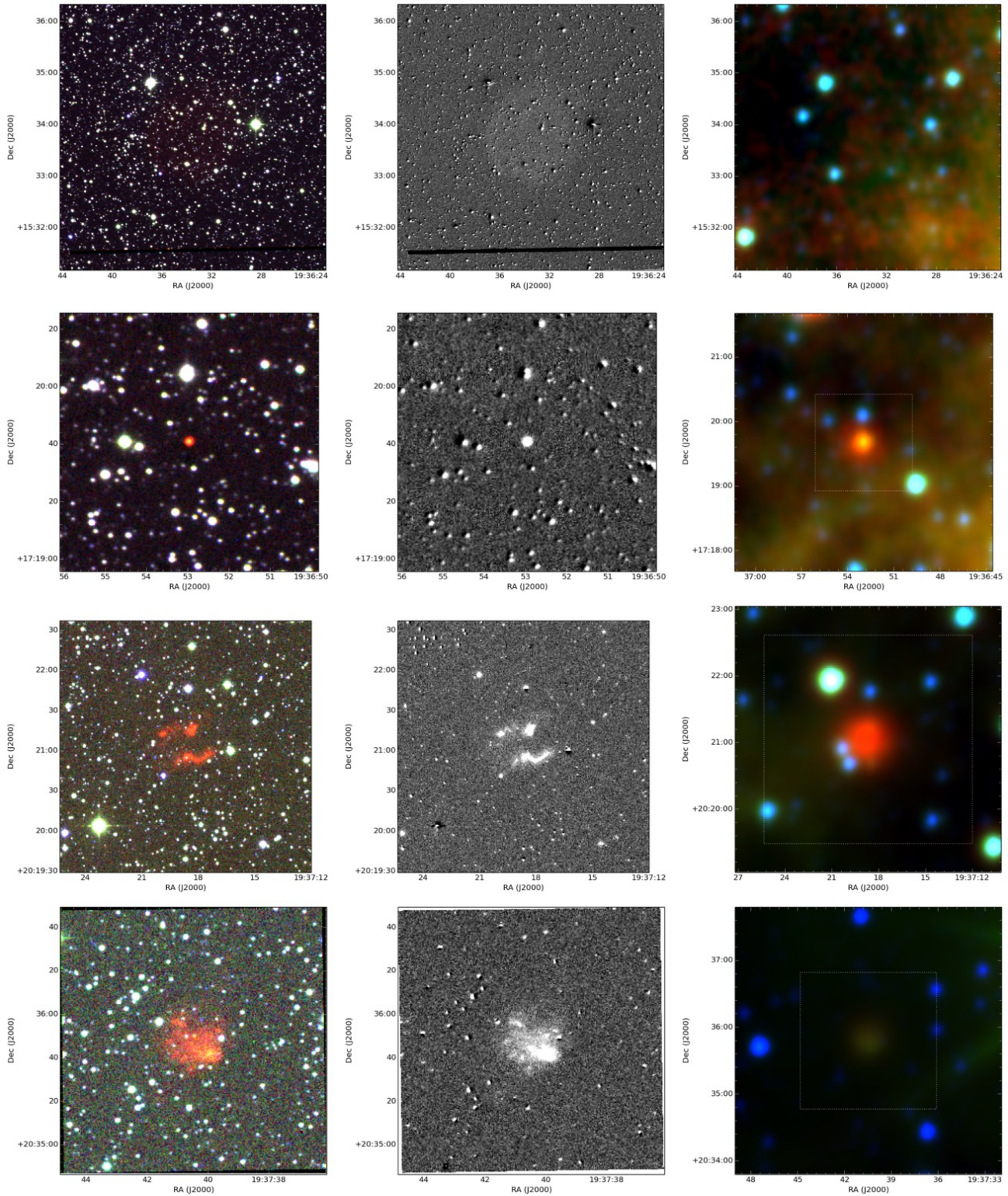


Figure A.25. Same as in Fig. A.1. Objects shown (from top to bottom): PN G051.9-02.5, PN G053.4-01.8, PN G056.1-00.4, PN G056.4-00.3

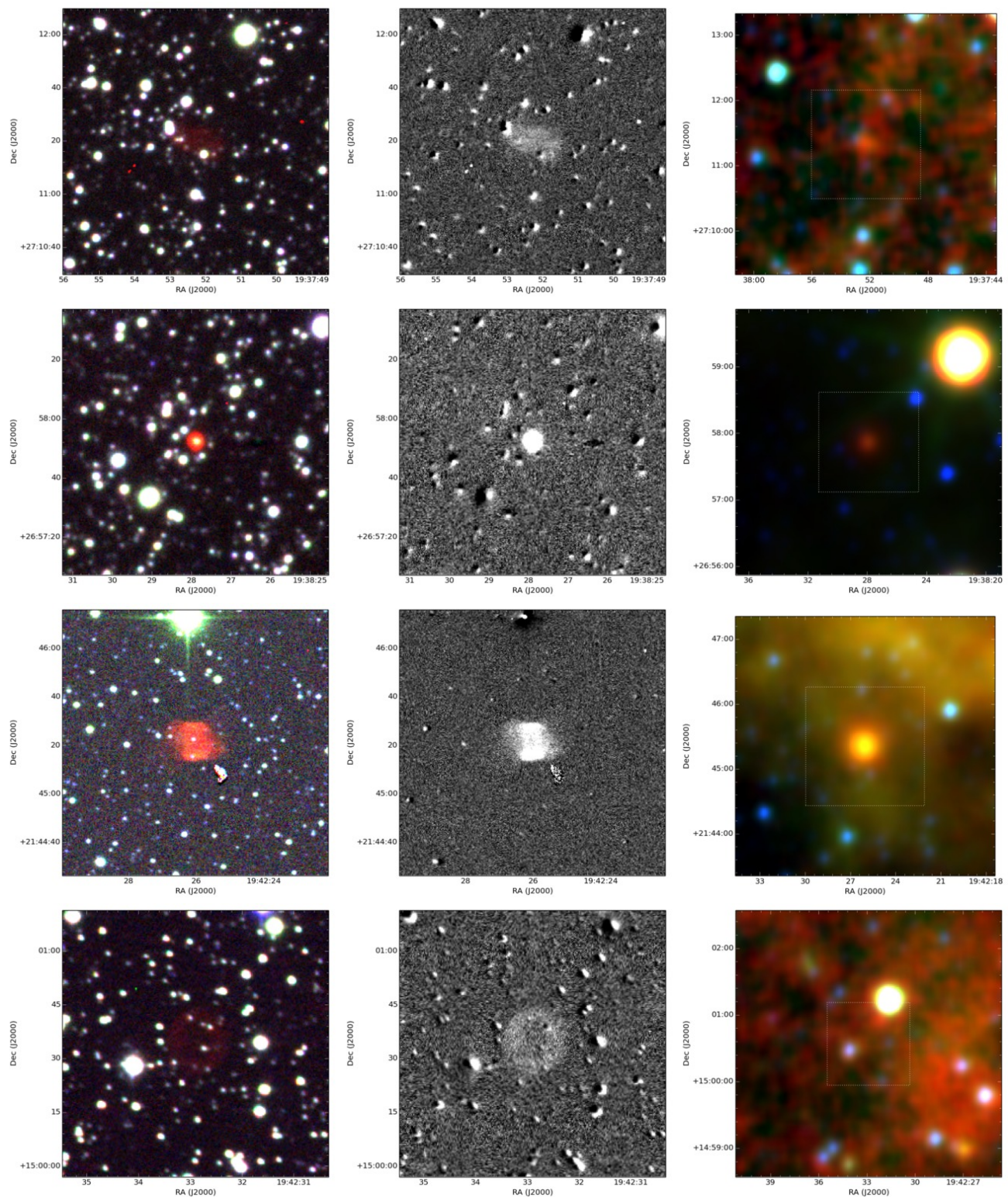


Figure A.26. Same as in Fig. A.1. Objects shown (from top to bottom): PN G062.1+02.8, PN G062.0+02.5, PN G057.9-00.7, PN G052.1-04.1

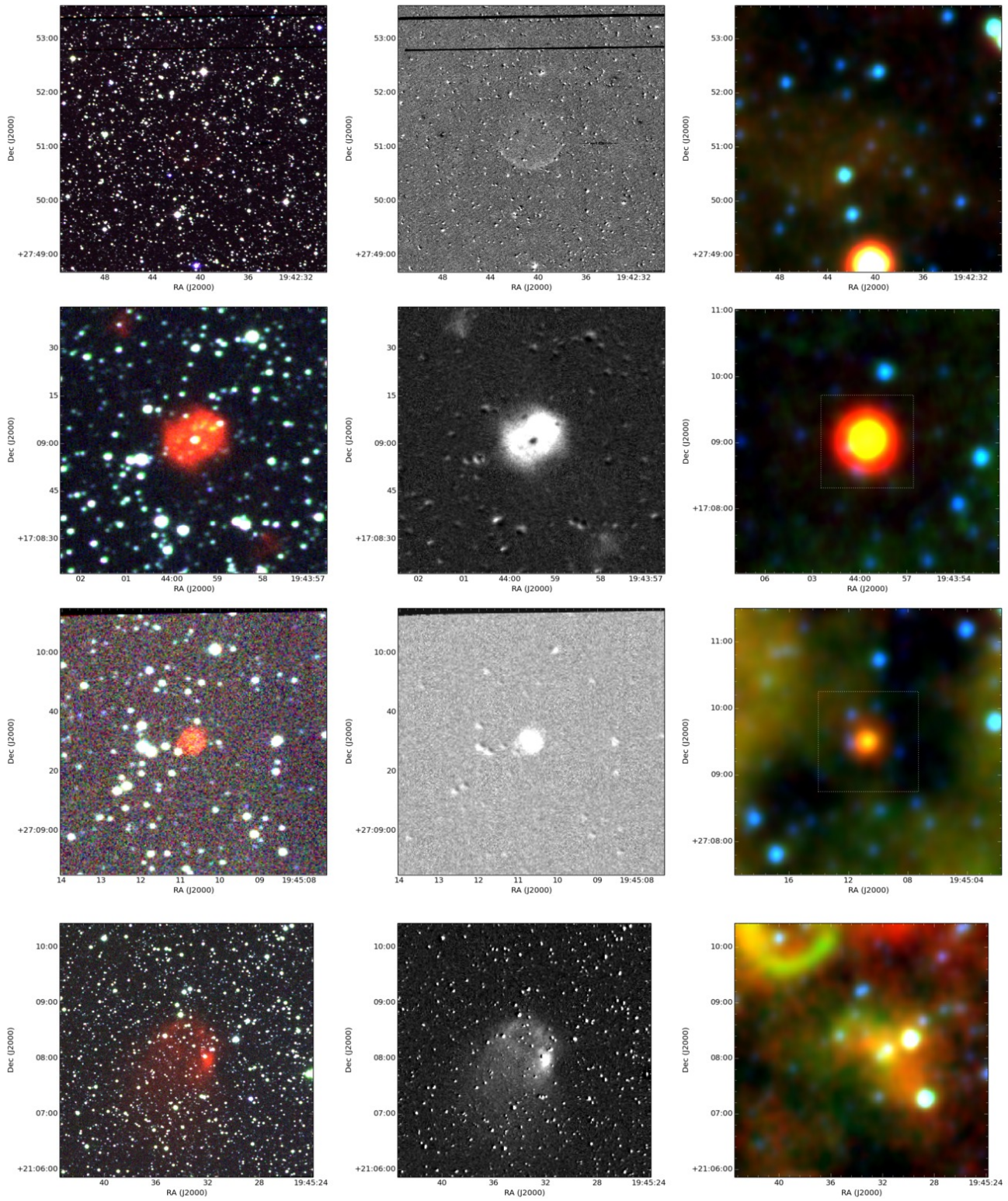


Figure A.27. Same as in Fig. A.1. Objects shown (from top to bottom): PN G063.3+02.2, PN G054.2-03.4, PN G062.9+01.3, PN G057.8-01.7

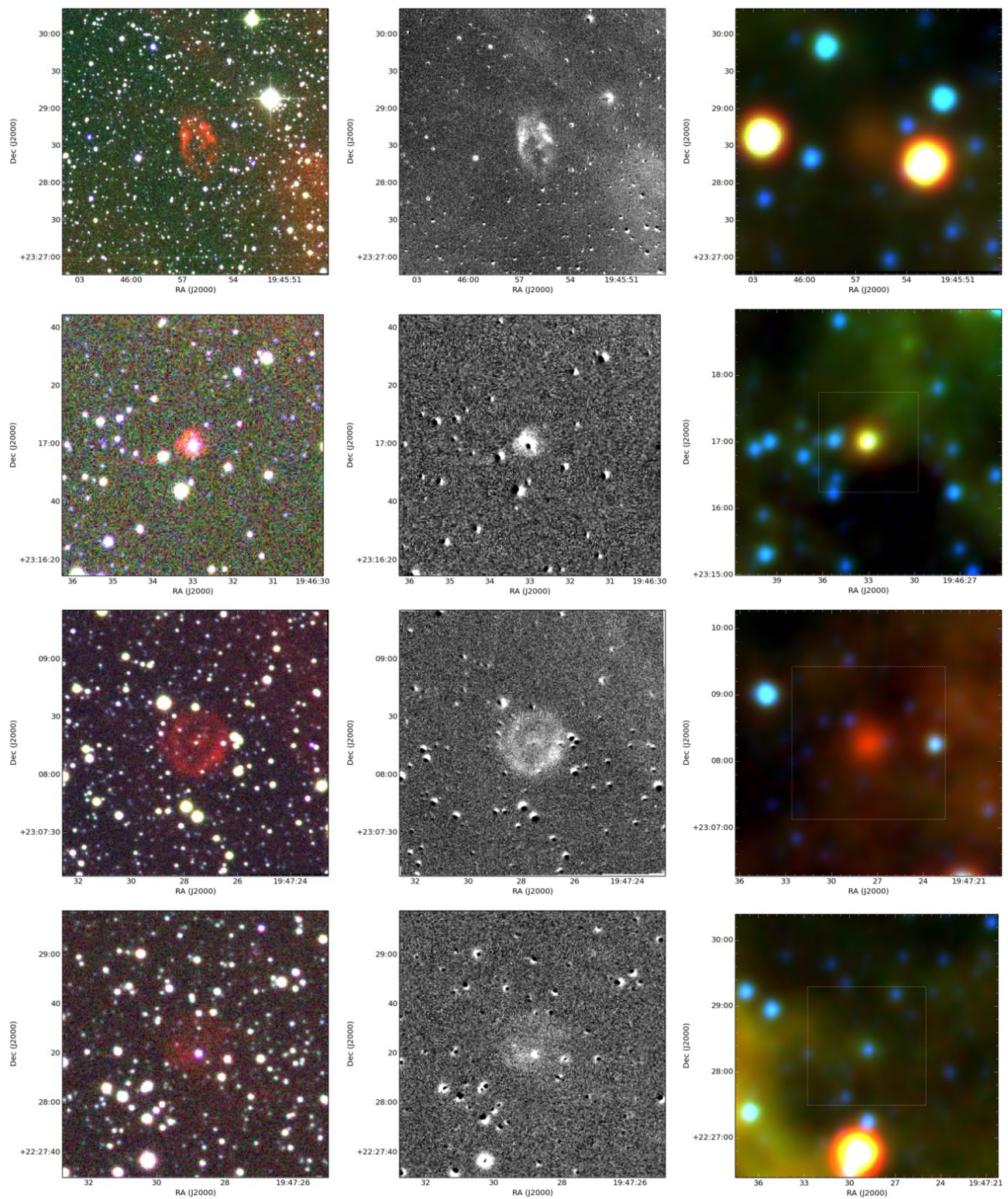


Figure A.28. Same as in Fig. A.1. Objects shown (from top to bottom): PN G059.8-00.6, PN G059.7-00.8, PN G059.7-01.0, PN G059.1-01.4

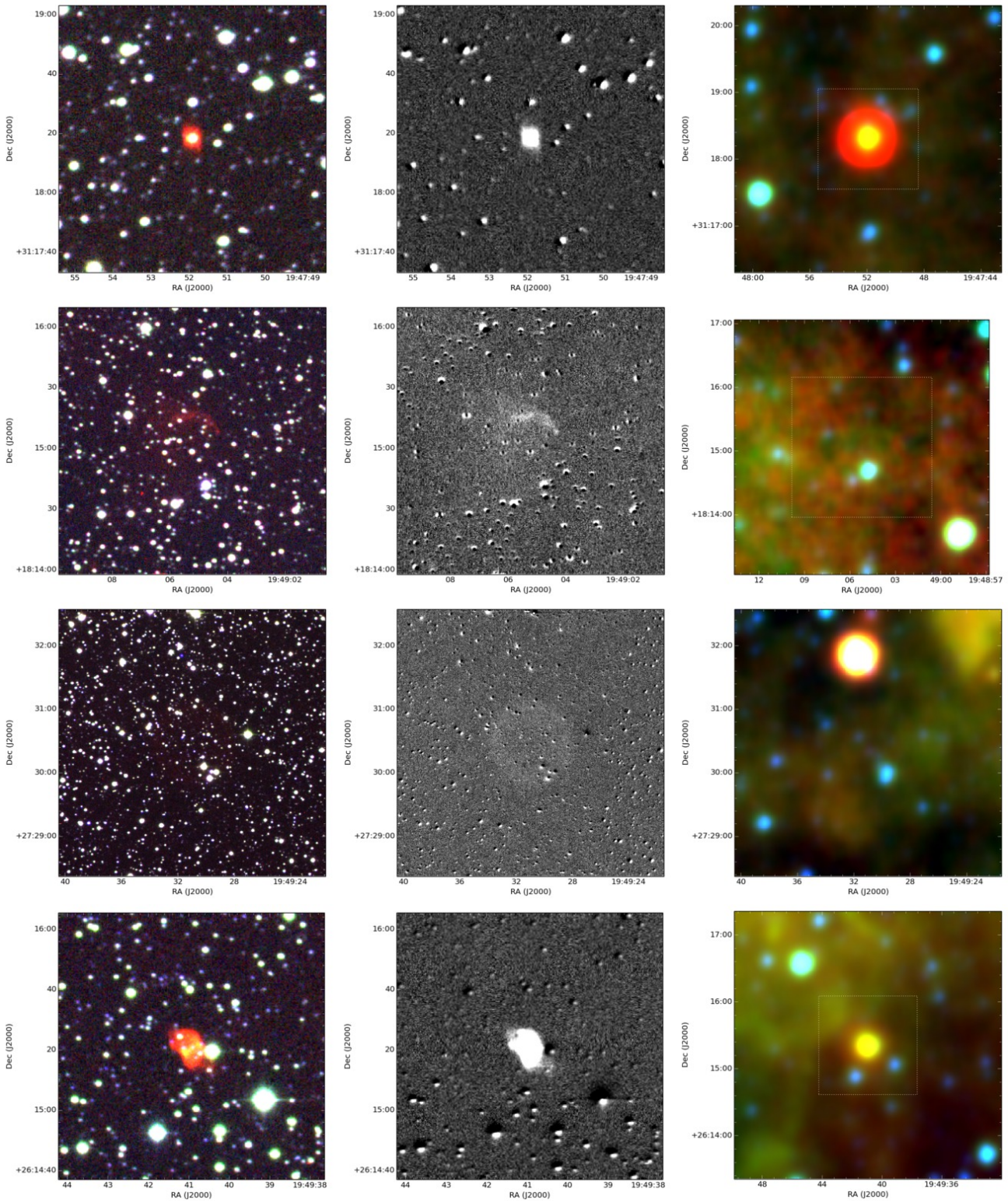


Figure A.29. Same as in Fig. A.1. Objects shown (from top to bottom): PN G066.8+02.9, PN G055.7-03.8, PN G063.7+00.7, PN G062.7+00.0

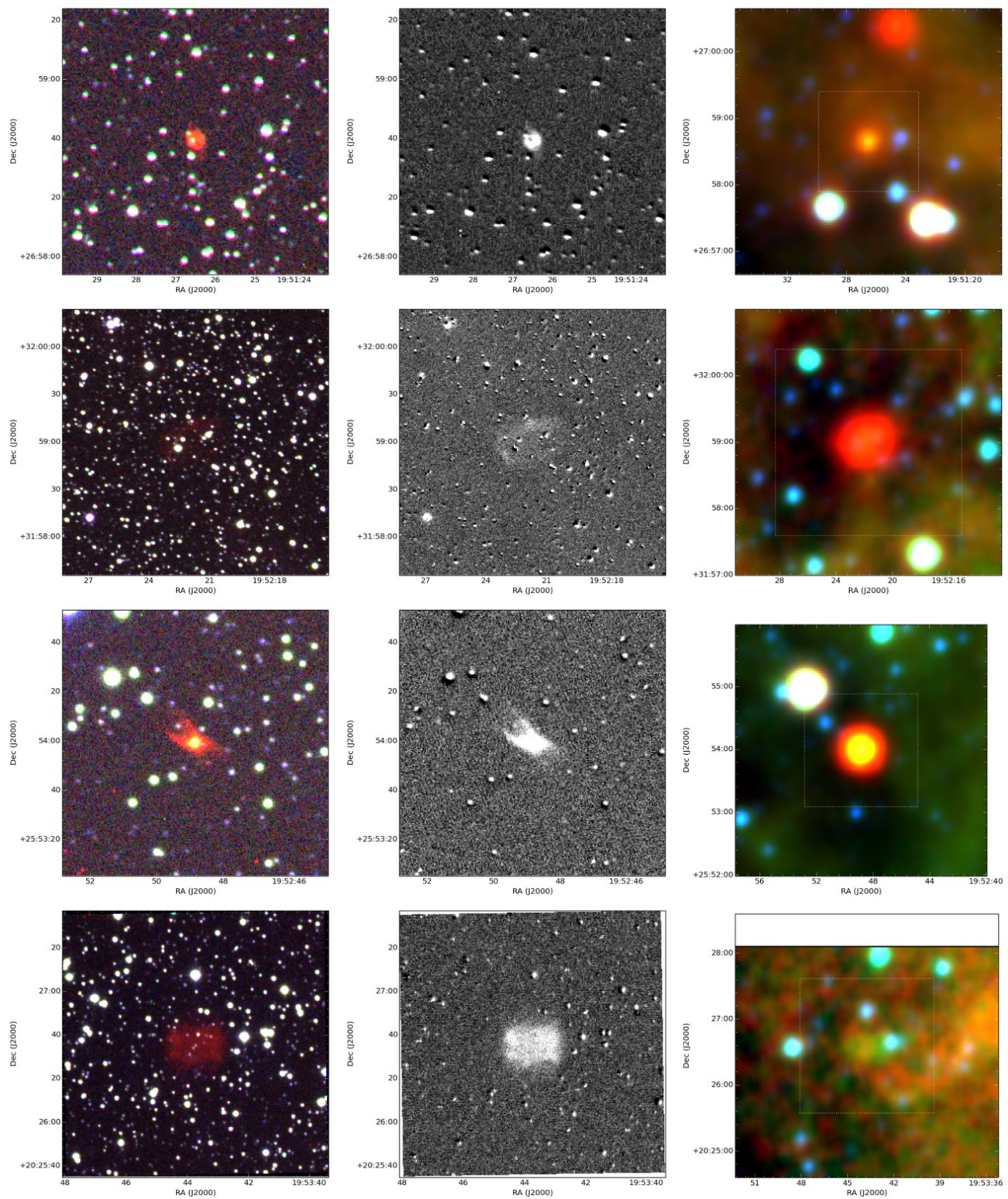


Figure A.30. Same as in Fig. A.1. Objects shown (from top to bottom): PN G063.5+00.0, PN G067.9+02.4, PN G062.7-00.7, PN G058.1-03.7

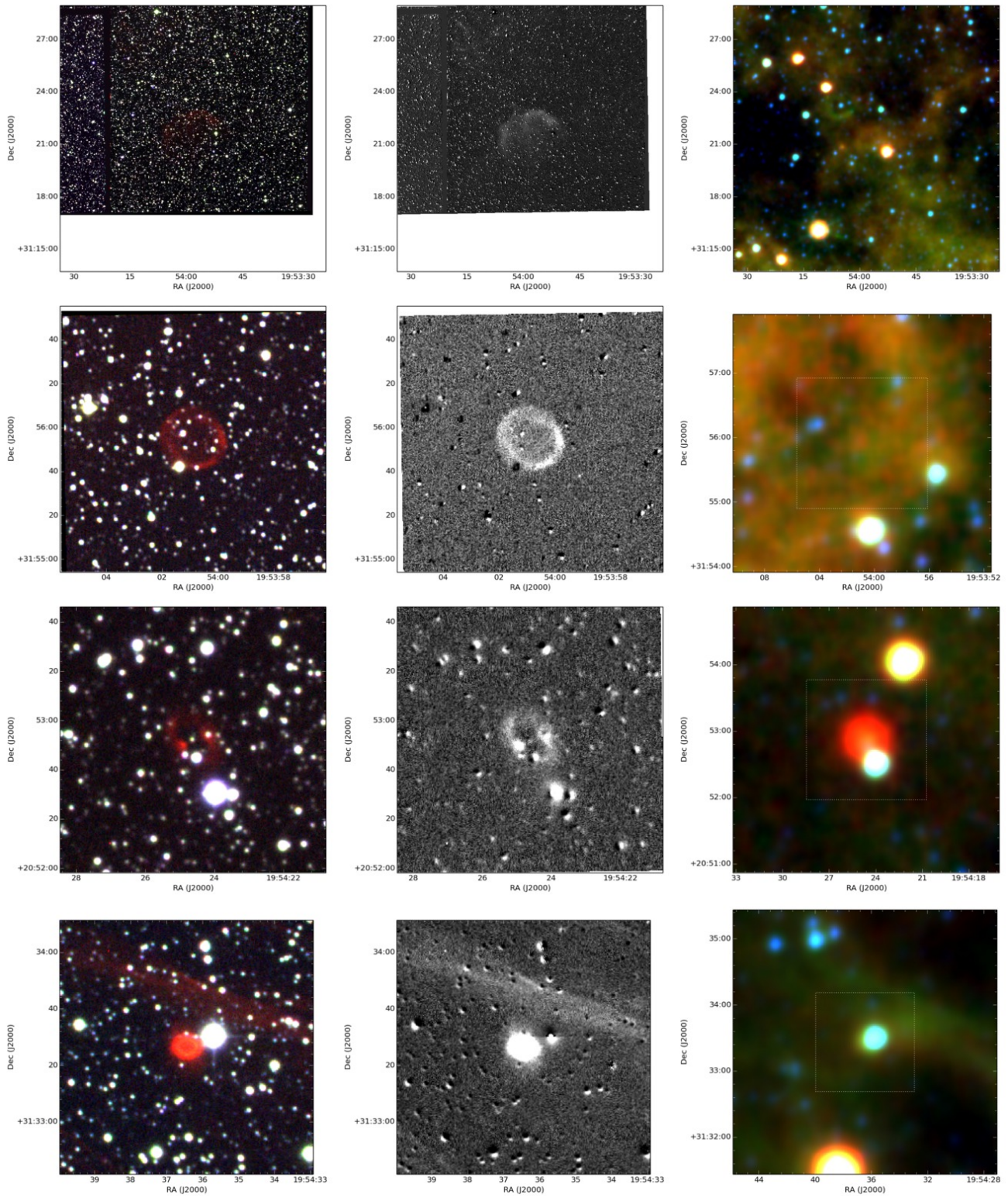


Figure A.31. Same as in Fig. A.1. Objects shown (from top to bottom): PN G067.5+01.8, PN G068.0+02.1, PN G058.6-03.6, PN G067.8+01.8

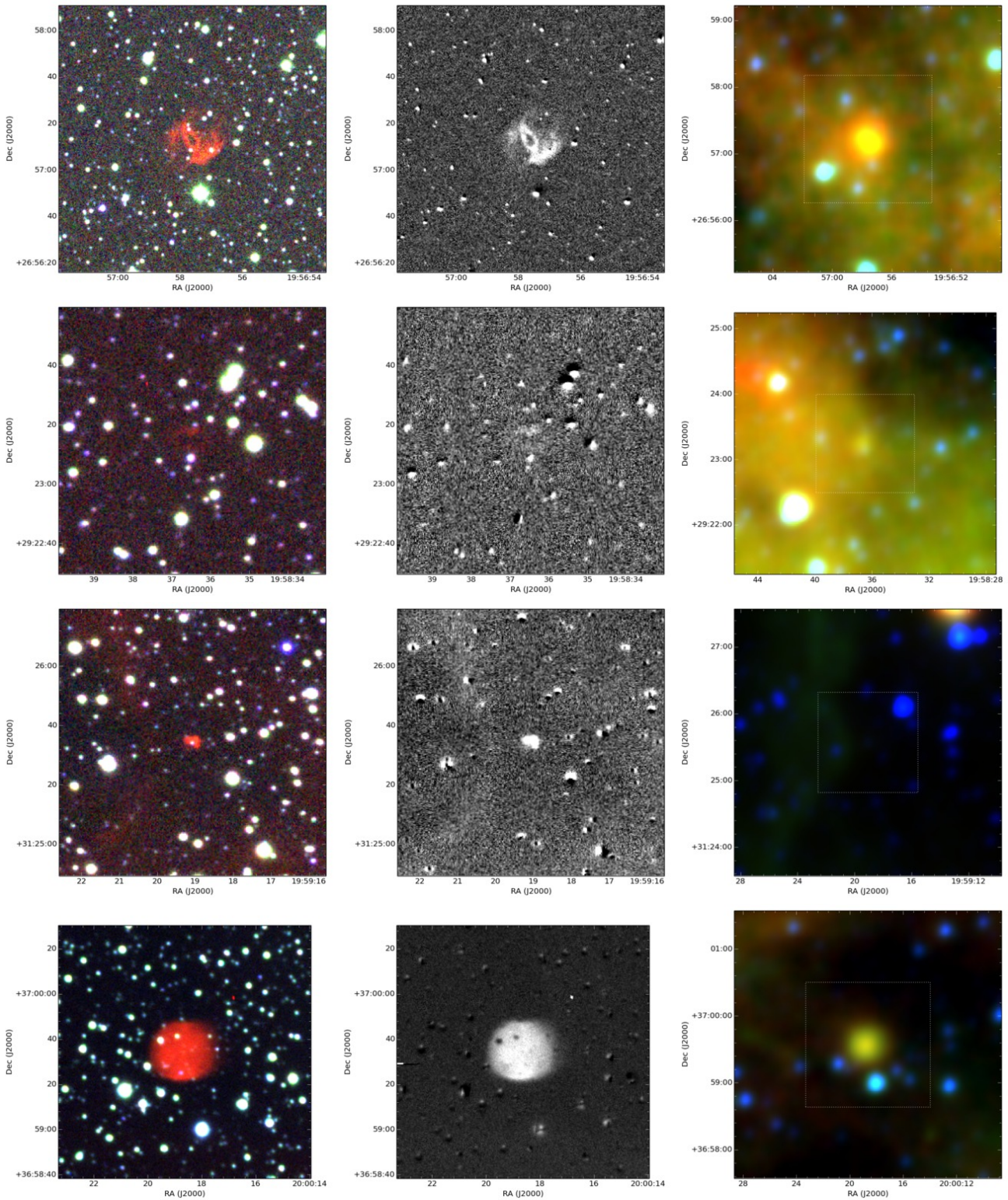


Figure A.32. Same as in Fig. A.1. Objects shown (from top to bottom): PN G064.1-00.9, PN G066.4-00.0, PN G068.2+00.9, PN G073.0+03.6

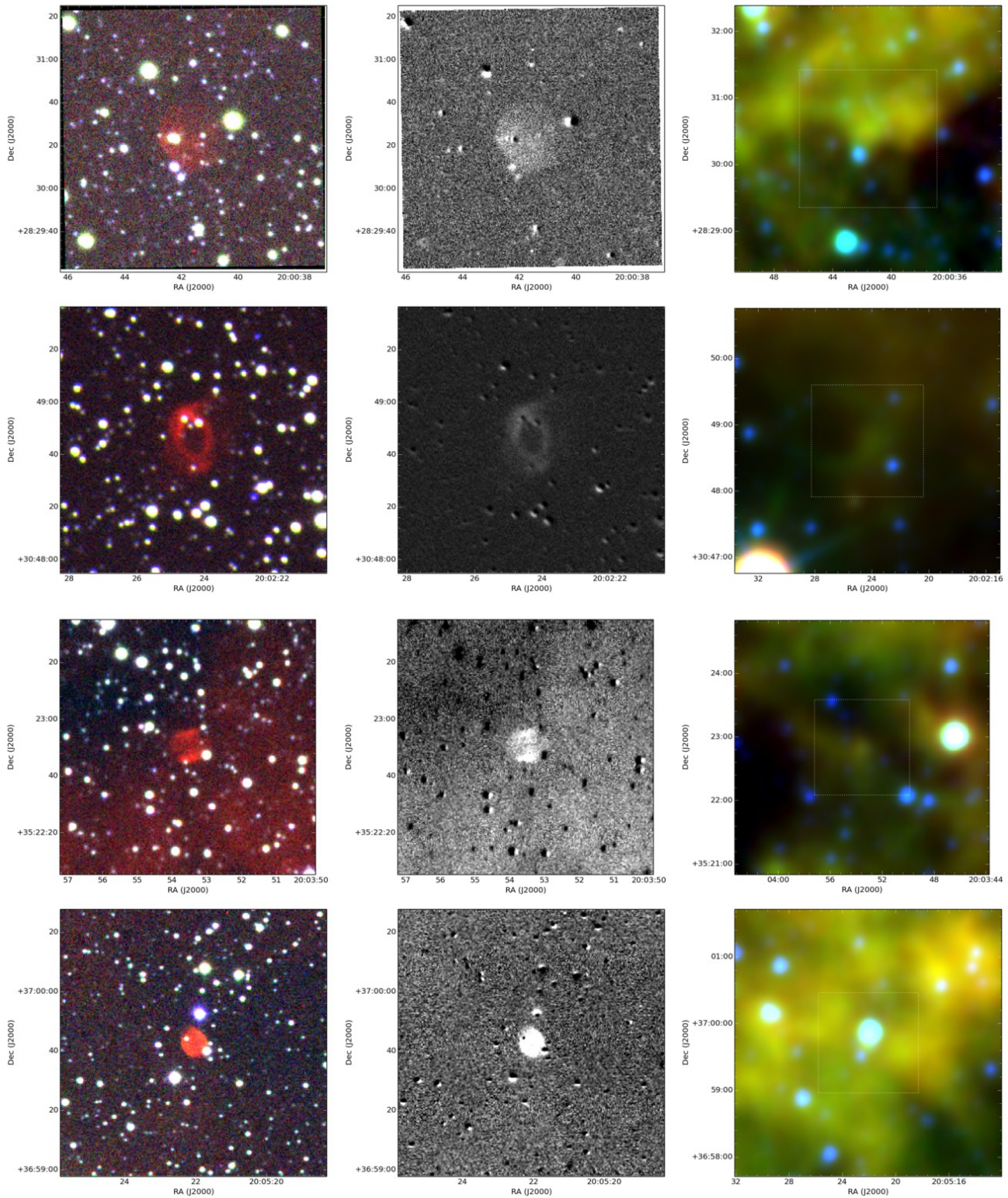


Figure A.33. Same as in Fig. A.1. Objects shown (from top to bottom): PN G065.8-00.8, PN G068.0+00.0, PN G072.0+02.2, PN G073.6+02.8

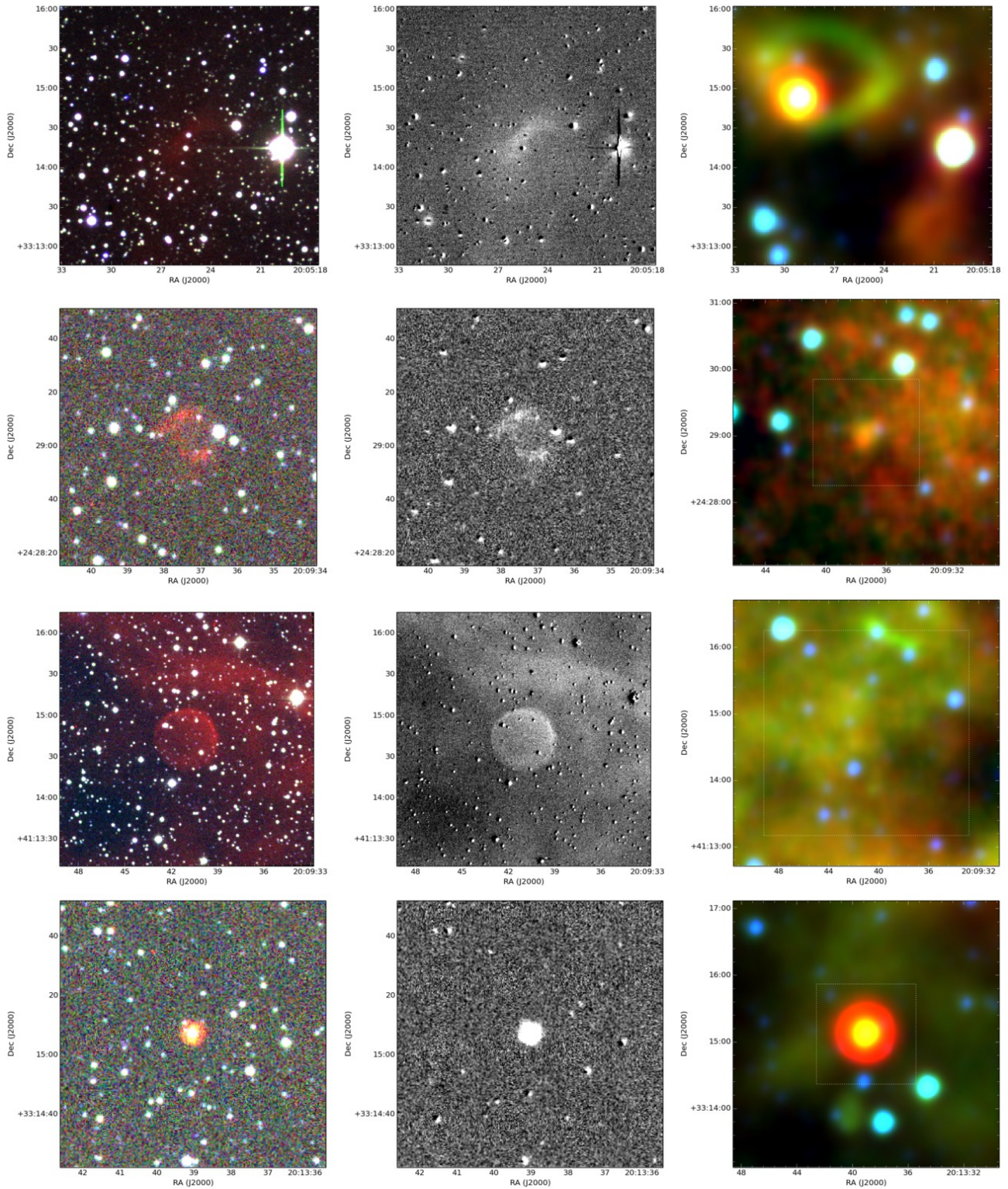


Figure A.34. Same as in Fig. A.1. Objects shown (from top to bottom): PN G070.4+00.7, PN G063.5-04.7, PN G077.6+04.3, PN G071.3-00.6

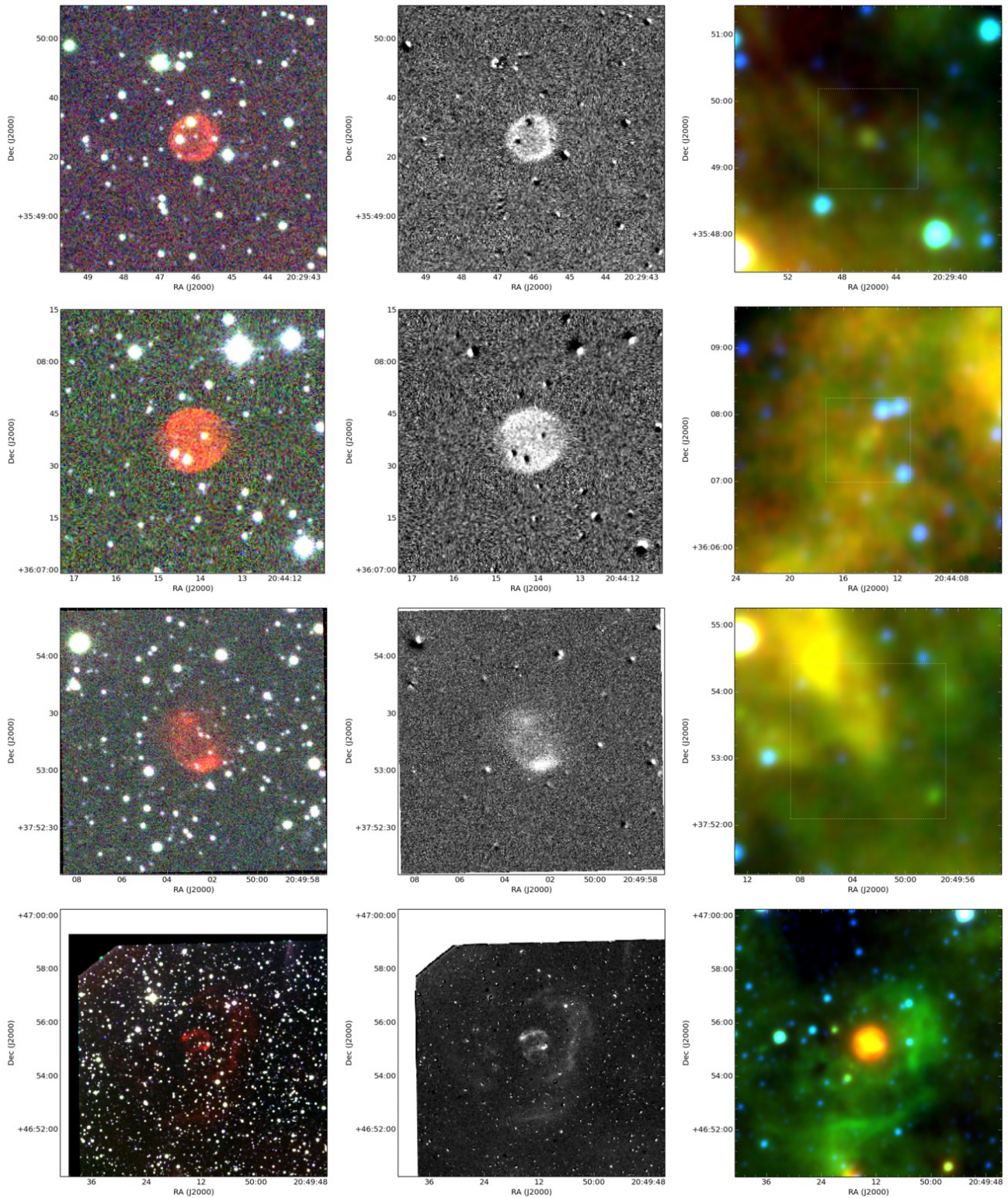


Figure A.35. Same as in Fig. A.1. Objects shown (from top to bottom): PN G075.3-01.9, PN G077.4-04.0, PN G079.5-03.8, PN G086.5+01.8

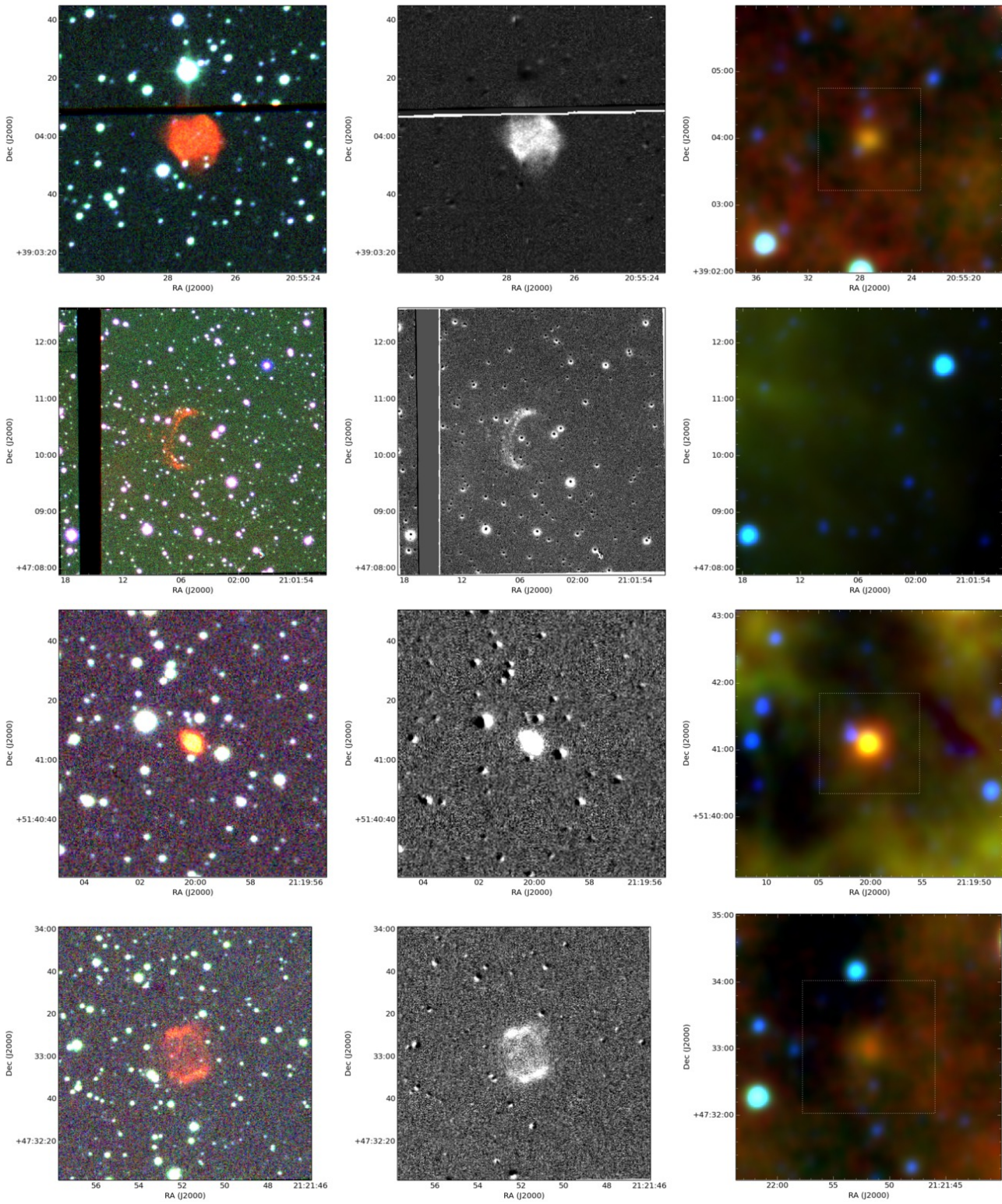


Figure A.36. Same as in Fig. A.1. Objects shown (from top to bottom): PN G081.0-03.9, PN G088.0+00.4, PN G093.3+01.4, PN G090.5-01.7

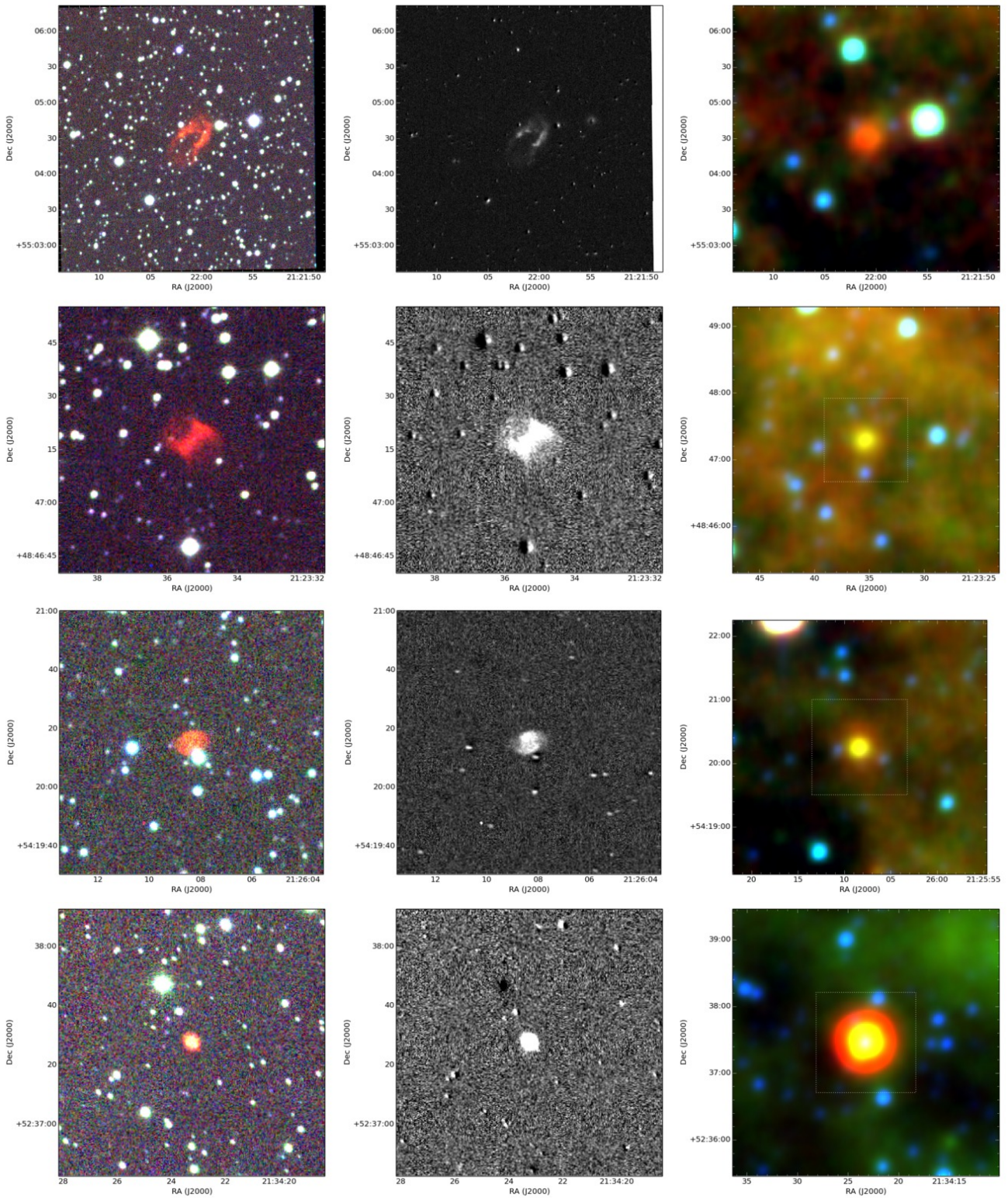


Figure A.37. Same as in Fig. A.1. Objects shown (from top to bottom): PN G095.9+03.5, PN G091.6-01.0, PN G095.8+02.6, PN G095.5+00.5

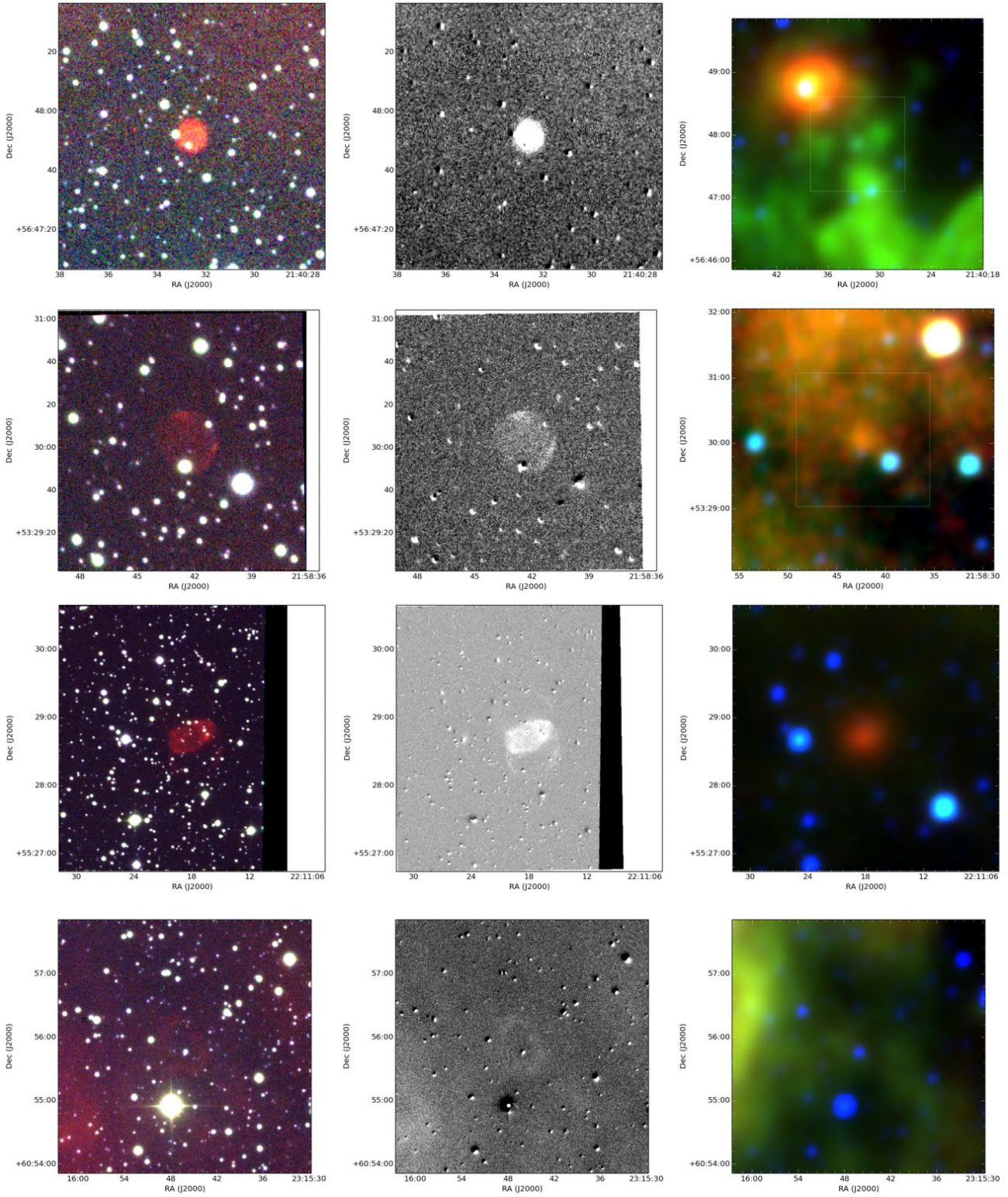


Figure A.38. Same as in Fig. A.1. Objects shown (from top to bottom): PN G098.9+03.0, PN G098.9-01.1, PN G101.5-00.6, PN G111.5+00.1

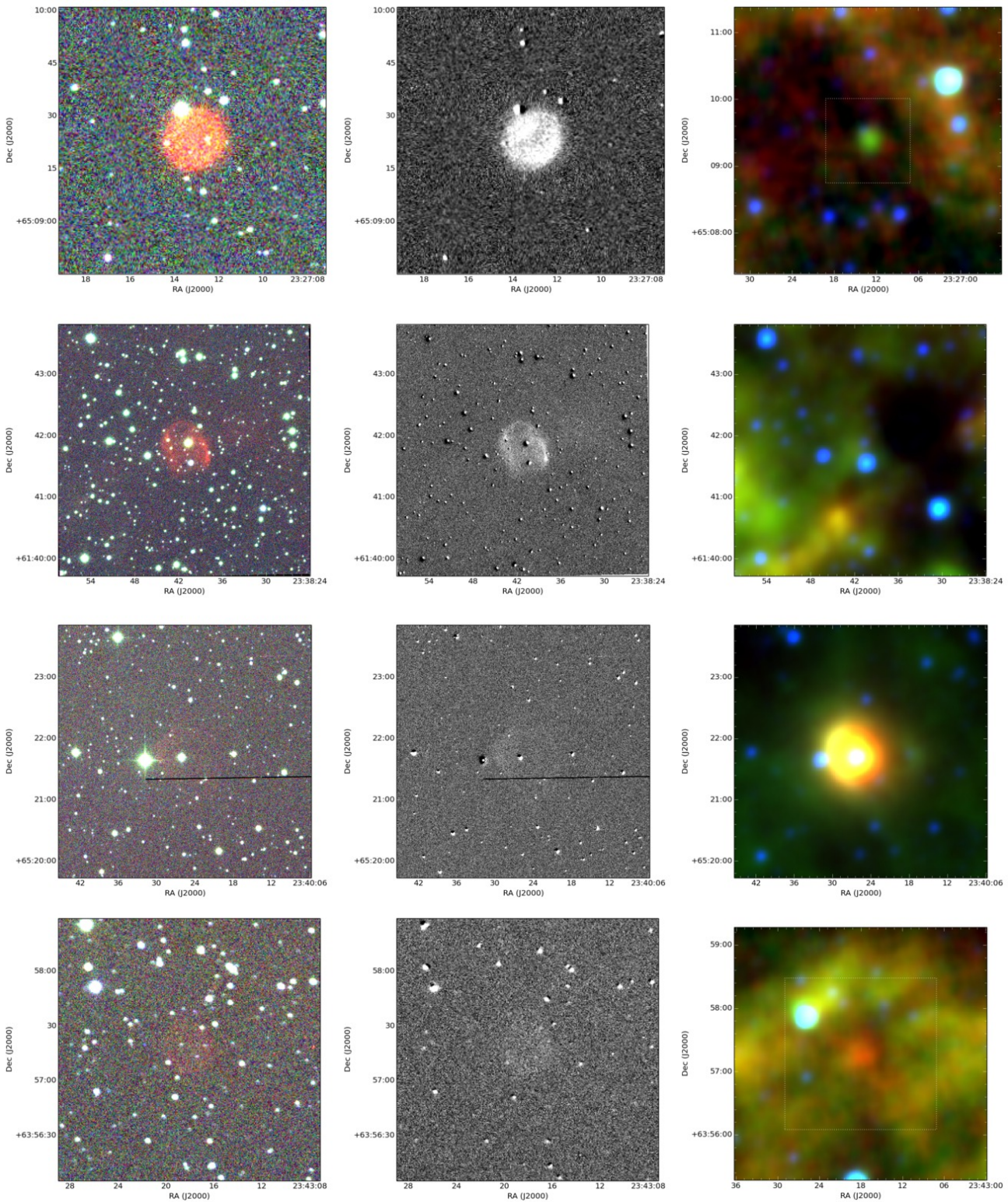


Figure A.39. Same as in Fig. A.1. Objects shown (from top to bottom): PN G114.2+03.7, PN G114.4+00.0, PN G115.6+03.5, PN G115.5+02.0

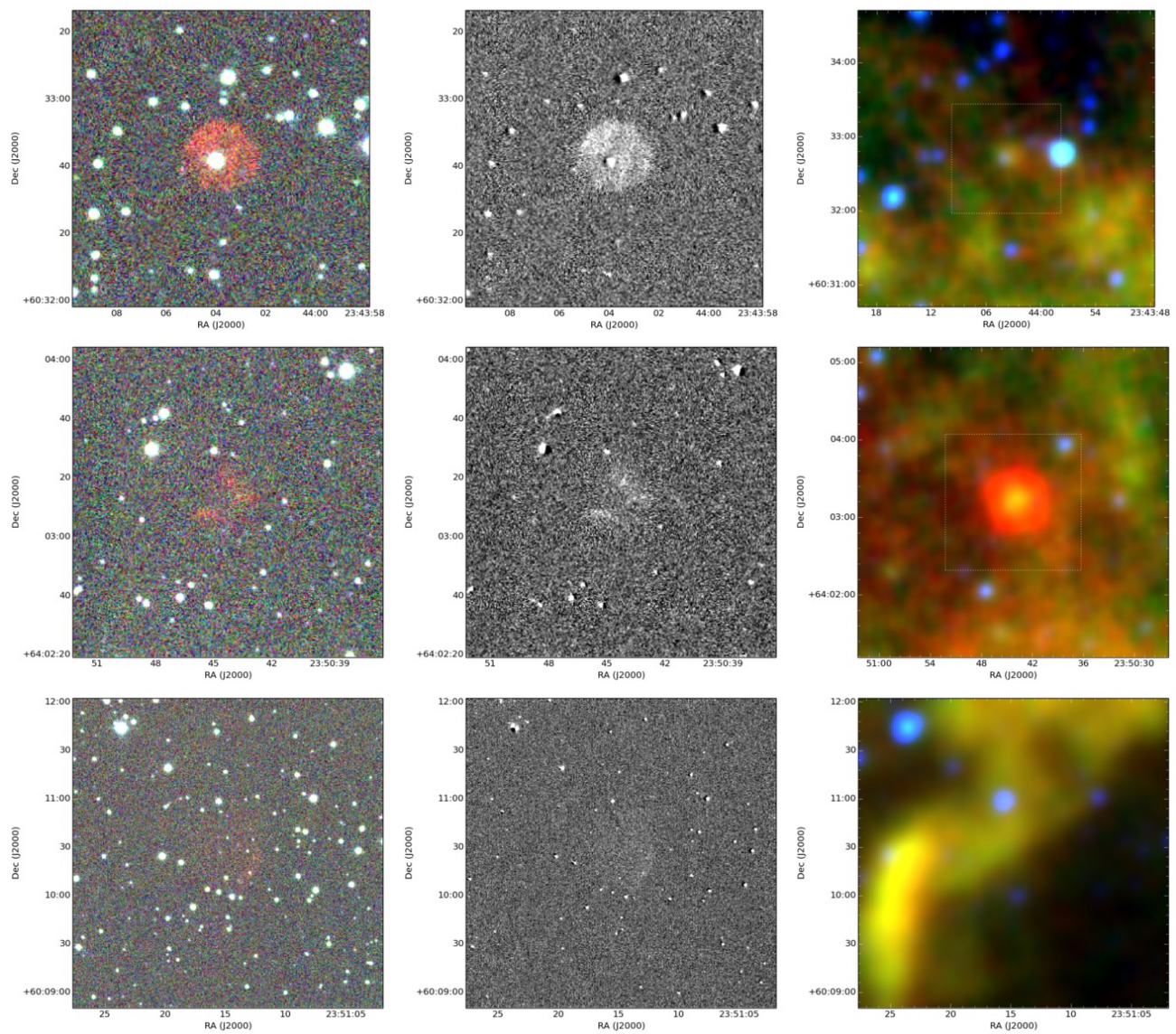


Figure A.40. Same as in Fig. A.1. Objects shown (from top to bottom): PN G114.7-01.2, PN G116.3+01.9, PN G115.5-01.8